Doklady Physics, Vol. 47, No. 5, 2002, pp. 329–331. From Doklady Akademii Nauk, Vol. 384, No. 1, 2002, pp. 28–30.

PHYSICS

Permeability of the Fullerene Cage of Endometallofullerene for Electron Spin Density[1]

V. K. Koltover*, T. A. Parnyuk*, V. P. Bubnov*, and R. M. Davydov**

Presented by Academician Yu.A. Osipyan December 21, 2001

Received December 24, 2001

Endohedral metallofullerene (M_m–C_{2n}) is a carbon cluster molecule containing one metal atom (sometimes, two or three metal atoms) inside a fullerene cage C_{2n} [1]. There are grounds for believing that this new class of compounds holds much promise for a variety of applications, including materials science, NMR imaging, and nuclear medicine [2–6]. It was demonstrated by EPR (electron paramagnetic resonance) that M–C_{2n} of Group III metals (M = La, Sc, Y, Gd) are paramagnetic and that unpaired electrons in these molecules are almost totally localized on the fullerene shell [2, 3].

This raises the question of whether the electron spin density may be localized beyond the fullerene shell. Recently, we observed new EPR signals for La–C_{82} and Y–C_{82} in dimethylformamide (DMF) with unusually small hyperfine splitting (HFS) constants A_{La} and A_Y [7, 8]. This decrease in the HFS constant was allegedly ascribed to a partial transfer of the unpaired electron onto the solvation shell atoms [7, 8]. Herein, we studied the EPR and ENDOR (electron-nuclear double resonance) spectra of La–C_{82} in the polycarbonate matrix and demonstrated for the first time that the area of localization of the electron spin density is indeed not limited by the fullerene cage.

The synthesis of La–C_{82}-containing soots in an electric-arc reactor and the technique of extraction of La–C_{82} from the soots were described earlier [5, 7, 8]. As probed by mass spectroscopy, the samples of La–C_{82} contained neither C_{60} nor other pristine fullerenes [7, 8]. Poly(bisphenol A carbonate) (PC, M_w = 64000; Aldrich) was used. An La–C_{82}-doped PC film was prepared as described in [9]. X-band EPR spectra (~9.5 GHz) were recorded on a Varian E-104A spectrometer. Q-band ENDOR spectra (~35 GHz) were recorded on a modified Varian E-110A at NWU. ENDOR stands for EPR-detected NMR spectroscopy. In an ENDOR experiment, the spectrometer magnetic field and microwave frequency are maintained at fairly constant values fitting to the electron spin resonance condition of the paramagnetic center and the microwave irradiation power is provided sufficiently large to saturate the EPR signal. Simultaneously, the sample is exposed to a variable radio-frequency field and the intensity of the saturated EPR signal is taken as a function of the radio frequency. If the radio frequency corresponds to a magnetic resonance frequency of a nuclear spin, then the reorientation of the nuclear spin takes place. As a result, the saturation of the EPR signal is relieved and this signal builds up [10].

The experimental results are depicted in Figs. 1 and 2. A solution of La–C_{82}-doped PC in *o*-dichlorobenzene (DCB) is a gel. The EPR spectrum of this gel at room temperature shows two partially overlapped octet signals with the intensity ratio ≈2 : 1. The HFS constant of the stronger octet is 0.115 mT, while that of the second one is 0.081 mT. Both octets are essentially identical to the well-known signals of La–C_{82} in DCB (without PC additions) and arise from the La–C_{82} isomers differing in the symmetry of their fullerene cages [2, 3]. The octet HFS appears due to the coupling of the unpaired electron to the ^{139}La nuclear magnetic moment (I = 7/2) [2, 3].

The individual spectral lines for this gel are almost as narrow as for pure DCB (H_{pp} ≈ 0.014 mT in the absence of oxygen), although significantly larger line widths should be observed for a viscous polymer solution. It is known that the widths of the HFS components for paramagnetic molecules in a liquid depend on the extent to which molecular rotation averages the HFS and *g*-factor anisotropy: the greater the mobility, the narrower the HFS lines (see, for example [11]). The low influence of the solution viscosity in our case may result from an essentially isotropic contact character of hyperfine coupling in La–C_{82} [2, 3].

In the room-temperature EPR spectrum of an La–C_{82}-doped PC film, the octet HFS is unobservable (Fig. 1, *2*). This is obviously caused by a low rotational mobility of La–C_{82} in the solid polymer. The octet HFS

[1] This article was submitted by the authors in English.

* *Institute of Problems of Chemical Physics, Russian Academy of Sciences, Chernogolovka, Moscow oblast, 142432 Russia*

** *Department of Chemistry, Northwestern University, 2145 Sheridan Road, Evanston, Illinois 60208, USA*

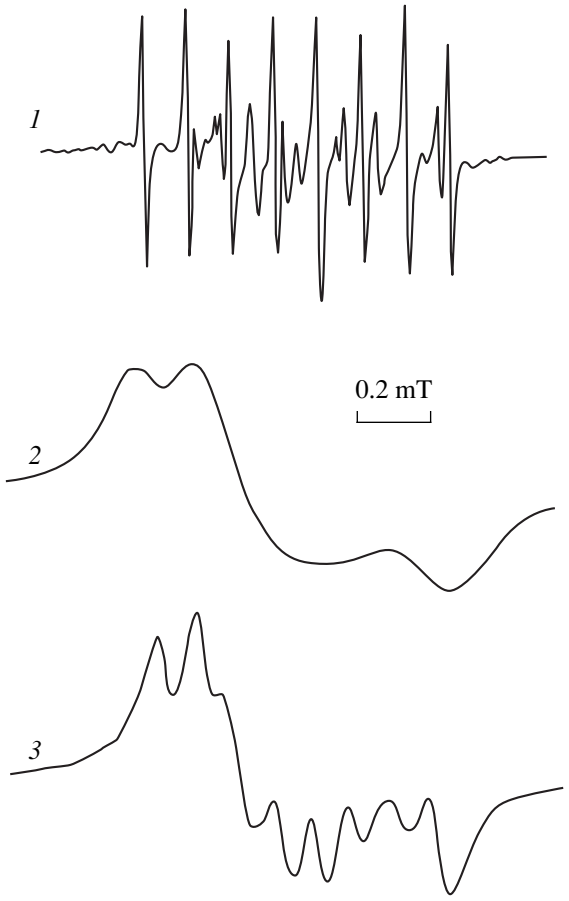

Fig. 1. X-band EPR spectra of La–C_{82} in polycarbonate (PC) samples: (*1*) a solution of PC in DCB (gel) at 293 K in the absence of oxygen (10^{-3} mm Hg), (*2*) an La–C_{82}-doped PC film at 293 K, and (*3*) an La–C_{82}-doped PC film at 425 K. The microwave power is P = 0.5 mW (frequency ~9.5 GHz), and the amplitude of modulation (100 kHz) of the spectrometer magnetic field H_m = 0.01 mT.

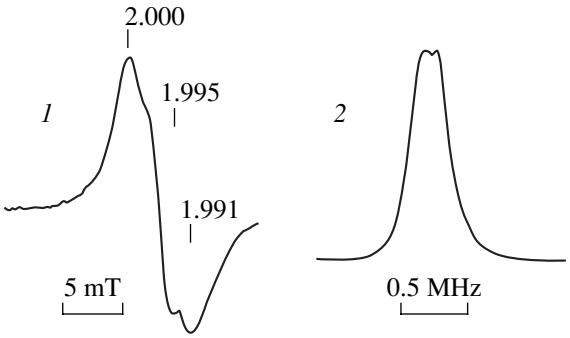

Fig. 2. Q-band (*1*) EPR and (*2*) ^{1}H ENDOR spectra of La–C_{82} in a polycarbonate film at 2 K. The EPR spectrum was recorded at the microwave frequency 38.218 GHz, P = 1 mW, and H_m = 0.25 mT (100 kHz). The ENDOR spectrum was recorded at the microwave frequency 35.218 GHz, spectrometer magnetic field strength H_0 = 1261 mT (at g = 1.995 of the EPR signal). The ENDOR doublet is centered at ν_0 = 53.691 MHz.

appears above the temperature of transition of polycarbonate from the glassy state into the high-elasticity state (≈400 K) when the mobility of the polymer segments becomes high enough (Fig. 1, *3*).

Figure 2 shows Q-band EPR and ENDOR signals of La–C_{82} in a PC film. The increase in the microwave frequency from X- to Q-band increases the Larmor frequency of protons from, thus eliminating the spectral overlap of ^{1}H ENDOR signals with those of other nuclei [10]. An intense ENDOR signal has been detected in the radio-frequency range in which reorientations of proton nuclear spins take place. It is known that the nuclear spin of ^{12}C is zero, while ^{13}C (natural abundance 1.1%, I = 1/2) and ^{139}La exhibit essentially different Larmor frequencies (~13 and 8 MHz, respectively) [10]. Since La–C_{82} molecules lack hydrogen atoms, the observed ^{1}H ENDOR spectrum unambiguously testifies to the coupling of the unpaired electron spin of La–C_{82} to the nuclear spins of the polymer hydrogen atoms.

The detected ENDOR signal consists of two lines, although poorly resolved, which is typical of ^{1}H ENDOR (I = 1/2) [10]. Obvious reasons for the poor resolution of the doublet are the existence of different types of protons in the polymer and the dipole–dipole interaction of the electron and proton spins.

The resonance radio frequencies for the ^{1}H ENDOR signal are determined by the formula [10]

$$\nu_\pm = (A^H/2 \pm g_N\beta_N H)/h.$$

Here, A^H is the hyperfine coupling constant resulting mainly from the electron-spin density localized on the proton, H is the magnetic field strength, g_N is the g-value of a proton, β_N is the nuclear Bohr magneton, and h is Planck's constant [10]. Hence, from the splitting of the doublet, one can estimate the upper limit of the contact hyperfine coupling with the polymer protons: $A^H \le 0.0028 \pm 0.0001$ mT.

Thus, the intense matrix ENDOR signal testifies to the fact that the area of localization of the electron spin density is indeed not restricted by the fullerene cage. This "spin leakage" of the fullerene shell can be of obvious importance in explaining such properties of M–C_{2n} as their tendency to form dimers and nonparamagnetic clusters in liquid solutions and solids.

ACKNOWLEDGMENTS

We are grateful to Dr. É.B. Yagubskiĭ (Institute of Problems of Chemical Physics) and Dr. B.M. Hoffman (Northwestern University, Evanston) for their interest to this research.

This research was supported by the Russian Foundation for Basic Research (project no. 01-03-32945) and the Russian Federal Program "Fullerenes and Atomic Clusters" (project no. 4-1-98).

REFERENCES

1. Y. Chai, T. Guo, C. Jin, *et al.*, J. Phys. Chem. **95**, 7564 (1991).
2. D. M. Poirier, M. Knupfer, J. M. Weaver, *et al.*, Phys. Rev. B **49**, 17403 (1994).
3. G. Seifert, A. Bartl, L. Dunsch, *et al.*, Appl. Phys. A **A66**, 265 (1998).
4. H. Shinohara, Rep. Prog. Phys. **63**, 843 (2000).
5. V. K. Kol'tover, E. É. Laukhina, Ya. I. Éstrin, *et al.*, Dokl. Akad. Nauk **353**, 57 (1997).
6. V. K. Koltover, Y. I. Estrin, L. T. Kasumova, *et al.*, J. Biosci. **24**, 188 (1999).
7. V. K. Koltover, V. P. Bubnov, E. E. Laukhina, and Y. I. Estrin, Mol. Mater. **13**, 239 (2000).
8. V. K. Kol'tover, Ya. I. Éstrin, V. P. Bubnov, and E. É. Laukhina, Izv. Akad. Nauk, Ser. Khim., No. 10, 1765 (2000).
9. V. K. Kol'tover, T. A. Parnyuk, V. P. Bubnov, *et al.*, Fiz. Tverd. Tela (St. Petersburg) **44**, 506 (2002) [Phys. Solid State **44**, 529 (2002)].
10. G. Feher, Phys. Rev. **114**, 1219 (1959).
11. V. K. Koltover, in *Biophysics* (G. K. Hall, Boston, 1977), Vol. 4, pp. 10–68.

Doklady Physics, Vol. 47, No. 5, 2002, pp. 332–336. Translated from Doklady Akademii Nauk, Vol. 384, No. 1, 2002, pp. 31–35.

PHYSICS

Propagation of Light from an Extended Source through an Optically Inhomogeneous Medium

Corresponding Member of the RAS V. V. Ragulsky* and V. G. Sidorovich**

Received January 21, 2002

As is well known, optical inhomogeneities exist in most transparent objects. They arise because of nonuniform concentration of particles in condensed media, turbulent air motion, roughness of interfaces between media, etc. These inhomogeneities, as well as phase aberrations in optical elements that form light beams, can noticeably affect the propagation of light beams, producing both static and dynamic distortions in them.

For example, the radiation of a point source (i.e., a spherical or plane wave with a uniform intensity distribution) in the case of propagation through a turbulent atmosphere turns into a wave characterized by a randomly curved unsteady wave front [1–3]. Then, due to the interference of different parts of the wave, amplitude inhomogeneities of the light field appear in the beam cross section, namely, local maxima and minima in which the light intensity may differ by many times from the average intensity.

The evolution of these inhomogeneities leads to scintillation of the light power recorded by a detector with a small (compared to inhomogeneity sizes) diameter. This phenomenon is quite familiar: this is the effect that is responsible for the twinkling of stars. In optical communication, location, and ranging, this effect causes strong fading of signals, which significantly affects the efficiency of the corresponding systems (see, e.g., [4]).

In this study, we attempt to decrease the effect of optical inhomogeneities on the amplitude distribution of the radiation transmitted through them by using an extended light source with a random angular spectrum.

From the conceptual standpoint, the possibility of such a decrease [5] is clear from the following reasoning. An extended source can be considered as a set of diffraction-size (i.e., virtually point-size) oscillators that closely adjoin each other. Therefore, we can expand the field produced by them as a sum of beams from distant point emitters. As is well known, spatial coordinates are readily transformed into angular ones by placing a source in the focal region of a proper lens. As a result of this transformation, the above "elementary" beams become noncollinear at the lens output. Therefore, the spatial distributions of their intensities in the far-field zone turn out to be shifted with respect to each other, which, generally speaking, should result in the smoothing of inhomogeneities in the light field.

From the simplest geometric construction, it follows that the relative shifts of the distributions mentioned above at a distance L from a lens with focal length F reach $\frac{d}{F}L$, where d is the source diameter and $F \ll L$. However, the effective smoothing of the inhomogeneities takes place only when these shifts exceed the spot diameter δ within which the emission of one elementary beam is smeared by the optical inhomogeneities, i.e., if the condition

$$\frac{d}{F}L > \delta \tag{1}$$

is satisfied.

We have performed experiments to verify the above concept. For this purpose, we applied two sources, namely, extended and point sources. We used the output end of a multimode lightguide 112 μm in diameter as the extended source. The source was located in the focal region of a lens with a focal length of 3.6 cm and a diameter of 1.6 cm. Coherent radiation with stabilized (with an accuracy no less than 0.4%) power from a semiconductor laser that generated at a wavelength λ = 0.785 μm was delivered to the lightguide input. Then, at the lens output, we observed a beam with a randomly nonuniform wave front and a uniform (on average) intensity distribution.

At distances significantly exceeding the initial cross section of the laser beam (1×3 μm^2), its wave front was quite close to spherical; i.e., this laser was virtually a point light source. Taking this fact into account, we placed a similar laser in the vicinity of the focal surface of another lens with the same characteristics mounted

* *Institute for Problems in Mechanics, Russian Academy of Sciences, pr. Vernadskogo 101, Moscow, 117526 Russia*

** *Sunflower Technologies, Povarskaya ul. 10, Moscow, 121069 Russia*
E-mail: sidor@opten.ru

1028-3358/02/4705-0332$22.00

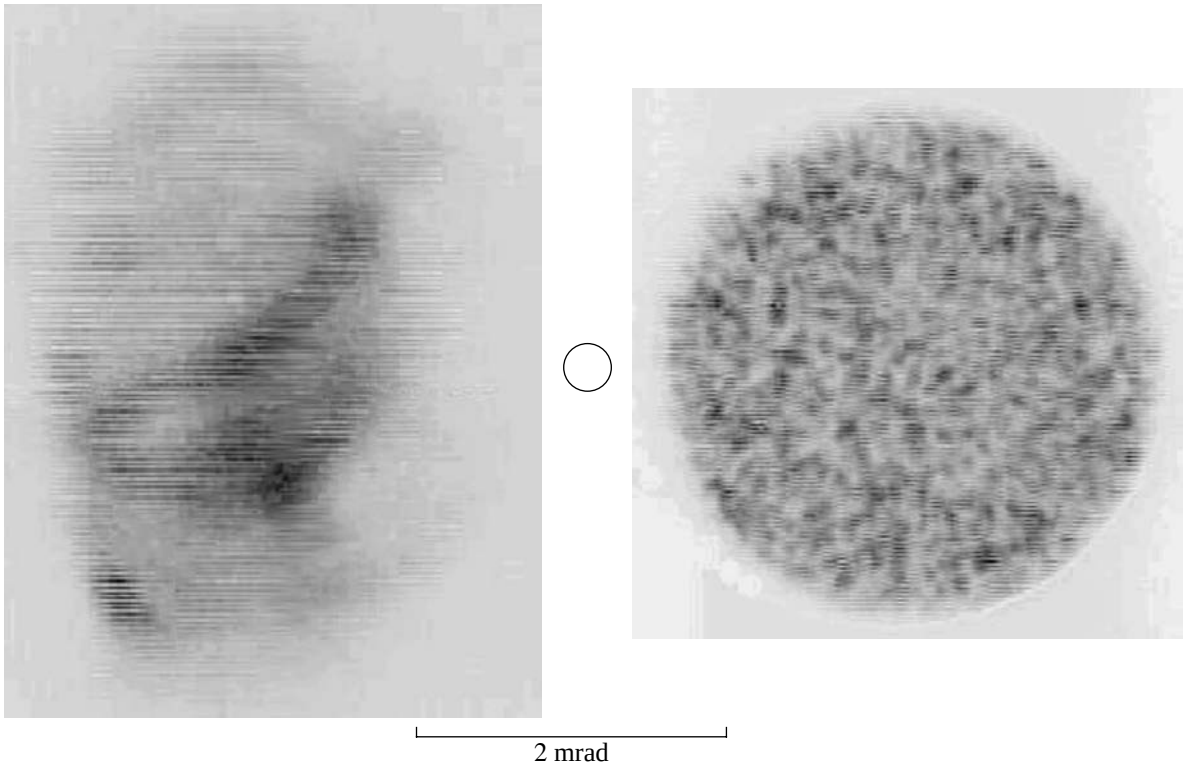

Fig. 1. Snapshot photograph of the far-field zone of light beams passing through turbulent air: (on the left) the beam from the point source; (on the right) the beam from the extended source; the circle between the photographs corresponds to the receiving aperture of the telescope.

near the first one. The outgoing light is a nearly spherical wave with a front curvature governed by the laser position with respect to the lens.

Both beams formed by these lenses were directed to another building 300 m away, where their parts, captured by a telescope with a diameter of 10 cm, were focused on a photodetector. Then, the photodetector signals were analyzed by a dedicated electronic system with a sampling frequency of about 20 kHz.

Since the beam from the extended source was, in fact, formed by overlapping coherent waves,[1] its intensity distribution contained small-scale inhomogeneities usually called speckles [6]. Their minimum possible size in the vicinity of the photodetector is equal to $\varepsilon = \frac{2\lambda}{D}L$, where D is the beam diameter at the lens output. In our case, $\varepsilon \approx 3$ cm. It is clear that averaging of speckle inhomogeneities of the light field is attained only when the aperture of the receiving device Ω exceeds ε, i.e., when the inequality

$$\Omega > \frac{2\lambda}{D}L \qquad (2)$$

is satisfied. Based on relation (2), we chose the diameter of the receiving telescope.

Near the telescope, the cross section of the beam from the extended source was a sharp light circle with a diameter of 0.9 m, whereas the second beam was blurred. By longitudinal displacement of the laser with respect to the lens, the divergence of this beam was adjusted in such a way that the brightness of the light in the center of its angular distribution was equal to the mean brightness of the beam from the extended source (provided that the total powers of these beams were identical).

The instability in the recorded light power can be conveniently characterized by the scintillation index Si, i.e., the rms deviation of the instantaneous power from the mean (over time) power, where the deviation magnitude is normalized to the mean power. It is known that in the case of well-pronounced air turbulence (arising, e.g., in summer due to strong heating of the Earth's surface by solar radiation), light propagation over long atmospheric paths can give rise to Si ~ 1. The results of this study were obtained in winter when turbulence is usually rather small and, correspondingly, the atmospheric value of Si is much lower. In our experiments with the point source, Si did not exceed 0.03, whereas with the extended source, it was 0.02.

To produce stronger turbulent inhomogeneities, we used a thermal radiator mounted 10 cm below the

[1] To be more precise, due to the depolarization of laser radiation in the lightguide, this beam consisted of two orthogonally polarized sets of coherent waves.

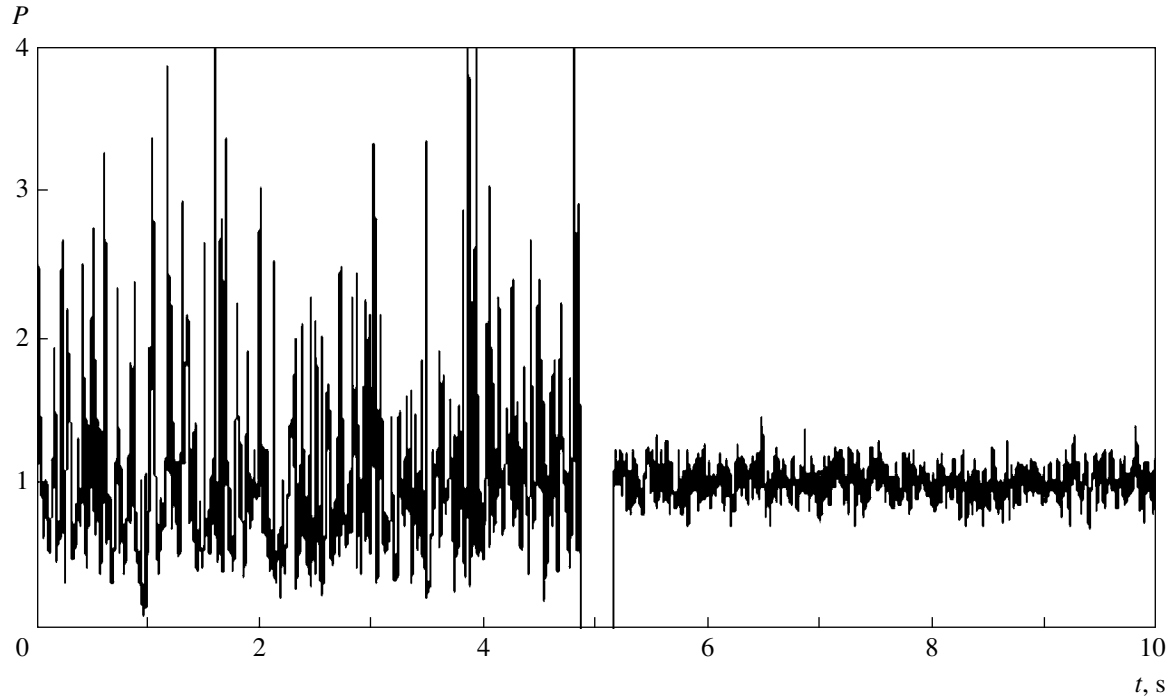

Fig. 2. Power of light impinging on the detector as a function of time: the first and second halves of the oscillogram were obtained with the point and extended sources, respectively.

beams and 1 m from the lenses. The radiator consisted of 12 electrically heated steel tubes with a diameter of 1 cm located 2.5 cm apart in the transverse (with respect to the beams) direction. The radiator temperature T could reach 300°C.

The experiments with the point source showed that its light scintillation index continuously rises with heating and reaches ~0.5 at the temperature indicated above. For the extended source, this index was equal to ~0.1; at $T > 70$°C, it weakly depended on the radiator temperature. It should be noted that the mean power (~10^{-5} W) of the received radiation was also almost independent of the degree of heating. This implies that condition (1) was satisfied in all the experiments.

The spectral analysis of intensity fluctuations for light passing through the turbulent air layer showed that changes in its optical inhomogeneities occurred during the time $t > 5 \times 10^{-3}$ s. With allowance for this fact, the far-field zone of the beams was photographed with an exposure of 10^{-3} s. Examples of pictures obtained by this method are shown in Fig. 1. As is seen, the initially uniform light distribution over the cross section of the point-source beam is strongly distorted in the case of propagation through an inhomogeneous medium. For the extended source, a beam passing through the same medium undergoes almost no changes that could be recorded by the receiving aperture whose size is shown in Fig. 1.

Correspondingly, when operating with the two different kinds of beams (emitted by point and extended light sources), the time characteristics of the light power P being received differ markedly from each other (see Fig. 2). In this case, the power P is normalized to its mean value averaged over time. In this representation, Si is the rms deviation from unity. For the case shown in this figure, Si = 0.48 and 0.105 for the point and extended sources, respectively. Thus, employment of the extended source leads to the suppression of scintillations by a factor of 4.6.

A statistical analysis of the observations, which is illustrated in Fig. 2, makes it possible to determine the probability of optical radiation with a specified power impinging on a detector (Fig. 3).[2] From the results shown in Fig. 3, it follows that, for the point source, the received power sometimes drops to the level of $P \approx 0.1$ and, with the same probability, can reach 4; i.e., the spread of extremal values reaches 40. For the extended source, the corresponding spread is lowered by a factor of 20.

It is worth noting that in order to decrease the effect of atmospheric distortions, it was previously proposed to simultaneously illuminate a detector with many light beams spaced in such a way that changes in optical inhomogeneities along different light paths for the beams would be uncorrelated with each other [7]. Technically, this method is much more complicated than that discussed above. In particular, in order to implement the method of [7], we need to use a large number of

[2] In this figure, the area under each curve, which represents the integral probability of receiving the signal from the detector, equals unity. The apparent difference in these areas is caused by using a logarithmic scale along the ordinate axis.

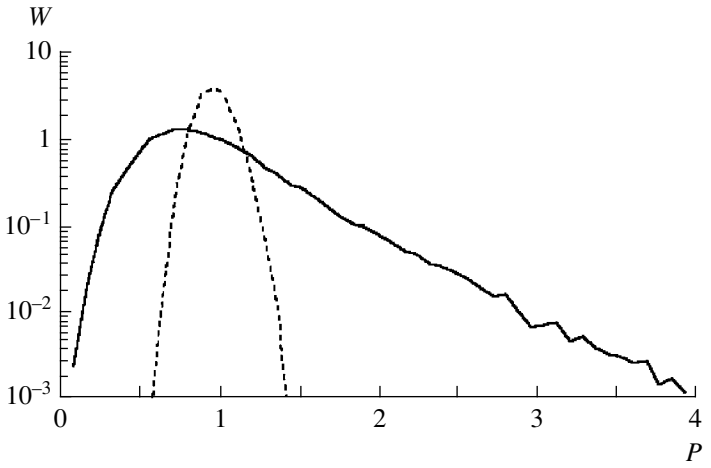

Fig. 3. Probability density W for an optical signal with a given power P incoming to a photodetector: solid and dashed lines correspond to the point and extended sources, respectively.

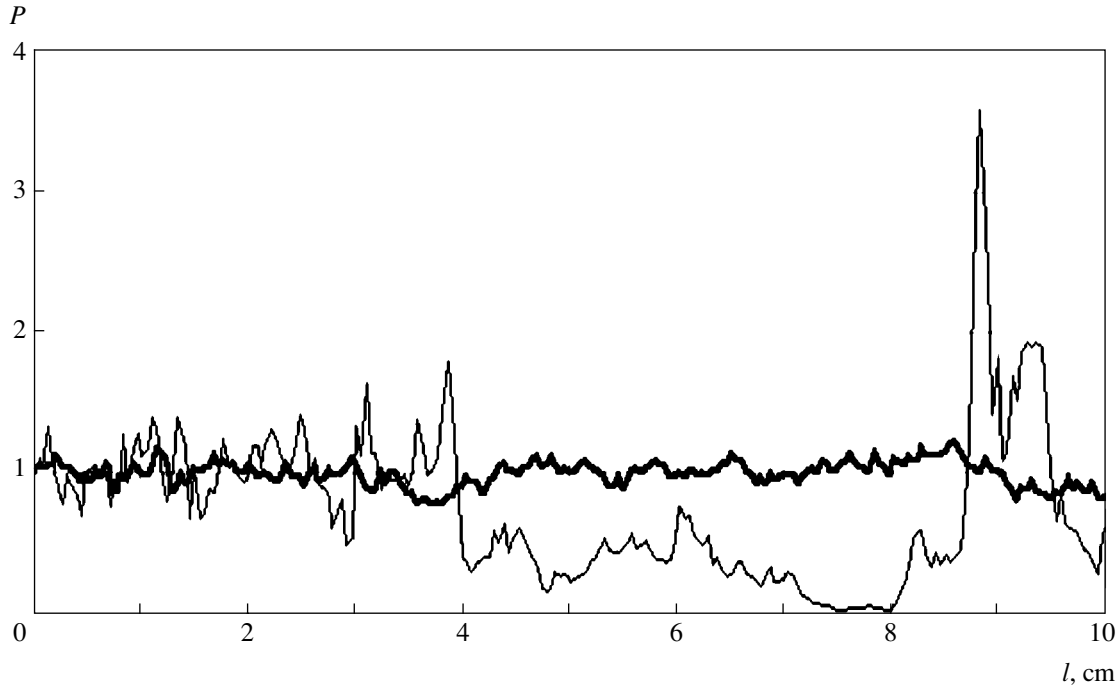

Fig. 4. Dependence of the received light power P on the cross-sectional displacement l of a glass sample placed in the light beam: thin and thick lines correspond to the point and extended sources, respectively. The power is normalized to that impinging on the detector if the inhomogeneous sample is replaced by a parallel-sided plate made of the same glass.

devices forming and aiming many beams. In addition, this method, generally, is not capable of eliminating the effect of static aberrations in the optical elements (lenses, glasses, etc.) through which the beams pass.

However, the mechanism of smoothing the light field considered in this study is able to effectively act independently of whether the optical inhomogeneities are dynamic or static. To verify this statement, we investigated the transmission of both beams through a sample made of low-grade glass. A 3-mm-thick sample was located 20 cm from the lenses and slowly moved in the transverse direction. As a result, various parts of the sample were in the light beam in turn and the aberrations were therefore also different. Correspondingly, the amount of light entering the receiving telescope varied. As was expected, the sensitivity to optical inhomogeneities sharply decreased (Fig. 4) when the extended source was used.

Thus, it has been established that the use of extended sources of light beams makes it possible to decrease by many times the effects of both dynamic and static inhomogeneities on the spatial distribution of light propagating through them.

ACKNOWLEDGMENTS

We are grateful to A.M. Prokhorov and E.M. Dianov for fruitful discussions and M.V. Vasil'ev and Yu.V. Nekrasov for their help in performing the experiments.

REFERENCES

1. L. A. Chernov, *Wave Propagation in a Medium with Random Inhomogeneities* (Izd. Akad. Nauk SSSR, Moscow, 1958).
2. A. M. Prokhorov, F. V. Bunkin, K. S. Gochelashvili, and V. I. Shishov, Usp. Fiz. Nauk **114** (3), 3 (1974) [Sov. Phys. Usp. **17**, 625 (1974)].
3. V. E. Zuev, V. A. Banakh, and V. V. Pokasov, *Optics of Turbulent Atmosphere* (Gidrometeoizdat, Leningrad, 1988).
4. I. I. Kim, J. Koontz, H. Hahakha, and R. Stieger, Proc. SPIE Int. Soc. Opt. Eng., No. 3232, 100 (1997).
5. V. V. Ragulsky and V. G. Sidorovich, Inventor's Certificate RF No. 22279 (2002).
6. J. W. Goodman, *Statistical Optics* (John Wiley and Sons, New York, 1985; Mir, Moscow, 1988).
7. E. Korevaar, US Patent No. 5777768 (1998).

Translated by Yu. Vishnyakov

Doklady Physics, Vol. 47, No. 5, 2002, pp. 337–340. Translated from Doklady Akademii Nauk, Vol. 384, No. 3, 2002, pp. 324–327.

PHYSICS

Diffusion of Interstitial Impurities through a Cylindrical Shell with Residual Stresses

N. M. Vlasov and Corresponding Member of the RAS I. I. Fedik

Received February 12, 2002

The cylindrical shell of a rod fuel element restricts the penetration of the products of nuclear fission. Residual stresses arising in the shell change the character of diffusion processes [1, 2]. For example, compressive stresses impede the migration of interstitial impurities through the shell, whereas tensile stresses give rise to the opposite effect. These effects are caused by the interaction between impurity atoms and residual stresses of different signs. In this study, the kinetics of diffusion migration of interstitial impurities through a cylindrical shell with residual stresses is analyzed. The choice of this model is explained by the following reasons. First, it is possible to obtain residual stresses of different signs in a cylindrical shell by cutting it, adding (excluding) a part of a material, and joining the cut edges. Second, the logarithmic dependence of the first invariant of the residual-stress tensor on the radial coordinate makes it possible to obtain the exact analytical solution of the diffusion equation in a field of forces. Third, this model analysis has a direct practical application. The depletion of a ceramic nuclear fuel (UO_2, UC, UN) is accompanied by an increase in the concentration of interstitial impurities (O, C, N) on the inner shell surface. Their diffusion migration through the shell depends on the level and character of the residual-stress distribution.

Residual stresses of different signs in a cylindrical shell can be as follows. In the first case, the edges of the shell cut are moved apart at an angle ω and the missing material is placed there. In this case, the regions near the inner and outer shell surfaces are in tension and compression states, respectively. In the second case, the shell is cut by an angle ω and the cut edges are joined. The residual stresses change in sign: the neighborhoods of the inner and outer shell surfaces are in tension and compression states, respectively.

Interstitial impurities interact with the field of residual stresses of different signs. The interaction potential for the dimensional effect (only size misfit between the atoms of an impurity and a basic metal is taken into account) is defined by the well-known relation [3]

$$V = -\frac{\sigma_{ll}}{3}\delta v, \quad (1)$$

where σ_{ll} is the first invariant of the residual-stress tensor and δv is the change in the volume of the shell material after the introduction of an interstitial impurity. If $\delta v > 0$, the potential V takes negative values for σ_{ll}. Therefore, interstitial impurities are attracted to the tension domain of residual stresses. For $\delta v > 0$ and $\sigma_{ll} < 0$, the potential V takes positive values. Therefore, impurity atoms are repulsed from the compression region of residual stresses. We consider zirconium, which is everywhere used in structural elements of nuclear power engineering, as a shell material. The first invariant of the residual-stress tensor depends logarithmically on the radial coordinate (planar deformation) [4]:

$$\sigma_{ll} = \frac{\mu\omega(1+\nu)}{2\pi(1-\nu)}\left\{1 + 2\ln\frac{r}{R} + \frac{2\left(\frac{r_0}{R}\right)^2}{1-\left(\frac{r_0}{R}\right)^2}\ln\frac{r_0}{R}\right\}, \quad (2)$$

where μ is the shear modulus, ν is the Poisson ratio, and ω is the rotation angle of the edges of the shell cut. When all other factors are the same, the sign of σ_{ll} depends on the rotation angle of the edges of the shell cut. Conditionally, we assume that $\omega < 0$ when $\sigma_{ll} > 0$ and $\sigma_{ll} < 0$ on the inner and outer shell surfaces, respectively. The rotation angle $\omega > 0$ corresponds to $\sigma_{ll} < 0$ and $\sigma_{ll} > 0$ on the inner and outer shell surfaces, respectively.

The equilibrium concentration of interstitial impurities depends exponentially on the potential V:

$$C_p = C_0\exp\left(-\frac{V}{kT}\right), \quad (3)$$

where C_0 is the concentration of interstitial impurities on the inner boundary of the shell without residual stresses, k is the Boltzmann constant, and T is the abso-

NPO Luch Research Institute,
ul. Zheleznodorozhnaya 24,
Podol'sk, Moscow oblast, 142100 Russia

1028-3358/02/4705-0337$22.00

lute temperature. Tensile and compressive stresses increase and decrease, respectively, the boundary concentration of impurity atoms (with respect to C_0) in accordance with Eq. (3).

The diffusion migration of interstitial impurities through a cylindrical shell with residual stresses is described by the time-dependent diffusion equation in the field of the potential V under the corresponding initial and boundary conditions:

$$\frac{1}{D}\frac{\partial C}{\partial t} = \Delta C \pm \frac{\nabla(C\nabla V)}{kT}, \quad r_0 < r < R,$$
$$C(r,0) = 0, \quad C(r_0,t) = C_p, \quad C(R,t) = 0, \tag{4}$$

where D is the diffusivity of interstitial impurities. The value of C_p depends on the sign of residual stresses on the inner shell boundary. The positive sign of the second term on the right-hand side of Eq. (4) corresponds to compressive stresses on the inner shell surface. They are logarithmically reversed to tensile stresses on the outer shell boundary. This distribution of residual stresses "extracts" interstitial impurities from the inner shell surface. The negative sign of the above term corresponds to the case where tensile stresses on the inner shell surface are logarithmically reversed to compressive stresses on the outer surface. This distribution of residual stresses retards the migration of interstitial impurities through the shell. The physical meaning of the initial and boundary conditions for problem (4) is evident. At the initial time instant, the concentration of interstitial impurities equals zero. The same concentration remains unchanged at the outer shell boundary. This means that impurity atoms leave the outer shell surface as soon as they arrive at it. This condition makes it possible to more clearly emphasize the role of residual stresses. The boundary condition at $r = r_0$ means that, on the inner shell surface, the constant equilibrium concentration of interstitial impurities is maintained in accordance with the interaction potential. Up to constants, the potential V has the form [5]

$$V = -A\ln\frac{r}{R}, \quad A = \frac{\mu\omega(1+\nu)}{3\pi(1-\nu)}\delta v. \tag{5}$$

Constant relations (2) are of no importance since the diffusion of impurity atoms depends on the gradient of the potential V. In this case, $\Delta V = 0$, because V is a harmonic function. With allowance for Eq. (5), problem (4) is mathematically formulated as follows:

$$\frac{1}{D}\frac{\partial C}{\partial t} = \frac{\partial^2 C}{\partial r^2} + \frac{1 \pm \alpha}{r}\frac{\partial C}{\partial r}, \quad r_0 < r < R,$$
$$C(r,0) = 0, \quad C(r_0,t) = C_p, \quad C(R,t) = 0. \tag{6}$$

The dimensionless parameter α specifies the ratio of the binding energy of an interstitial impurity in the field of residual stresses to the thermal motion energy:

$$|\alpha| = \frac{\mu|\omega|(1+\nu)\delta v}{3\pi(1-\nu)kT}.$$

If $|\alpha| \ll 1$, the field of residual stresses is a weak disturbance of the impurity diffusion flux induced by the concentration gradient. At $|\alpha| \gg 1$, the dominant contribution to the diffusion process comes from the field of residual stresses. For $|\alpha| \approx 1$, the diffusion fluxes of interstitial impurities, which are caused by the gradients of concentration and potential V, are approximately equal to each other. Let us estimate $|\alpha|$ for a Zr–H system. If $kT = 10^{-20}$ J, $\mu = 4 \times 10^{10}$ Pa, $\nu = 0.3$, $|\omega| = 0.3$ rad, and $\delta v = 3 \times 10^{-30}$ m^3, we have $|\alpha| \approx 1$. For this reason, without loss of generality, the dimensionless parameter α is taken to be equal to unity in absolute value. The sign of this parameter depends on the type of residual stresses in the cylindrical shell. If $\omega < 0$ (tensile stresses on the inner surface), it is assumed that $\alpha = -1$. In this case, the kinetics of the diffusion of interstitial impurities with allowance for the sign of Eq. (4) are found by solving the problem

$$\frac{1}{D}\frac{\partial C}{\partial t} = \frac{\partial^2 C}{\partial r^2} + \frac{2}{r}\frac{\partial C}{\partial r}, \quad r_0 < r < R,$$
$$C(r,0) = 0, \quad C(r_0,t) = C_p^1, \quad C(R,t) = 0, \tag{7}$$

where

$$C_p^1 = C_0\exp\left(-\frac{V}{kT}\right)_{r=r_0} = C_0\left(\frac{R}{r_0}\right).$$

At $\alpha = -1$, the equilibrium concentration of interstitial impurities at the inner shell boundary exceeds the corresponding value in the absence of residual stresses. Problem (7) shows that residual stresses of this type change the symmetry of the diffusion equation: the diffusion process in the cylindrical shell is spherically symmetric. The transformation of the coordinate dependence decreases the rate of formation of the concentration profile. Mathematically, this fact immediately follows from the form of the diffusion equation. At $\frac{\partial C}{\partial r} < 0$, the variation rate of the concentration $\frac{\partial C}{\partial t}$ in Eq. (7) is less than the rate in Eq. (6) for $\alpha = 0$. The retardation of the process kinetics is physically caused by the fact that tensile stresses decrease in the radial direction and are even reversed to compressive stresses. The solution of problem (7) gives the concentration field of interstitial impurities for a given type of residual stresses:

$$\frac{C}{C_0} = \frac{R}{r}$$
$$\times\left\{\frac{R-r}{R-r_0} - \frac{2}{\pi}\sum_{n=1}^{\infty}\frac{\sin\frac{\pi n(r-r_0)}{R-r_0}}{n}\exp\left[-\frac{\pi^2 n^2 Dt}{(R-r_0)^2}\right]\right\}. \tag{8}$$

For $\omega > 0$ (compressive stresses on the inner shell surface), it is assumed that $\alpha = 1$. In this case, the kinet-

ics of the diffusion of the interstitial impurities with allowance for the sign of Eq. (4) are determined by solving the problem

$$\frac{1}{D}\frac{\partial C}{\partial t} = \frac{\partial^2 C}{\partial r^2}, \quad r_0 < r < R, \tag{9}$$

$$C(r, 0) = 0, \quad C(r_0, t) = C_p^2, \quad C(R, t) = 0,$$

where

$$C_p^2 = C_0 \exp\left(-\frac{V}{kT}\right)_{r = r_0} = C_0\left(\frac{r_0}{R}\right).$$

At $\alpha = 1$, the equilibrium concentration of interstitial impurities on the inner shell surface is less than the corresponding value in the absence of residual stresses. Residual stresses of the other type again change the symmetry of the problem. The diffusion of interstitial impurities in the cylindrical shell is now plane symmetric. This change in the coordinate dependence increases the rate of formation of the concentration profile. Mathematically, this conclusion follows from the form of the diffusion equation. When $\frac{\partial C}{\partial r} < 0$, the variation rate of the concentration $\frac{\partial C}{\partial t}$ for $\alpha = 1$ in Eq. (9) is higher than the rate in Eq. (6) at $\alpha = 0$. Compressive stresses in the radial direction are changed to tensile stresses, and therefore the diffusion migration of interstitial impurities is accelerated. The field of the impurity-atom concentration for this distribution of residual stresses has the form

$$\frac{C}{C_0} = \frac{r_0}{R} \times \left\{\frac{R - r}{R - r_0} - \frac{2}{\pi}\sum_{n=1}^{\infty} \frac{\sin\frac{\pi n(r - r_0)}{R - r_0}}{n} \exp\left[-\frac{\pi^2 n^2 Dt}{(R - r_0)^2}\right]\right\}. \tag{10}$$

We now compare Eqs. (8) and (10), which are represented in the form

$$\frac{C}{C_0} = \frac{R}{r} f(r, t), \tag{11a}$$

$$\frac{C}{C_0} = \frac{r_0}{R} f(r, t), \tag{11b}$$

respectively. Here, $f(r, t)$ is the expression in braces in Eqs. (8) and (9). At $C(R, t) = 0$, the diffusion flux of impurity atoms through the outer shell surface has the form

$$\mathbf{j} = -D\left(\frac{\partial C}{\partial r} + \frac{C}{kT} + \frac{\partial V}{\partial r}\right)_{r = R} = -D\left.\frac{\partial C}{\partial r}\right|_{r = R} \tag{12}$$

and makes it possible to separate the contribution of residual stresses of different signs to the diffusion of interstitial impurities. The diffusion flux of interstitial impurities has the form

$$|\mathbf{j}| = DC_0\left.\frac{\partial f}{\partial r}\right|_{r = R}, \tag{13a}$$

$$|\mathbf{j}| = \frac{DC_0 r_0}{R}\left.\frac{\partial f}{\partial r}\right|_{r = R} \tag{13b}$$

for Eqs. (11a) and (11b), respectively.

The analysis of Eqs. (13) shows that the dominant contribution to the diffusion flux of interstitial impurities comes from the equilibrium concentration on the inner shell surface. If the inner domain of the cylindrical shell is in the compression state, the flux of impurity atoms through the outer surface is much less than the flux for residual stresses of the opposite sign. Therefore, in order to decrease the penetration of interstitial impurities through the shell of a fuel element in the process of nuclear fuel depletion, one must create compressive stresses near the inner shell surface. This action can also prevent the penetration of products of nuclear fission. For the same initial concentration of interstitial impurities on the inner shell surface, the distribution of residual stresses is of crucial importance.

The diffusion fluxes of interstitial impurities through the cylindrical shell can be best illustrated for a steady-state process. Here, the effects of two distributions of residual stresses on diffusion are compared with each other and with the case of the absence of stresses. In addition, the stationary distribution of the concentration of interstitial impurities makes it possible to obtain their integral value in the shell when the total diffusion flux at the outer boundary is equal to zero. The steady-state field of the interstitial-impurity concentration in the cylindrical shell with two types of residual stresses and in the absence of them has the form

$$\frac{C}{C_0} = \frac{R}{r}\frac{R - r}{R - r_0}, \tag{14a}$$

$$\frac{C}{C_0} = \frac{r_0}{R}\frac{R - r}{R - r_0}, \tag{14b}$$

$$\frac{C}{C_0} = \frac{\ln\frac{R}{r}}{\ln\frac{R}{r_0}}, \tag{14c}$$

respectively. Expressions (14a) and (14b) describe the concentration of the interstitial impurities when the inner region of the cylindrical shell is in the tension and compression states, respectively. Relationship (14c) describes the concentration of interstitial impurities in the absence of residual stresses. The diffusion fluxes for

Eqs. (14) determine the migration of impurity atoms through the cylindrical shell:

$$|\mathbf{j}| = \frac{DC_0}{R - r_0}, \quad (15a)$$

$$|\mathbf{j}| = \frac{DC_0 r_0}{R(R - r_0)}, \quad (15b)$$

$$|\mathbf{j}| = \frac{DC_0}{R \ln \frac{R}{r_0}}. \quad (15c)$$

The analysis of Eqs. (15a) and (15b) shows that, in the steady-state regime, the diffusion flux of interstitial impurities in the first case is greater than the flux in the second case. Tensile residual stresses on the inner shell surface increase the flux of impurity atoms through the outer boundary. In the absence of residual stresses [Eq. (15c)], the flux of interstitial impurities is intermediate between the above cases.

Thus, the theoretical analysis of the above model of the diffusion of interstitial impurities through a cylindrical shell with residual stresses leads to the following conclusions. If the inner region of the shell is in a tension state, the diffusion flux of impurity atoms through the outer boundary is maximal, which is due to the high concentration of impurity atoms at the inner shell boundary. Tensile stresses increase the equilibrium concentration of interstitial impurities compared to the case where stresses are absent. If the inner region of the shell is in a compression state, the diffusion flux of interstitial impurities through the outer boundary is minimal, which is due to a low value of the equilibrium concentration of impurity atoms at the inner shell boundary. Compressive stresses decrease the equilibrium concentration of interstitial impurities compared to the case where stresses are absent. The analysis showed that the promotion or retardation of the process kinetics due to a change in the coordinate dependence of the diffusion equation is of minor importance. As a rule, the diffusion migration of interstitial impurities through the cylindrical shell is determined by their concentration at the inner boundary. Therefore, in order to decrease the penetration of interstitial impurities and fission products through the shell of a fuel element, it is necessary to create compressive stresses on its inner surface.

REFERENCES

1. N. M. Vlasov and I. I. Fedik, Dokl. Akad. Nauk **375**, 334 (2000) [Dokl. Phys. **45**, 623 (2000)].
2. N. M. Vlasov and I. I. Fedik, Dokl. Akad. Nauk **382**, 186 (2002) [Dokl. Phys. **47**, 47 (2002)].
3. C. Teodosiu, *Elastic Models of Crystal Defects* (Editura Academia, Bucuresti, 1982; Springer, Heidelberg, 1982).
4. A. I. Lur'e, *Theory of Elasticity* (Nauka, Moscow, 1970).
5. N. M. Vlasov, Dokl. Akad. Nauk **377**, 464 (2001) [Dokl. Phys. **46**, 219 (2001)].

Translated by Yu. Vishnyakov

Doklady Physics, Vol. 47, No. 5, 2002, pp. 341–345. Translated from Doklady Akademii Nauk, Vol. 384, No. 3, 2002, pp. 328–333.

PHYSICS

Universal Properties of Metals in the Phenomenon of Dynamic Failure

Corresponding Member of the RAS R. I. Il'kaev, A. Ya. Uchaev, S. A. Novikov, N. I. Zavada, L. A. Platonova, and N. I. Sel'chenkova

Received June 28, 2001

The response of metal to an external physicomechanical action is determined by both the thermodynamic state of the metal and the characteristics of the loading process.

By convention, the phenomenon of failure can be divided into two regions, namely, the quasistatic longevity region ($t > 10^{-4}$ s) and the dynamic longevity region ($t < 10^{-6}$ s).

In [1–7], a thermal shock caused by high-current beams of relativistic electrons is described in detail. In this case, in contrast to traditional loading methods, the failure process proceeds over times $t < 10^{-8}$ s and at the energy-supply rate $\frac{dT}{dt} \sim 10^{12}$ K/s, which is accompanied by temperature variation up to the melting temperature T_{melt}. This makes it possible to obtain more comprehensive data on the time–temperature dependences of the process, because the effect of the actual crystal-lattice structure is less pronounced under these testing conditions. Thus, the results of these investigations yield additional information about the behavior of specific substances and are important on their own for failure physics, e.g., in constructing failure models of high-rate deformation.

We have investigated the regularities of dynamic failure for a series of metals with atomic numbers $Z \sim$ 13–92 (Al, Ti, Ta, Ni, Pb, Cu, Cd, Sn, Zn). The experiments were carried out in the time-to-rupture range $t \sim 10^{-5}$–10^{-10} s at initial temperatures T_0 between 4 K and T_{melt}. The energy-supply rates were $\frac{dT}{dt} \sim 10^6$–10^{12} K/s $\left[\frac{dE}{dt} \sim 10^5\text{–}10^{11}\ \text{J/(g s)}\right]$ and $\frac{dE}{dm} \sim 1\text{–}10^4$ J/g. The results are presented in the table.

Russian Federal Nuclear Center,
All-Russia Scientific-Research Institute
of Experimental Physics,
Sarov, Nizhni Novgorod oblast, 607190 Russia
E-mail: uchaev@expd.vniief.ru

Evidently, the formation of a dynamic-strength database by combining results obtained by analysis of partial properties is not optimal. The main task is to reveal general regularities that characterize the behavior of metals and remain invariable with respect to changes in external conditions. It was demonstrated in [1–7] that, in the dynamic failure of metals, the resistance to external effects arises due to the appearance of a certain dissipative structure formed in a sample, namely, a cascade of failure centers. The use of the method for spectral determination of the failure-center size distribution at various stages of the process made it possible to establish general regularities in the formation of a cascade of failure centers. Using the similarity transformation, we obtained the size distribution of failure centers for various materials in terms of universal coordinates. This shows that the dynamic failure of metals obeys a single dominant process. This process combines the accumulation and growth of failure centers, which determine a major part of the longevity time. The developing cascade of failure centers is a fractal cluster. The process of accumulation of failure centers (development of damage capability) can be described within the self-similar approximation [1]. The spectral distribution of the failure centers by size

Time regularities of dynamic failure for a number of metals

Metal	P, GPa				
	$t = 10^{-6}$ s	$t = 10^{-7}$ s	$t = 10^{-8}$ s	$t = 10^{-9}$ s	$t = 10^{-10}$ s
Cd	0.54	0.76	1.12		
Ni	3.48	5.82	9.68	14.4	
Ta	4.96	7.47	10.87	15.0	
W		9.0	14.9	21.35	25.25
Fe	4.61	7.98	12.09	18.8	
Cu	1.66	3.77	6.99	10.21	
Pb	0.37	0.7	1.0		
Ti	2.13	4.93	10.42	14.0	
Sn	0.61	0.76	1.34		

1028-3358/02/4705-0341$22.00

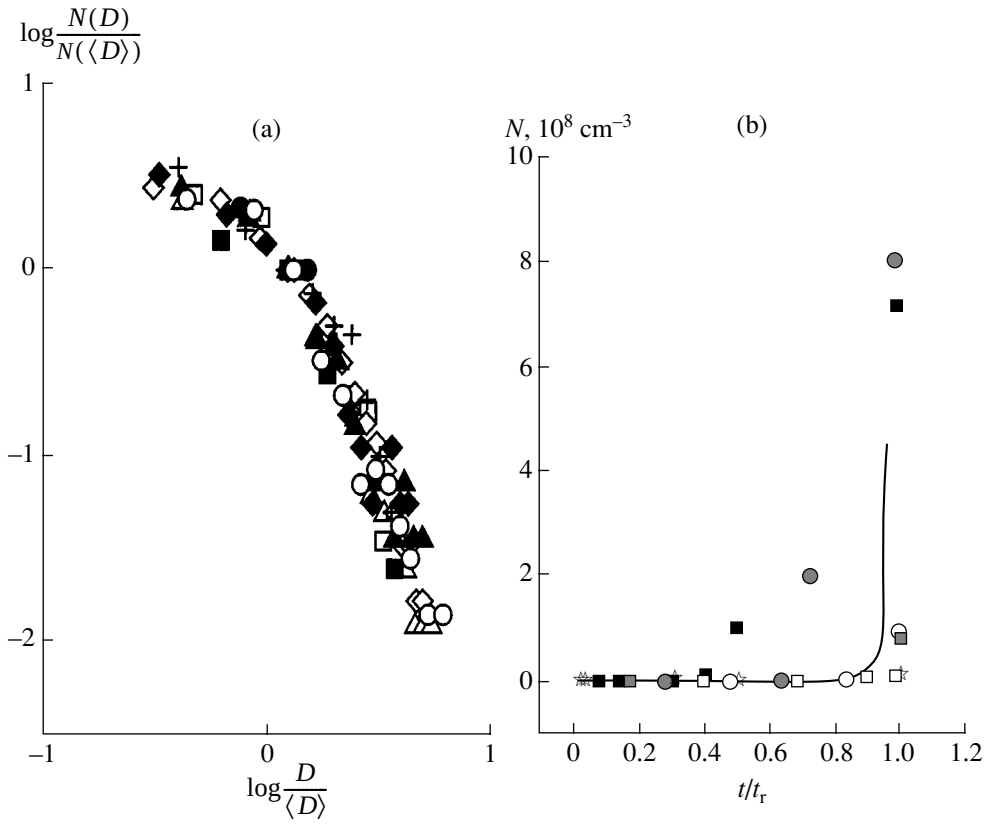

Fig. 1. (a) Size distribution of failure centers in Fe samples with a thickness $\Delta = 4 \times 10^{-4}$ m (closed symbols) and Cu samples with a thickness $\Delta = 10^{-3}$ m in metallographic sections parallel to the failure surface [$\delta_\bullet(\delta_\circ) > \delta_\blacksquare(\delta_\square) > \delta_\blacktriangle(\delta_\triangle) > \delta_\blacklozenge(\delta_\diamond) > \delta_+$ (Here, δ is the depth measured from the failure surface.)]. (b) Accumulation rate of failure centers (mathematical-simulation results and experimental data) for various metals at the longevity scale t_r: (■) Pbσ_1, $\Delta = 3 \times 10^{-4}$ m; (□) Pbσ_2, $\Delta = 4 \times 10^{-4}$ m; (●) Cuσ_1, $\Delta = 2 \times 10^{-4}$ m; (○) Cuσ_2, $\Delta = 4 \times 10^{-4}$ m, (☆) Cu; $\Delta = 5 \times 10^{-5}$ m; (■) Pb, $\Delta = 2.3 \times 10^{-4}$ m ($\sigma_1 > \sigma_2$); and (curve) results of calculations by Eq. (1).

has the form $N(D) \sim D^{-\alpha}$, where D is the failure-center size and $\alpha > 1$ (Fig. 1). The accumulation rate of failure centers can be described by an evolutionary equation of the form (Fig. 1)

$$\frac{dN}{dt} \sim N^{\beta}, \quad \beta > 1. \tag{1}$$

The data displayed in Fig. 1 show the correlated behavior and the onset of self-organization of a cascade of failure centers in the scale of a sample undergoing failure. The results of fractographic studies have shown that the violation of continuity and the presence of failure centers is observed only in the loading zone of a sample.

The use of interactive image analysis systems made it possible to reveal the appearance of plastic-flow zones as in the case of turbulence, even at low initial temperatures ($T \sim 4$ K). The appearance of these zones results in loss of the long-range order of the crystal lattice in the vicinity of failure centers that form and grow. We imply micro- and mesolevels of the deformation structure (Fig. 2).

Zones of crystal-lattice flow in the vicinity of an individual failure center separated from a neighboring center by a distance exceeding the size of the failure center itself are structured. This process occurs in such a manner that the tangents drawn to the boundaries of both the failure centers and slip bands, which relate to the same radius vector, are nearly parallel (Fig. 2). In the state preceding rupture, the average size of the failure centers reaches a few percent of the sample thickness. The zones of crystal-lattice flow (instability zones) in the vicinity of failure centers spaced by distances on the order of their size have no preferential directions. Here, the crystal lattice loses its long-range order. These zones determine the correlated behavior of a cascade of failure centers near the percolation threshold.

In percolation theory, there is a method that makes it possible to quantitatively describe the phase connectedness, including the connectedness of failure centers arising in the process of dynamic failure (in the case of a many-center failure). We analyzed the problem of spheres, i.e., a spherical region that exists around failure centers in which plastic-flow fields affect the pro-

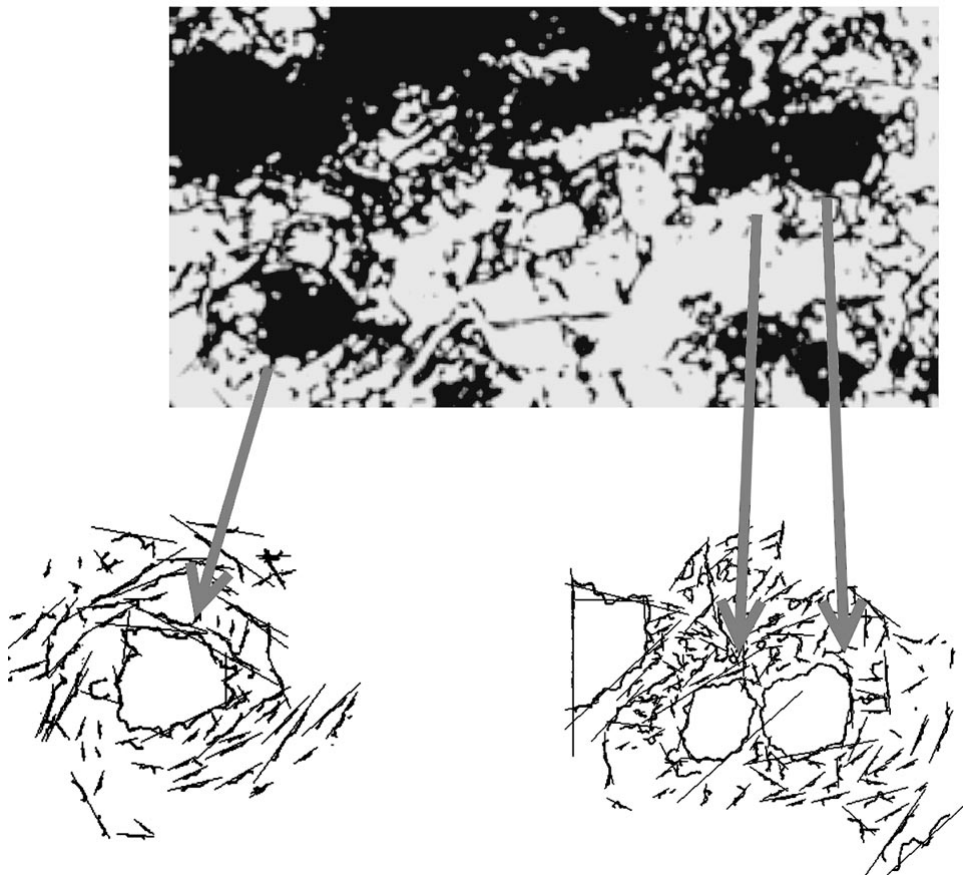

Fig. 2. Structuring of crystal-lattice slip bands in the vicinity of growing failure centers and tangents to the slip bands.

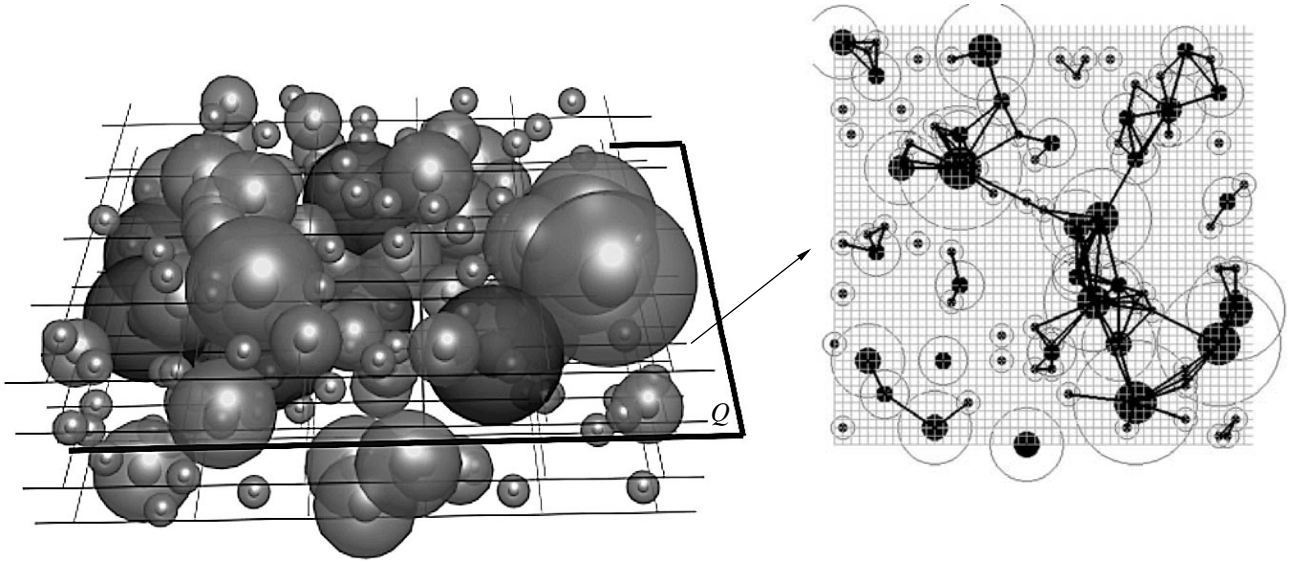

Fig. 3. Failure-center percolation cluster obtained with the help of a random-number generator with allowance for the $N(D) \sim D^{-\alpha}$ distribution law and the rate $N(t)$ of failure-center accumulation. The pattern is a computer version of a percolation metallographic section obtained by cutting the volume cluster by a Q plane. Solid lines show the appearance of connectedness between neighboring failure centers. The broken line intersecting the entire section shows the appearance of an infinite cluster changing the connectedness of the sample. Closed circles represent failure centers of the crystal lattice. The circles around the failure centers bound the zones with plastic-flow fields affecting the failure centers.

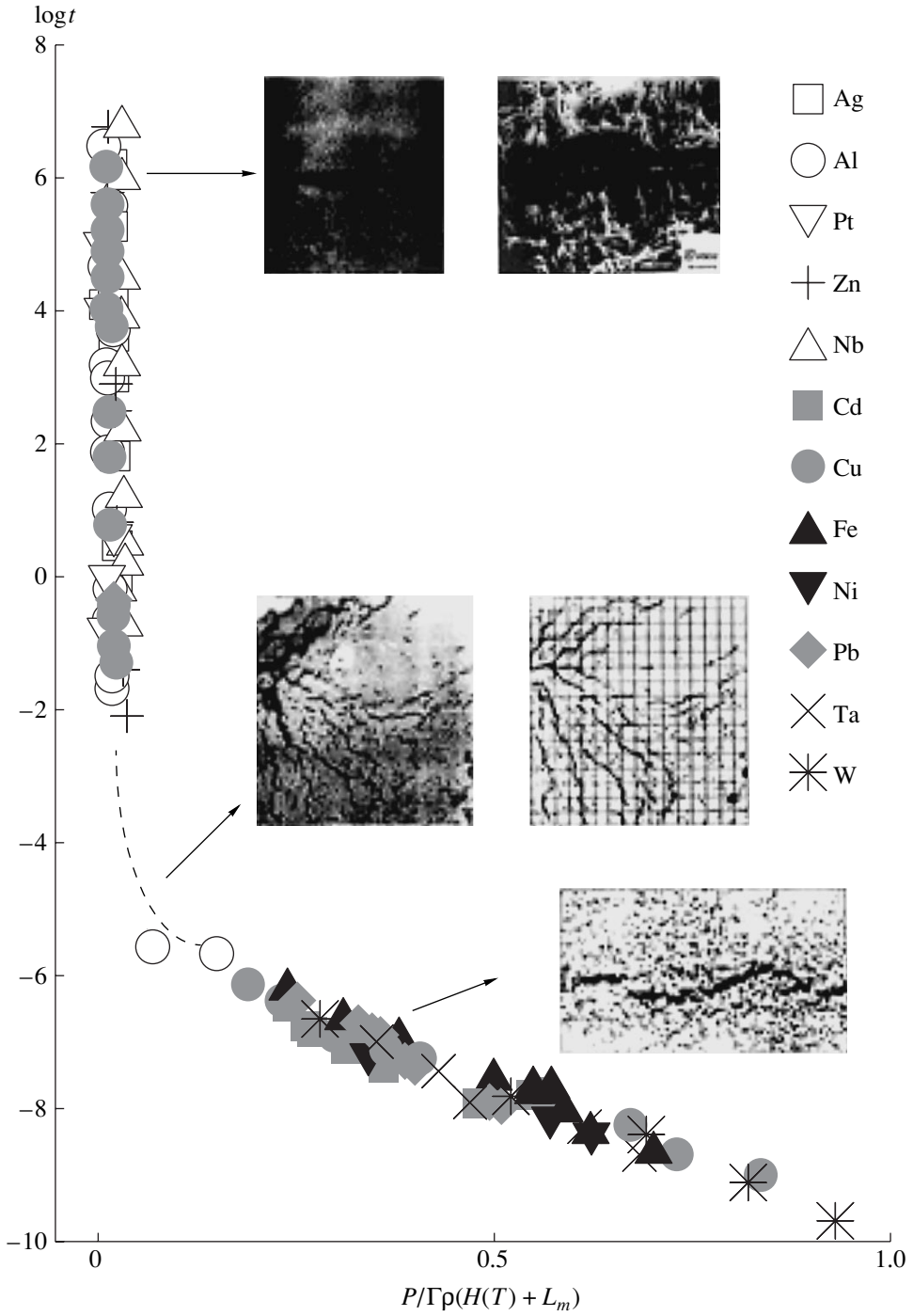

Fig. 4. Longevity for various metals in terms of the universal coordinates. The data for $\rho(T, P)$, $H(T)$, $\Gamma(T, P)$, and $\rho(T, P)$, $H(T)$, $\Gamma(T, P)$, L_m are taken from tables. The data for $E = P/\Gamma\rho$ are measured in this study. Here, H is the enthalpy, Γ is the Grüneisen parameter, and ρ is the material density.

cess of dynamic failure. For a sphere of radius R, taking into account the data of fractographic analysis, we can derive the expression

$$N^{-1/3} \simeq 1.2R \qquad (2)$$

(N is the density of the failure centers). This expression enables us to estimate the passage from microfracture to macrofracture both qualitatively and quantitatively. Figure 3 shows the computer version of a percolation metallographic section for a cascade of failure centers. According to expression (2), the failure process is controlled at its final stage by the concentration criterion [1] for all linear size scales under consideration. It was

demonstrated that, at the final stage, the cascade of failure centers is a percolation cluster. In this case, a connectedness of the failure-center system arises. Figure 3 presents the results of a mathematical simulation of the volume of a failure-center percolation cluster. The computer version of a metallographic section obtained by cutting the percolation-cluster volume by the plane Q is also presented.

According to the structural and energy analogy in the behavior of metal when thermal and mechanical energy are delivered, in either case, violation of the long-range crystal lattice takes place. With allowance for this fact, we present data on longevity for a set of metals in terms of universal coordinates (Fig. 4). On the basis of data taken from the literature, we can conclude that, in the quasistatic longevity range, regions of plastic flow of the crystal lattice also appear in the mouth of a growing crack. The universal coordinates make it possible to determine the time dependence for ratios of the critical density of the absorbed energy (which leads to failure) to the energy parameters of the crystal lattice (enthalpy H and melting heat L_m). The data in Fig. 4 present the absolute values of the dissipative energy loss of an unloading wave by failure in the dynamic range. These data are close to the unified curve and determine the boundary. The failure region lies above this boundary. The inserts in Fig. 4 show a change in the failure mechanism from a single-center to a many-center failure. Systematized data are presented for pure metals in the quasistatic range [8].

The generalized approach (including micro-, meso-, and macrolevels of failure) to investigating the dynamic-failure process made it possible to reveal the universal attributes of the evolution of arising structures. These attributes can be considered as a manifestation of self-similarity in the behavior of metals under pulsed loading. Here, the universality is a consequence of the space–time self-organization in ensembles of failure centers within a size range exceeding four orders of magnitude. This fact testifies to the absence of any specific length scale within the range under consideration, which is associated with the physics of formation of a cascade of failure centers.

Taking into account the self-similarity of the process of accumulating damage capability in the dynamic longevity range, we can obtain the relation between the critical energy density and the longevity, namely, $E^{\gamma}t = \text{const}$ [1, 5, 6], where $\gamma \sim 3.8$. The resulting expression specifies the amplitude–time coordinate irrespective of the method of loading and geometry. Hence, we can impose certain conditions on a nonhomogeneous wave equation that describes the motion of an elastoplastic continuum. The self-consistency in the calculation of the amplitude $P(x, t)$ $[E(x, t)]$ at each point of the coordinate axis makes it possible to describe the wave motion of the medium and the accumulation of the damage capability for various profiles of the absorbed energy. Thereby, the absolute value of the dissipative energy loss in the one-dimensional case (amplitude–time dependence) is established. Its computational and theoretical justification in two- and three-dimensional cases allows us to describe the dynamic-failure process for various geometries of the system under study and to predict the behavior of unexplored materials.

It should also be noted that the data presented in Fig. 4 can be used in computer-aided design of resistant materials for specific operating conditions (e.g., when choosing a material for the screen of an output window of a pulsed relativistic-electron accelerator, etc.).

Thus, we have demonstrated that, in the dynamic longevity range, the thermodynamic potential (enthalpy) is a parameter that controls the dynamic-failure process. The ratio of the absorbed-energy density to the energy parameters of the crystal lattice (enthalpy and phase-transition heat) is an invariant of the behavior of a metal with respect to external actions.

At pulsed-pressure amplitudes $P \sim 1$–30 GPa and in the longevity range $t \sim 10^{-6}$–10^{-10} s, the evolution of micro- and mesoscopic defects in the phenomenon of dynamic failure is a defining feature in the invariant behavior of metals under a thermal shock.

REFERENCES

1. E. K. Bonyushkin, N. I. Zavada, S. A. Novikov, and A. Ya. Uchaev, *Kinetics of Dynamic Failure of Metals in the Mode of Pulse Volumetric Heating* (Sarov, 1998).
2. A. Ya. Uchaev, S. A. Novikov, V. A. Tsukerman, *et al.*, Dokl. Akad. Nauk SSSR **310**, 611 (1990) [Sov. Phys. Dokl. **35**, 91 (1990)].
3. A. I. Pavlovskiĭ, E. K. Bonyushkin, A. Ya. Uchaev, *et al.*, Dokl. Akad. Nauk SSSR **317**, 1376 (1991) [Sov. Phys. Dokl. **36**, 326 (1991)].
4. E. K. Bonyushkin, B. L. Glushak, N. I. Zavada, *et al.*, Prikl. Mekh. Tekh. Fiz., No. 6, 105 (1996).
5. E. K. Bonyushkin, N. I. Zavada, S. A. Novikov, *et al.*, in *High Energy Density* (Vseross. Fiz. Yadernyĭ Tsentr–Vseross. Nauchn. Issled. Inst. Énerg. Fiz., Sarov, 1997), pp. 368–383.
6. E. K. Bonyushkin, N. I. Zavada, S. A. Novikov, *et al.*, *Fractals in Applied Physics* (Russian Federal Nuclear Center, All-Russia Scientific Research Institute of Experimental Physics (RFNC–VNIIEF), Sarov, 1995), pp. 123–174.
7. E. K. Bonyushkin, N. I. Zavada, S. A. Novikov, and A. Ya. Uchaev, *Applied Problems in Strength and Plasticity* (Moscow, 1999), pp. 25–37.
8. V. R. Regel', A. I. Slutsker, and E. E. Tomashevskiĭ, *Kinetic Nature of Strength in Solids* (Nauka, Moscow, 1974).

Translated by T. Syromyatnikova

Doklady Physics, Vol. 47, No. 5, 2002, pp. 346–352. Translated from Doklady Akademii Nauk, Vol. 384, No. 3, 2002, pp. 334–340.

PHYSICS

Refinement of the Crystal Structure of $K_2Zn_2V_{10}O_{28} \cdot 16H_2O$

O. V. Yakubovich, E. N. Anan'eva, O. V. Dimitrova, and Corresponding Member of the RAS V. S. Urusov

Received December 21, 2001

Orange crystals of the $Ca_3V_{10}O_{28} \cdot 16H_2O$ pascoite mineral and the $K_2Mg_2V_{10}O_{28} \cdot 16H_2O$ hummerite mineral were found in the vanadium-containing uranium ores of the Colorado plateau [1]. Later on, synthetic analogs of these minerals were obtained and then described by a general formula $A_2M_2V_{10}O_{28} \cdot nH_2O$, where A = K, Cs, NH_4, or Rb and M = Mg, Zn, Mn, or Co. A distinctive structural feature of these compounds is the presence of the $(V_{10}O_{18})^{6-}$ decavanadate complex in their structure.

The decavanadate ion is formed when V_2O_5 vanadium oxide is placed in an acid solution with pH ranging from 2 to 6 [2]. The divanadate ion V_2O_5 is polymerized in the solution and forms the $V_{10}O_{28}$ molecular group. The structure of the $V_{10}O_{28}$ complex is formed by ten VO_6 octahedrons linked by common edges into a ten-nuclear octahedral cluster (Fig. 1). The ideal symmetry of the $V_{10}O_{28}$ decavanadate ion is *mmm*.

In the crystal structures of the group of compounds under consideration, the decavanadate complexes combine with M-octahedrons and A-ten-vertex polyhedrons, forming layers parallel to the *ab* plane. Water molecules are situated in the interlayer space.

The crystal structures of pascoite and hummerite minerals differ in the number and character of coordination of cations linking $(V_{10}O_{28})^{6-}$ cluster anionic groups into a unified configuration. In a $Ca_3V_{10}O_{28} \cdot 16H_2O$ pascoite unit cell [3], two calcium atoms are in seven-vortex polyhedrons formed by two oxygen atoms of a decavanadate group and five water molecules. The distorted octahedron around the third calcium atom is formed by water molecules. In the structure of $K_2Mg_2V_{10}O_{28} \cdot 16H_2O$ hummerite [4], magnesium ions are located in octahedrons composed of water molecules. Of the ten oxygen atoms participating in the coordination of potassium atoms, five atoms belong to three neighboring decavanadate ions and the other five belong to water molecules.

The crystal structure of the synthetic $K_2Zn_2V_{10}O_{28} \cdot 16H_2O$ compound representing a zinc analog of the hummerite mineral was recognized on the basis of experimental data obtained by X-ray photography [2]. In this paper, we present results on refining the structure of this phase. This refinement is aimed at both the localization of hydrogen atoms and analysis of the features of hydrogen bonds.

Semitransparent crystals of a prismatic habitus and orange color were prepared by a conventional method of hydrothermal synthesis [5] in a $ZnO–V_2O_5–KF–K_3PO_4–H_2O$ system at a temperature T = 250°C and pressure P = 100 atm. The mass ratios of the components were

$$ZnO : V_2O_5 : KF : K_3PO_4 = 2 : 2 : 1 : 1.$$

The dependence of the degree of vanadate-ion polymerization on the pH in a solution is well known. For example, in alkaline solutions, colorless orthovanadates, pyrovanadates, and methavanadates crystallize at pH > 12.6, pH from 12.6 to 9.6, and pH from 9.6 to 6.5,

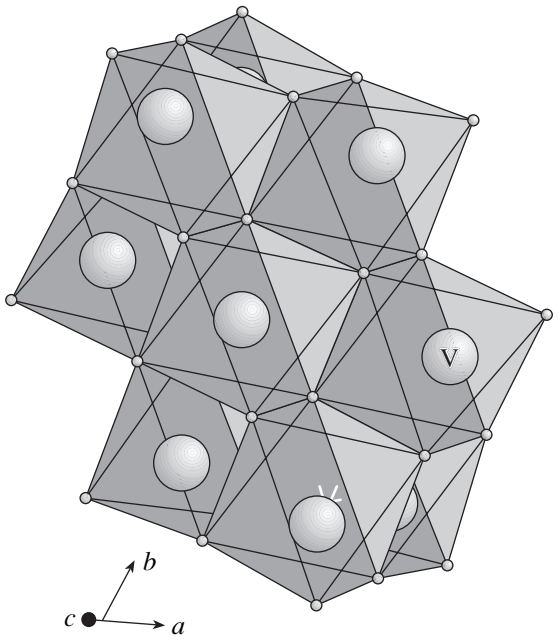

Fig. 1. $V_{10}O_{28}$ ten-nuclear octahedral cluster.

Moscow State University, Vorob'evy gory, Moscow, 119899 Russia

1028-3358/02/4705-0346$22.00

Table 1. Crystallographic characteristics, experimental data, and refinement of the structure

Crystallographic characteristics	
Formula	$K_2Zn_2V_{10}O_{28} \cdot 16H_2O$
Absorption μ, mm^{-1}	4.16
Space group	*P* 1*bar*
Number of formula units *Z*	1
Parameters of the unit cell	
a, Å; α	10.802(2); 104.83(3)°
b, Å; β	11.157(2); 109.43(3)°
c, Å; γ	8.770(2); 64.99(3)°
Volume, $Å^3$	895.0(3)
Density ρ, g/cm^3	2.697
Experimental data	
Diffractometer	SYNTEX $P\bar{1}$
Radiation	MoK_α (graphite monochromator)
Temperature, K	293
Survey region θ_{max}	30.0°
Index constraints	$-15 \le h \le 14$, $-15 \le k \le 15$, $0 \le l \le 12$
Data for structure refinement	
Number of reflections: independent/observed with $I > 1.96\sigma(I)$	3608/3275
Refinement method	According to F^2
Number of refined parameters	327
Correction for absorption	(semiempirical over equivalents)
T_{max}, T_{min}	1.000, 0.742
Extinction coefficient	0.0004(3)
Uncertain factors	
R (for the observed reflections)	0.039
wR_2 (for all independent reflections)	0.094
s	1.110
Residual electron density, $e/Å^3$	
ρ_{max}, ρ_{min}	0.58, –0.58

respectively. In acid solutions, typical orange polyvanadates and light yellow pervanadates are crystallized at pH ranging from 6.5 to 2.0 and pH < 0.8. It is shown [2] that three types of $(V_{10}O_{28})^{6-}$, $(HV_{10}O_{28})^{5-}$, and $(H_2V_{10}O_{28})^{4-}$ complex ions are present in the orange solution (pH from 2.0 to 6.5), decavanadate ions being the prevailing component in the solution. Qualitative X-ray spectral analysis based on a CamScan 4DV device showed the presence of K, Zn, and V atoms in the crystal compositions we obtained. These data, the orange color of the crystals, and their synthesis in an acid solution admitted the possibility of the participation of $(V_{10}O_{28})^{6-}$ decavanadate ions in forming the structure of the compound we obtained.

The parameters of the unit cell and triclinic crystal symmetry were determined by the photographic method with a rotating-crystal X-ray camera and refined while investigating a crystal with average linear dimensions of ~0.1 mm by means of a SYNTEX P-1 four-circle diffractometer. These parameters turned out to be *a* = 10.802(2), *b* = 11.157(2), *c* = 8.770(2) Å, α = 104.83(3)°, β = 109.43(3)°, and γ = 64.99(3)°. Taking into account the elemental composition of the given phase and based on the data obtained for both the metric of the unit cell and crystal symmetry, we identified the crystal with the $K_2Zn_2V_{10}O_{28} \cdot 16H_2O$ water potassium and zinc decavanadate.

We obtained the experimental material needed to refine the structure of this crystal by the 2θ : θ scanning method and with the same diffractometer using Mo-K_α radiation. The recorded reflection intensities were corrected with allowance for the Lorentz factor and the

Table 2. Coordinates of basis atoms and equivalent temperature parameters

Atom	*x*	*y*	*z*	U_{eq}, Å^2
V1	−0.00274(9)	0.47729(8)	0.67734(10)	0.0170(2)
V2	0.28103(9)	0.44692(8)	0.61576(10)	0.0188(2)
V3	0.94915(9)	0.27565(8)	0.35303(10)	0.0183(2)
V4	0.23696(9)	0.24458(9)	0.30811(11)	0.0207(2)
V5	0.22779(9)	0.19733(8)	0.63439(11)	0.0210(2)
Zn	0.77078(7)	0.20981(6)	0.77442(8)	0.0236(2)
K	0.5831(1)	0.2258(1)	0.3146(2)	0.0352(3)
O1	0.3052(4)	0.1288(3)	0.4583(4)	0.0219(7)
O2	0.1002(3)	0.3785(3)	0.4855(4)	0.0171(7)
O3	0.8573(3)	0.4101(3)	0.5240(4)	0.0162(6)
O4	0.0976(4)	0.3368(3)	0.7682(4)	0.0211(7)
O5	0.8617(3)	0.4469(3)	0.2593(4)	0.0179(7)
O6	0.3428(4)	0.3452(3)	0.4366(4)	0.0211(7)
O7	0.3976(4)	0.5133(4)	0.7059(5)	0.0272(8)
O8	0.3387(4)	0.3026(3)	0.7217(4)	0.0216(7)
O9	0.0624(4)	0.1634(3)	0.5087(4)	0.0208(7)
O10	0.8267(4)	0.2173(4)	0.2602(4)	0.0259(8)
O11	0.0690(4)	0.2045(3)	0.2216(4)	0.0211(7)
O12	0.6917(4)	0.9225(4)	0.2572(5)	0.0303(9)
O13	0.1087(4)	0.4158(3)	0.2028(4)	0.0205(7)
O14	0.3233(4)	0.1610(4)	0.1727(5)	0.0309(9)
O15 (H_2O)	0.3233(5)	0.6322(4)	0.3650(5)	0.0304(9)
O16 (H_2O)	0.6534(5)	0.3356(5)	0.9410(6)	0.0363(10)
O17 (H_2O)	0.1276(5)	0.8986(4)	0.4076(6)	0.0356(10)
O18 (H_2O)	0.3941(4)	0.8564(4)	0.3734(5)	0.0290(9)
O19 (H_2O)	0.0597(6)	0.7330(6)	0.0977(6)	0.0499(14)
O20 (H_2O)	0.1559(5)	0.9398(4)	0.0817(5)	0.0339(10)
O21 (H_2O)	0.3459(6)	0.4093(5)	0.0702(6)	0.0452(12)
O22 (H_2O)	0.4179(7)	0.8878(7)	0.0055(7)	0.0498(13)
H1	0.472(7)	0.824(6)	0.366(7)	0.02(2)
H2	0.033(7)	0.744(7)	0.011(9)	0.03(2)
H3	0.384(6)	0.928(6)	0.397(7)	0.03(2)
H4	0.272(7)	0.613(6)	0.397(8)	0.02(2)
H5	0.093(7)	0.978(7)	0.424(8)	0.05(2)
H6	0.677(9)	0.311(9)	0.023(11)	0.04(3)
H7	0.051(7)	0.886(7)	0.395(8)	0.03(2)
H8	0.004(7)	0.722(7)	0.138(8)	0.05(2)
H9	0.118(8)	0.014(7)	0.106(9)	0.04(2)
H10	0.221(8)	0.930(7)	0.046(9)	0.06(2)
H11	0.345(8)	0.389(8)	−0.007(10)	0.08(3)
H12	0.281(9)	0.409(8)	0.089(10)	0.03(3)
H13	0.401(12)	0.958(12)	0.019(13)	0.08(5)
H14	0.639(9)	0.414(9)	0.963(11)	0.11(3)
H15	0.368(7)	0.566(7)	0.320(8)	0.05(2)
H16	0.487(12)	0.866(11)	0.064(14)	0.16(5)

Note: For hydrogen atoms, the values of isotropic temperature factors are given.

Table 3. Interatomic distances, Å

V1-octahedron		V2-octahedron		V3-octahedron		V4-octahedron	
V1–O13	1.686(3)	V2–O7	1.608(4)	V3–O10	1.605(4)	V4–O14	1.608(4)
O4	1.701(3)	O6	1.830(4)	O11	1.814(3)	O1	1.835(4)
O5	1.905(3)	O8	1.838(4)	O9	1.843(4)	O6	1.849(4)
O3	1.936(3)	O5	1.974(3)	O5	1.995(3)	O11	1.915(4)
O2	2.117(3)	O3	2.012(3)	O3	2.016(3)	O13	2.058(4)
O2	2.131(3)	O2	2.243(3)	O2	2.229(3)	O2	2.304(3)
Average	1.913	Average	1.918	Average	1.917	Average	1.928
V5-octahedron		Zn-octahedron		K-ten-vertex polyhedron			
V5–O12	1.602(4)	Zn–O17	2.066(4)	K–O22	2.767(5)		
O1	1.839(4)	O19	2.066(5)	O10	2.786(4)		
O8	1.876(4)	O20	2.074(4)	O6	2.802(4)		
O9	1.897(4)	O16	2.096(4)	O15	2.936(5)		
O4	2.022(4)	O15	2.097(4)	O14	2.979(4)		
O2	2.342(3)	O18	2.119(4)	O18	3.006(5)		
Average	1.930	Average	2.086	O12	3.040(4)		
				O7	3.060(4)		
				O21	3.084(6)		
				O17	3.260(6)		
				Average	2.972		

Table 4. Geometrical characteristics of hydrogen bonds

D–H···*A*	*d*(*D*–H), Å	*d*(H···*A*), Å	Angle *DHA*, degrees	*d*(*D*–*A*), Å
O18–H1···O8	0.78(8)	2.19(8)	162(6)	2.947(6)
O18–H1···O6		2.60(6)	118(5)	3.045(6)
O18–H1···O1		2.58(8)	131(5)	3.145(7)
O19–H2···O11	0.74(7)	2.07(7)	171(8)	2.802(6)
O18–H3···O1	0.74(6)	2.03(6)	164(8)	2.750(5)
O15–H4···O3	0.82(8)	1.88(8)	173(7)	2.692(7)
O17–H5···O9	0.80(7)	1.93(7)	163(8)	2.707(5)
O16–H6···O10	0.77(9)	2.33(9)	161(12)	3.066(6)
O17–H7···O9	0.86(9)	2.01(8)	148(6)	2.774(7)
O19–H8···O4	0.85(9)	1.96(9)	170(7)	2.793(8)
O20–H9···O11	0.76(8)	2.03(8)	164(9)	2.770(5)
O21–H10···O22	0.82(9)	2.11(10)	167(7)	2.909(10)
O21–H11···O8	0.65(8)	2.32(8)	175(10)	2.970(6)
O21–H12···O13	0.78(11)	2.35(10)	169(8)	3.115(8)
O22–H13···O14	0.71(12)	2.29(12)	150(12)	2.926(8)
O16–H14···O21	0.81(10)	2.14(11)	152(10)	2.877(8)
O15–H15···O7	0.78(7)	2.37(8)	132(7)	2.951(7)
O15–H15···O21		2.44(7)	141(7)	3.090(6)
O22–H16···O12	0.73(12)	2.51(12)	148(12)	3.155(9)

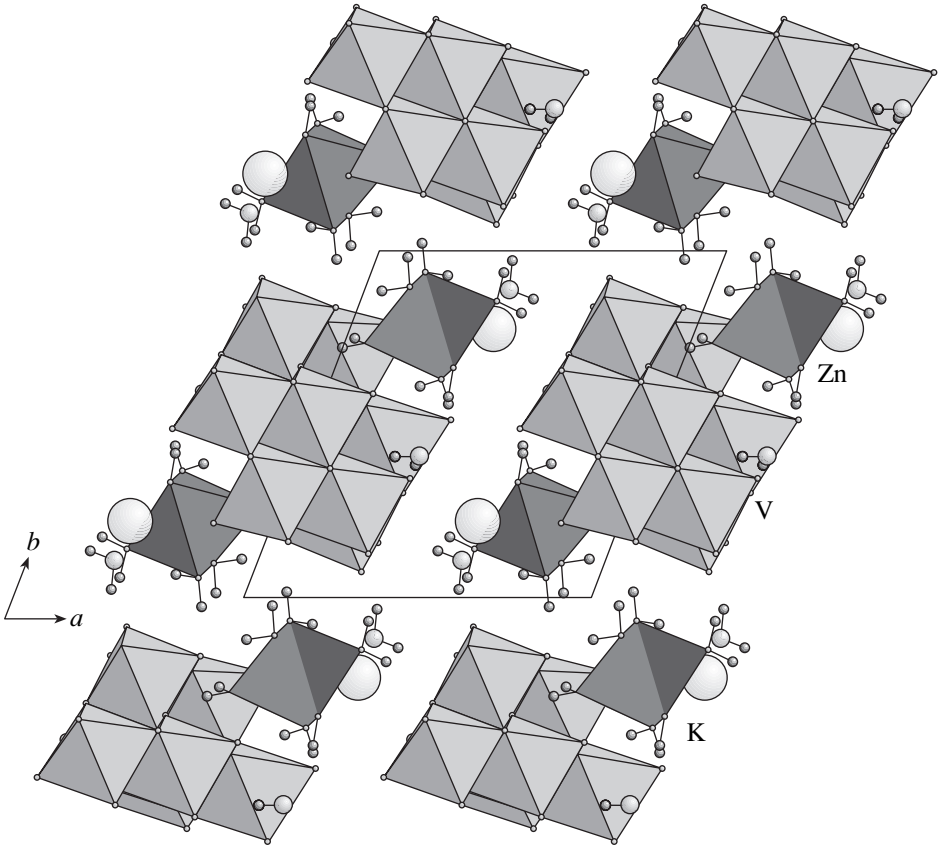

Fig. 2. Crystalline structure of $K_2Zn_2V_{10}O_{28} \cdot 16H_2O$ in the *ab* projection. Potassium (K) atoms are shown as spheres.

polarization effect. The crystallographic characteristics of Zn-vanadate, data of the X-ray experiment, and parameters of the crystal-structure refinement are presented in Table 1.

All calculations were carried out using the SNELXL software package [6]. Curves of atomic scattering and corrections for anomalous dispersion, which had been taken from [7], were used. The structure was refined in a full-matrix anisotropic approximation with due regard for absorption and secondary isotropic extinction. The positions of 16 independent hydrogen atoms were localized on the basis of a difference synthesis of the electron density and then refined in the isotropic approximation. The coordinates of basis atoms with equivalent temperature parameters and interatomic distances are given in Tables 2 and 3, respectively. The geometric characteristics of hydrogen bonds are listed in Table 4.

Zinc atoms form isolated $[Zn(H_2O)_6]^{2+}$ octahedral complexes in the crystal structure. The Zn–O interatomic distances in the octahedron vary from 2.066 to 2.119 Å. These distances are regularly longer than the corresponding values in the Mg octahedron for the $K_2Mg_2V_{10}O_{28} \cdot 16H_2O$ isostructural hummerite, in which they lie within the range from 2.052 to 2.100 Å. The coordination potassium polyhedron is an irregular ten-vortex polyhedron in which interatomic distances are within the range 2.767–3.260 Å.

Five crystallographically independent vanadium atoms form a ten-nuclear decavanadate cluster. V-octahedrons linked by their edges are strongly distorted, and, in this case, two types of V-octahedron distortion can be distinguished in the structure. Two shortened bonds, namely, V1–O13 = 1.686 Å and V1–O4 = 1.701 Å in the V1O6 octahedron (with an angle of 107.49(2)° between them), against the background of the other four V–O distances lying within the range 1.905–2.131 Å testify to a tendency of vanadium to the VO_2 configuration. This configuration is characteristic of some vanadium-containing compounds (e.g., KVO_3 and $KVO_3 \cdot H_2O$) [2]. VO vanadyl ions can be separated, since they are connected to the other four independent vanadium atoms. Thus, in the octahedral complexes around V2, V3, V4, and V5 atoms, we can isolate one shortened (1.602–1.608 Å) and one elongated (2.229–2.342 Å) V–O bond and vanadium polyhedrons can be interpreted as distorted pseudotetragonal bipyramides.

$V_{10}O_{28}$ decavanadate clusters and $Zn(H_2O)_6$ octahedrons in the crystal structure are combined with each other by hydrogen bonds and form layers parallel to the *ab* plane. Potassium atoms are situated in the same layers alternating with decavanadate groups along the *a*

Table 5. Local balance of valences

Atom	V1	V2	V3	V4	V5	Zn	K	H1	H2	H3	H4	H5	H6
O1				0.92	0.91			0.02		0.20			
O2	0.43	0.30	0.34	0.26	0.23								
	0.41												
O3	0.70	0.57	0.56								0.23		
O4	1.32				0.55								
O5	0.76	0.63	0.60										
O6		0.93		0.88			0.16	0.04					
O7		1.69					0.08						
O8		0.91			0.82			0.05					
O9			0.90		0.78							0.22	
O10			1.71				0.17						0.09
O11			0.97	0.74					0.17				
O12					1.72		0.09						
O13	1.37			0.50									
O14				1.69			0.10						
O15						0.35	0.11				0.77		
O16						0.35							0.91
O17						0.38	0.05					0.78	
O18						0.33	0.09	0.89		0.80			
O19						0.38			0.83				
O20						0.36							
O21							0.08						
O22							0.18						
ΣS_{ij}	4.99	5.03	5.08	4.99		2.15	0.11	1.00	1.00	1.00	1.00	1.00	1.00

Atom	H7	H8	H9	H10	H11	H12	H13	H14	H15	H16	ΣS_{ij}	$\lvert\delta\rvert$
O1											2.05	0.05
O2											1.97	0.03
O3											2.06	0.06
O4		0.18									2.05	0.05
O5											1.99	0.01
O6											2.01	0.01
O7									0.06		1.83	0.17
O8					0.11						1.89	0.11
O9	0.18										2.08	0.08
O10											1.97	0.07
O11			0.18								2.06	0.06
O12							0.13			0.07	2.01	0.01
O13						0.08					1.95	0.05
O14											1.79	0.21
O15									0.89		2.12	0.12
O16								0.86			2.12	0.12
O17	0.82										2.03	0.03
O18											2.11	0.11
O19		0.82									2.03	0.03
O20			0.82	0.87							2.05	0.05
O21					0.89	0.92		0.14	0.05		2.08	0.08
O22				0.13			0.87			0.93	2.11	0.11
ΣS_{ij}	1.00	1.00	1.00	1.00	1.00	1.00	1.00	1.00	1.00	1.00		

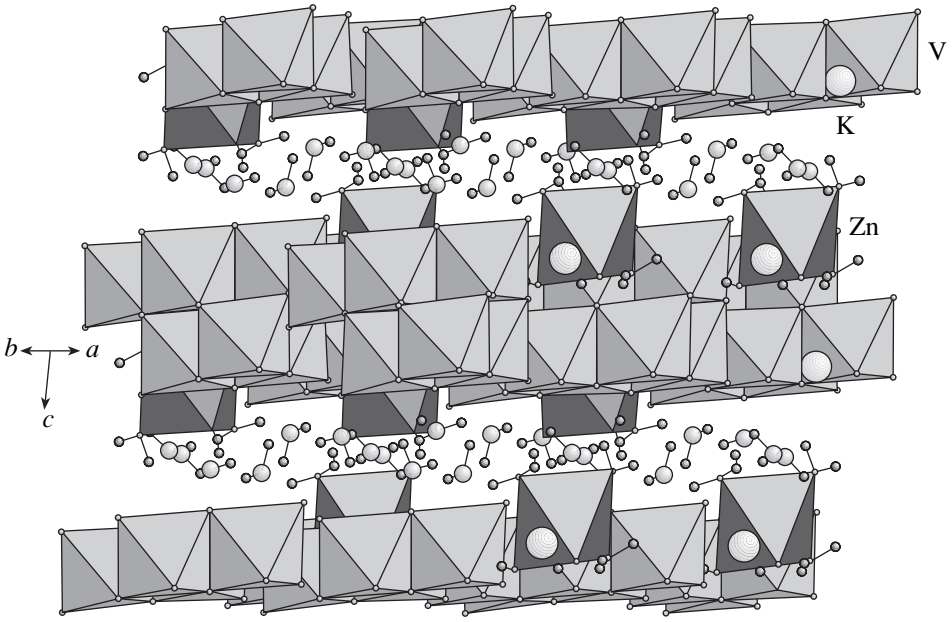

Fig. 3. K, V, and Zn layers in $K_2Zn_2V_{10}O_{28} \cdot 16H_2O$ structure linked along the *c* axis by water molecules in a common crystalline construction.

axis (Fig. 2). In the direction of the *c* axis, the layers are interleaved by water molecules (Fig. 3).

Eight independent water molecules in the structure play a different crystal-chemistry role. Six of them, O15–O20, coordinate Zn atoms. In this case, O15, O17, and O18 also participate in the coordination of potassium atoms. Two additional water molecules, O21 and O22, belong only to the potassium coordination sphere. O21 and O22 atoms not only function as donors (H_2O molecules) in the structure but also as acceptors for hydrogen bonds (Table 4).

Hydrogen bonds, which play an important role in stabilizing the given structure, as is usual for inorganic compounds, are asymmetric and significantly nonlinear. The system of hydrogen bonds is complicated by the presence of so-called bifurcation bonds acting in the structure between the water molecule containing O15 and two acceptors on one side and the water molecule containing O18 and three acceptors of hydrogen bonds on the other side (Table 4).

After the localization of 16 hydrogen atoms had been established, we managed to calculate the local valence balance [8] in the structure with consideration of the proton contribution [9] (Table 5). The criterion of the balance quality, which was calculated for oxygen atoms [10] and equaled 3.6%, shows the reliability of the obtained structural data. Employing the parameters and the function calculated in [10] yields close results with a balance quality criterion of 3.2%.

ACKNOWLEDGMENTS

This work was supported by the Russian Foundation for Basic Research, project nos. 00-05-64312 and 00-15-98582.

REFERENCES

1. H. T. Evans, M. E. Mrose, and R. Marvis, Am. Mineral. **40**, 314 (1955).
2. H. T. Evans, Inorg. Chem. **5**, 967 (1966).
3. A. G. Swallow, F. R. Ahmed, and W. H. Barnes, Acta Cryst. **21**, 397 (1966).
4. N. V. Avtamonova, V. K. Trunov, and L. G. Makarevich, Izv. Akad. Nauk SSSR, Ser. Neorg. Mater. **26**, 350 (1990).
5. A. A. Chernov, E. I. Givargizov, Kh. S. Bagdasarov, *et al.*, in *Modern Crystallography*, Ed. by B. K. Vainshtein, A. A. Chernov, and L. A. Shuvalov (Nauka, Moscow, 1980), Vol. 3.
6. G. M. Sheldrisk, *SHELXL97. Program for the Refinement of Crystal Structures from Diffraction Data* (Göttingen Univ., Göttingen, 1997).
7. *International Tables of Crystallography*, Ed. by I. T. Hahn (D. Riedel, Dordrecht, 1995).
8. V. S. Urusov and I. P. Orlov, Kristallografiya **44**, 736 (1999) [Crystallogr. Rep. **44**, 686 (1999)].
9. I. D. Brown, Acta Cryst. **32**, 24 (1976).
10. Yu. A. Pyatenko, Kristallografiya **17**, 773 (1972) [Sov. Phys. Crystallogr. **17**, 677 (1972)].

Translated by T. Galkina

Doklady Physics, Vol. 47, No. 5, 2002, pp. 353–355. Translated from Doklady Akademii Nauk, Vol. 384, No. 1, 2002, pp. 36–38.

TECHNICAL PHYSICS

Evolution of Nanostructural Ensembles in Boride–Nitride Films

R. A. Andrievski, G. V. Kalinnikov, A. E. Oblezov, and D. V. Shtansky

Presented by Academician A.G. Merzhanov, October 5, 2001

Received November 21, 2001

Thermal stability plays the principal role in the process of developing efficient nanostructural materials. Nonetheless, information on the influence of thermal effects on nanostructures is rather scarce, being limited to only a few studies (e.g., [1–5]). The evolution of nanostructural ensembles has been analyzed only for nitride films [3]. Therefore, it is of interest to study this evolution for boride–nitride nanostructural films, which have both a rather small crystallite size (about 1–2 nm) and high hardness (40–60 GPa [6]). Our preliminary results were reported in [7, 8].

Methods of preparing films by nonreactive magnetron sputtering were described previously in [9]. The temperature of silicon substrates and stainless-steel blades was held constant at about 150°C. The films were deposited by means of hot-pressed targets containing both separate compounds (TiB_2 and TiN) and their mixtures with mass ratios of 25/75, 50/50, and 75/25. The structure of the films deposited on the blades was analyzed with JEOL-200CX and JEM-3010 microscopes. Foils were prepared from the films by electrolytic dissolution of the blades with subsequent ion polishing. The grain-size distributions were obtained on the basis of dark-field electron-microscopy images at magnifications of 50 000–100 000 (JEOL-200CX) and 700 000 (JEM-3010) with the use of the Image-Pro Express 4.0 and Statistica computer programs. Crystallite clusters containing no less than 1000–2000 grains were used for each of the distributions. The measurements were performed for crystallite sizes exceeding 1 nm. According to the recommendations of [10], the minimum effective resolution achieved for dark-field images is about 1 nm.

The phase composition of the films was studied by X-ray phase analysis (XRPA) and microelectron diffraction structural analysis (MDSA). The hardness of films sputtered onto the silicon substrates was determined in the course of 7–10 measurements on a PMT-3 microhardness meter for loads of 0.2, 0.3, and 0.5 N. As before [6, 9], values of H_{V_0} related to the intrinsic hardness of the films were estimated by the method of [11]. This method excludes, to a sufficient degree, the effect of both film thickness and substrate type on measurement results. The method allows us, at least to a first approximation, to normalize the measured hardness values and to simplify their comparison. Information about the film composition according to data of Auger-electron spectroscopy is given in [6, 9]. Annealing was carried out in vacuum (10^{-4} Pa) at 700 and 1000°C for 15 min.

A typical dark-field electron-microscopy image and the results of data processing are presented in the figure and Table 1, respectively. All the films are characterized by a very fine nanostructure, with crystallite sizes that are minimum for films II and III and maximum for the TiN film (V). The sizable value of the root-mean-square error for the original films is evidence of rather broad grain-size distributions. The analysis of histograms has shown that these distributions are well described by the log-normal function. It is important that in the condi-

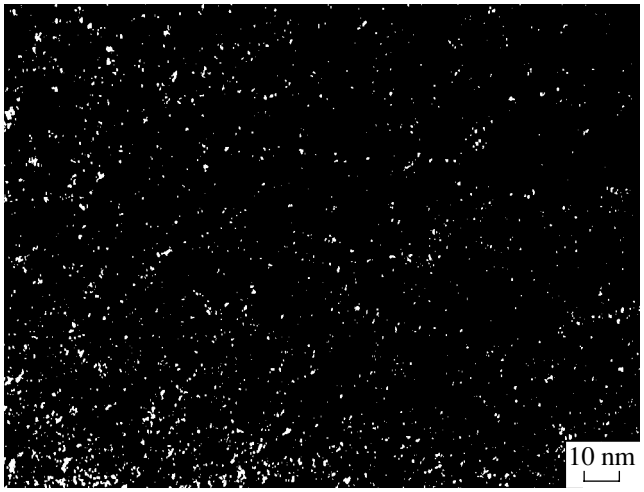

Dark-field electron-microscopy image (film III).

Institute for Problems of Chemical Physics, Russian Academy of Sciences, Chernogolovka, Moscow oblast, 142432 Russia
Moscow Institute of Steels and Alloys, Leninskiĭ pr. 4, Moscow, 119991 Russia

1028-3358/02/4705-0353$22.00 © 2002 MAIK “Nauka/Interperiodica”

Table 1. The average size (L) of crystallites in the original and annealed films (1–2 nm thick) deposited with the use of various targets

Target	Film	L, nm		
		Original films	T_{ann} = 700°C	T_{ann} = 1000°C
TiB_2	I	3–5 [9]	Unannealed	Unannealed
TiB_2 + 25%TiN	II	2.3 ± 1.1	4.4 ± 1.4	Unannealed
TiB_2 + 50%TiN	III	2.9 ± 1.1	3.7 ± 1.2	3.4 ± 1.9
TiB_2 + 75%TiN	IV	5.4 ± 4.0	8.1 ± 4.4	7.9 ± 3.8
TiN	V	9.9 ± 8.8	13.0 ± 6.6	10.2 ± 7.0

Table 2. Effect of annealing on the microhardness. H_V is the microhardness for a load of 0.3 N, and H_{V_0} is the intrinsic microhardness (GPa) estimated by the method of [11]

Film	Original films		T_{ann} = 700°C		T_{ann} = 1000°C	
	H_V	H_{V_0}	H_V	H_{V_0}	H_V	H_{V_0}
I	20 ± 1	41–46	20 ± 2	40–46	17 ± 2	35–39
II	20 ± 2	40–46	20 ± 1	40–45	16 ± 2	32–38
III	18 ± 2	46–52	19 ± 1	47–54	16 ± 1	38–45
IV	22 ± 2	53–59	22 ± 2	52–58	15 ± 3	32–42
V	16 ± 1	36–40	17 ± 1	38–42	15 ± 2	33–40

tions under consideration, the annealing slightly affects the average value of the crystallite size. The characteristics of original and annealed nanostructural ensembles are found to be virtually the same.

We should note that according to XRPA and MDSA data obtained before and after annealing, the films have an identical single-phase composition. Films I, II, and III–V have hexagonal (AlB_2-type) and cubic (NaCl-type) structures, respectively; i.e., decomposition of the supersaturated Ti(B, N) solid solutions does not occur.

Values of the microhardness for the original and annealed films are listed in Table 2. The range of H_{V_0} values allows for measurements with loads not only of 0.3 N but also of 0.1 and 0.5 N. As is seen, a temperature of 700°C, in fact, does not affect the microhardness value. However, after annealing at 1000°C, a certain decrease in the values of H_V and H_{V_0} is noticed. For films I–III and IV, this decrease reaches 15–20 and 30%, while for the coarsest grained film V, the decrease in hardness is quite insignificant (only about 4%). It is difficult to suggest a conclusive explanation for the results obtained or for differences in both the grain-size variations (Table 1) and microhardness (Table 2) after annealing at 1000°C. Most likely, this should be associated with different levels of residual stresses for films of different compositions and with possible features of the temperature dependences for the processes of recrystallization and relaxation of residual stresses. It is known that high values of film hardness are caused not only by a small grain size but also by the presence of significant residual compressive stresses (see, e.g., [4, 12]). We can certainly assume that relaxation of stresses at the interface between a high-melting compound (film) and silicon (substrate) occurs more intensely than recrystallization of the refractory compound in itself. As a result, we observe a certain reduction of the hardness in the case of a very minor change in grain sizes.

In the structures of films II and III, we should note the presence of a significant number of crystallites with a size of about 1 nm and smaller (Fig. 1, Table 1). The presence of these small crystallites in films was indicated previously in [4, 6, 13]. It is rather difficult to obtain perfect high-resolution images of such grains, since it is almost impossible to find small diffracting crystallites in the plane of the foil being studied. Nonetheless, one of the authors (D.V. Shtansky) has succeeded in finding them in (Ti, Al)(B, N) films: cubic particles 1.5–2 nm in size were distinctly identified with high resolution.

We recall that the period of a cubic crystal lattice, e.g., titanium nitride, is 0.424 nm (for the hexagonal TiB_2, $a \simeq 0.303$ nm and $c \simeq 0.323$ nm) [14]; i.e., there are only 8 or 27 unit cells in the TiN and TiB_2 crystallites with sizes of about 1 nm and even fewer in the crystallites with sizes of about 0.5 nm. Thus, in this

case, we, in fact, are dealing with cluster-consolidated materials. The fraction corresponding to the interface area is rather large in such objects. From simplest estimates (the fraction of the near-boundary regions is about $3s/L$, where s is the boundary width), it follows that for a grain size of ~2 nm and a reasonable boundary width of ~0.5 nm, this fraction can equal about 75%. The module design of such cluster-consolidated materials obviously needs more detailed analysis (see, e.g., [15]). However, it is important to note the necessity of thoroughly studying the properties of these objects in combination with a detailed structural certification. A fact of especial importance is that within the nanometer range, crystallite sizes are close to those of the de Broglie wavelengths for nitrides, borides, and carbides of transition metals. The properties of these metals resemble Bi-type semimetals. Therefore, in this case, we can expect the manifestation of dimensional quantum effects.

Thus, in the conditions under study of vacuum annealing (temperatures up to 1000°C, duration of 15 min), the structure and phase composition of boride–nitride films turned out to be rather stable, although their microhardness was reduced, on average, by about 4–30%. This fact is associated with a possible relaxation of compressive stresses. We also pay attention to the presence in the structure of certain films of a considerable number of crystallites with a size of ~1 nm and smaller. For such cluster-consolidated materials, we can expect the manifestation of dimensional quantum effects.

ACKNOWLEDGMENTS

This work was supported by the "Integratsiya" Federal Purposeful Program, project no. 855, and by the NATO Program "Science for Peace," project no. 973529.

REFERENCES

1. R. A. Andrievski, I. A. Anisimova, and V. P. Anisimov, Thin Solid Films **205**, 171 (1991).
2. H. Holleck and M. Lahres, Mater. Sci. Eng. **140**, 609 (1991).
3. R. A. Andrievski, I. A. Anisimova, V. P. Anisimov, *et al.*, Thin Solid Films **261**, 83 (1995).
4. D. V. Shtansky, E. A. Levashov, A. N. Sheveiko, and J. J. Moore, J. Mater. Synth. Process. **7**, 187 (1999).
5. S. Veprek, J. Vac. Sci. Technol. A **17**, 2401 (1999).
6. R. A. Andrievski, G. V. Kalinnikov, and D. V. Shtansky, Fiz. Tverd. Tela (St. Petersburg) **42**, 741 (2000) [Phys. Solid State **42**, 760 (2000)].
7. A. E. Oblezov, G. V. Kalinnikov, and R. A. Andrievski, in *Program and Abstracts of the NATO Advanced Study Institute "Functional Gradient Materials and Surface Layers Prepared by Fine Particles Technology," Kiev, Ukraine, 2000* (Kiev, 2000), Poster P-13, p. 66.
8. R. A. Andrievski, G. V. Kalinnikov, and A. E. Oblezov, in *Proc. Int. Conf. on Metall. Coat. and Thin Films, San Diego, USA, 2001* (San Diego, 2001), Report B3-1-11, p. 19.
9. R. A. Andrievski, G. V. Kalinnikov, N. P. Kobelev, *et al.*, Fiz. Tverd. Tela (St. Petersburg) **39**, 1859 (1997) [Phys. Solid State **39**, 1661 (1997)].
10. C. E. Krill, R. Haberkorn, and R. Birringer, in *Handbook of Nanostructured Materials and Nanotechnology* (Acad. Press, New York, 2000), Vol. 2, p. 155.
11. B. Jonsson and S. Hogmark, Thin Solid Films **114**, 257 (1984).
12. R. A. Andrievski, Usp. Khim. **66**, 57 (1997).
13. W. Gissler, Surface Coat. Technol. **68**, 556 (1994).
14. R. A. Andrievski and I. I. Spivak, *The Strength of Refractory Compounds and of Materials Based on Them* (Metallurgiya, Chelyabinsk, 1989).
15. N. A. Bul'enkov and D. A. Tytik, Izv. Akad. Nauk, Ser. Khim., No. 1, 1 (2000).

Translated by T. Galkina

Doklady Physics, Vol. 47, No. 5, 2002, pp. 356–359. Translated from Doklady Akademii Nauk, Vol. 384, No. 1, 2002, pp. 39–42.

TECHNICAL PHYSICS

Longitudinal Acoustic Wave in a Thin Fiber Immersed in the Bulk of a Low-Modulus Matrix

S. L. Bazhenov and Corresponding Member of the RAS A. A. Berlin

Received January 10, 2002

There exists a practical problem of determining the elastic modulus for rubbers deposited onto a glass fiber. In this connection, the problem of propagation of a longitudinal acoustic wave in a thin elastic fiber immersed in the bulk of a low-modulus elastic matrix is theoretically solved in this paper.

The basic parameters that determine the propagation velocity c_0 of a longitudinal acoustic wave in an elastic bar are its density ρ_0 and elastic modulus E [1]:

$$c_0 = \sqrt{\frac{E}{\rho_0}}. \quad (1)$$

The velocity of a longitudinal ultrasound wave in a bar in the shape of a thin elastic strip decreases if the bar is immersed in the bulk of a low-modulus matrix [2] or in a viscous liquid [3]. The decrease in the wave velocity is caused by the involvement in vibrations of a matrix (liquid) boundary layer that moves as an associated mass together with the strip.

The goal of the present paper is to solve the problem of the propagation of a longitudinal acoustic wave in a thin elastic bar in the shape of a fiber and immersed in the bulk of a low-modulus matrix.

We consider a longitudinal acoustic wave in an elastic cylindrical bar (fiber) immersed in the unbounded volume of a low-modulus matrix (Fig. 1). The presence of the matrix is taken into account by adding to the oscillatory equation a term describing the interaction of the fiber with the liquid [3, 4]:

$$\pi R^2 \rho_0 \frac{\partial^2 u}{\partial t^2} = \pi R^2 E \frac{\partial^2 u}{\partial y^2} + 2\pi R\tau. \quad (2)$$

Here, u is the fiber displacement from the equilibrium position, ρ_0 is the fiber density, R is the fiber radius, πR^2 is the cross-sectional area of the fiber, and E is the elastic modulus of the fiber. Furthermore, τ is the shear stress and y is the axis along which the longitudinal acoustic wave propagates.

Semenov Institute of Chemical Physics, Russian Academy of Sciences, ul. Kosygina 4, Moscow, 117977 Russia

In order to find stresses τ, we consider stimulated transverse shear vibrations of a matrix in contact with a fiber. The matrix motion in cylindrical coordinates is described by the equation

$$\rho \frac{\partial^2 u}{\partial t^2} = G\left(\frac{\partial^2 u}{\partial r^2} + \frac{1}{r}\frac{\partial u}{\partial r}\right), \quad (3)$$

where ρ is the matrix density, G is the matrix shear modulus, and r is the radial coordinate.

Let the bar execute longitudinal harmonic vibrations along its axis y with the angular frequency ω. We seek a periodic solution to Eq. (3) in the form

$$u(r, t) = s(r)\exp(i\omega t).$$

Replacing the variables

$$r = \sqrt{\frac{G}{\omega^2 \rho}}\, x = \frac{x}{k_\perp},$$

where $k_\perp = \sqrt{\frac{\omega^2 \rho}{G}}$, we reduce Eq. (3) to the Bessel equation of the zeroth order:

$$\frac{d^2 s}{\partial x^2} + \frac{1}{x}\frac{ds}{dx} + s = 0. \quad (4)$$

The general solution to this equation has the form $CJ_0(x) + BY_0(x)$, where C and B are constant and $J_0(x)$

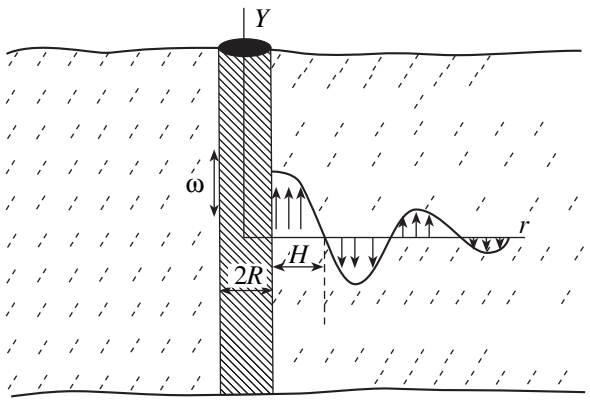

Fig. 1. Calculation scheme. Y is the fiber axis, R is the fiber radius, and ω is the angular frequency of the vibrations.

1028-3358/02/4705-0356$22.00

and $Y_0(x)$ are Bessel functions of the first and second kinds, respectively.

If the matrix was in the quiescent state at the initial moment, then a longitudinal wave in the fiber initiates the appearance of a divergent wave in it. The divergent cylindrical wave is described by the complex Hankel function of the second kind [5]

$$s = AH_0^{(2)}(x) = A[J_0(x) - iY_0(x)], \quad (5)$$

where A = const and $i = \sqrt{-1}$.

The stress with which the matrix acts on the fiber is $\tau = -G\frac{du}{dr}$ for $r = R$. Using the relationship $H_0^{(2)'}(x_0) = -H_1^{(2)}(x_0)$, where $H_1^{(2)}(x_0)$ is the first-order Hankel function [5, 7], we arrive at the relationship

$$\tau = AGk_\perp H_1^{(2)}(x_0)\exp(i\omega t). \quad (6)$$

Here, $x_0 = k_\perp R = \sqrt{\frac{\omega^2\rho}{G}}R$ is a dimensionless parameter characterizing the ratio of the fiber radius and the length of the transverse wave in the matrix.

The solution to Eq. (2) for longitudinal fiber vibrations has the form

$$u = u_0\exp[i(\omega t - k_\parallel y)],$$

where $k_\parallel$ is the wave number. The boundary conditions are reduced to the equality of the displacements of the strip and matrix at their interface $x = x_0$. The substitution of the solution into Eq. (2) with allowance for the boundary conditions $u_0 = AH_0^{(2)}(x_0)$ and relationship (1) leads to the equation

$$k_\parallel^2 = \frac{\omega^2}{c_0^2}\left(1 + \frac{2\sqrt{\rho G}H_1^{(2)}(x_0)}{R\rho_0\omega H_0^{(2)}(x_0)}\right). \quad (7)$$

From here, we can find the wave number $k_\parallel$:

$$k_\parallel = \frac{\omega}{c_0}\sqrt{1 + \alpha + i\beta}, \quad (8)$$

where c_0 is the speed of sound in the fiber in the absence of the liquid and

$$\alpha = \frac{2\sqrt{\rho G}[J_0(x_0)J_1(x_0) + Y_0(x_0)Y_1(x_0)]}{R\rho_0\omega[J_0^2(x_0) + Y_0^2(x_0)]},$$
$$\beta = \frac{2\sqrt{\rho G}[Y_0(x_0)J_1(x_0) - J_0(x_0)Y_1(x_0)]}{R\rho_0\omega[J_0^2(x_0) + Y_0^2(x_0)]}. \quad (9)$$

The wave number $k_\parallel$ is complex-valued, and its imaginary part determines the wave attenuation. Evidently, the wave attenuation is caused by a loss of energy within the fiber, which is spent on exciting a wave in the matrix. The speed of sound is determined by the ratio $\frac{\omega}{k_\parallel}$ of the angular frequency to the wavenumber modulus:

$$c = \frac{c_0}{\sqrt[4]{(1+\alpha)^2 + \beta^2}}. \quad (10)$$

For asymptotic values $x \gg 1$, the functions J_0, Y_0, J_1, and Y_1 take the form [5, 7]

$$J_0(x) = \sqrt{\frac{2}{\pi x}}\cos\left(x - \frac{\pi}{4}\right), \quad J_1(x) = \sqrt{\frac{2}{\pi x}}\cos\left(x - \frac{3\pi}{4}\right),$$
$$Y_0(x) = \sqrt{\frac{2}{\pi x}}\sin\left(x - \frac{\pi}{4}\right), \quad Y_1(x) = \sqrt{\frac{2}{\pi x}}\sin\left(x - \frac{3\pi}{4}\right). \quad (11)$$

At the same time, Eq. (9) can be reduced to the form

$$\alpha = 0, \quad \beta = \frac{2\sqrt{\rho G}}{R\rho_0\omega}. \quad (12)$$

For $\alpha = 0$ and weak attenuation of a longitudinal wave, i.e., $\beta \ll 1$, the expansion of formula (10) yields

$$c \approx c_0\left(1 - \frac{\rho G}{R^2\rho_0^2\omega^2}\right). \quad (13)$$

The attenuation of a plane wave in the fiber is described by the expression

$$u = u_0\exp(-\beta z) = \exp\left(-\frac{\sqrt{\rho G}}{R\rho_0 c_0}y\right). \quad (14)$$

The effect of a liquid on the speed of sound in a cylindrical fiber is similar to that in a thin strip [2]. In this case, in the asymptotic region $x \gg 1$, formulas (13) and (14) coincide with the solution to the plane problem of an elastic strip with a thickness R that is immersed in a low-modulus matrix.

In the calculations, the functions J_0 and J_1 were found by numerical integration of the Bessel function [7]:

$$J_n(x) = \frac{1}{2\pi}\int_0^{2\pi}\cos(n\theta - x\sin\theta)d\theta, \quad (15)$$

where $n = 0, 1$ is the Bessel function index.

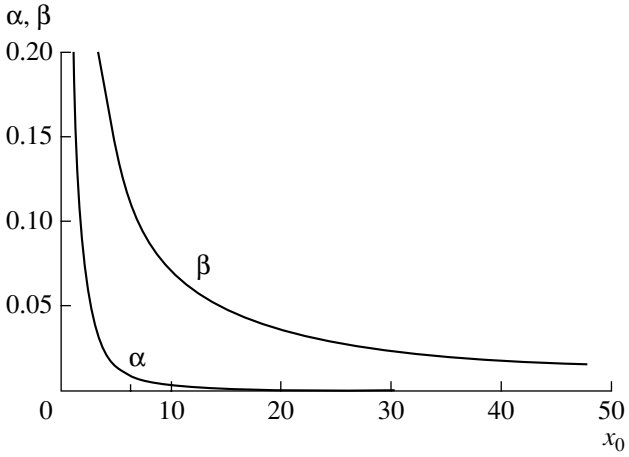

Fig. 2. Dependence of the coefficients α and β on the parameter x_0. The calculations are performed for densities of the coating and substrate ρ = 930 kg/m^3 and ρ_0 = 2600 kg/m^3, respectively. The matrix shear modulus is G = 1 MPa, the vibration frequency is f = 250 kHz, and the speed of sound in the fiber is c_0 = 5.1 km/s. The parameter x_0 was varied by a change in the fiber radius.

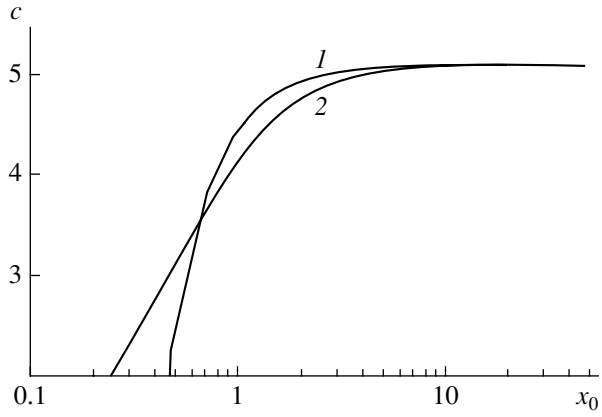

Fig. 3. Longitudinal-wave velocity as a function of the parameter x_0. The calculation parameters correspond to Fig. 2.

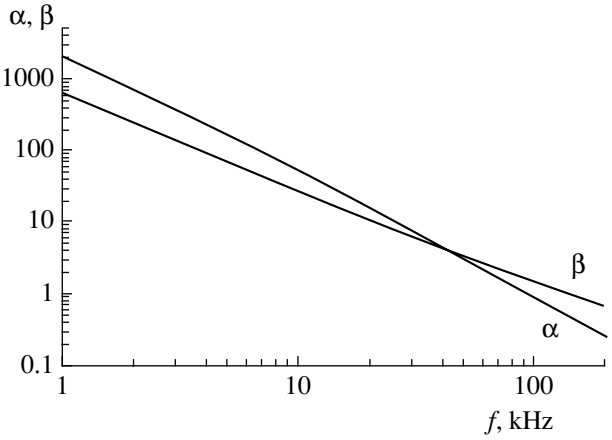

Fig. 4. Coefficients α and β as functions of the vibration frequency. The calculation parameters correspond to Fig. 2; the fiber radius is R = 30 μm.

The function Y_0 was calculated by numerical integration according to the formula from [7]:

$$Y_0(x) = -\frac{2}{\pi}\int_1^\infty \frac{\cos xt}{\sqrt{t^2-1}}dt.$$

In turn, the function Y_1 was determined by numerical differentiation: $Y_1(x) = -\dfrac{\Delta Y_0}{\Delta x}$.

The coefficients α and β calculated according to Eq. (10) as functions of the dimensionless parameter x_0 are plotted in Fig. 2. These coefficients monotonically decrease, the decrease rate being much more rapid for the coefficient α than for coefficient β. This behavior is quite consistent with asymptotic formula (12).

Curves *1* and *2* in Fig. 3, which were calculated according to expressions (10) and (13), respectively, show the dependences of the speed of sound on the parameter x_0. The speed monotonically increases and, at high x_0, attains the ultimate value of the speed of sound in an isolated fiber. It is worth noting that formula (13) was derived under the assumption $x_0 \gg 1$. This fact explains the deviation of this formula from the exact solution for small x. Analysis of the numerical solution shows that formulas (10) and (13) differ from each other at large values of the parameter x_0 as well. This can be explained by the fact that, at high values of the parameter x_0, the deviation of the speed of sound from that in the initial fiber is on the order of β^2. The values of the parameter α are also on the order of β^2. Therefore, formula (13) is not exact in the asymptotic region $x_0 \gg 1$.

Figure 4 presents the coefficients α and β calculated according to Eq. (10) as functions of the vibration frequency f. The slopes of the curves in the high-frequency region, in which the inequality $x_0 \gg 1$ is fulfilled, are equal to –1 (for α) and –2 (for β). It follows from here that $\alpha \backsim \dfrac{1}{f}$ and $\beta \backsim \dfrac{1}{f^2}$.

The effect of the presence of the matrix on the coefficients α and β and, correspondingly, on the speed of sound is noticeable provided that $x_0 \approx 2\pi$, whence it follows that the critical frequency is $f^* < \sqrt{\dfrac{G}{\rho R^2}}$. At frequencies lower than f^*, the wave attenuation is so much strong that it loses the capability of propagating along the bar. This conclusion is also valid in analysis of the effect of the fiber diameter. If the diameter is smaller than the length of the transverse wave in the matrix, the longitudinal wave attenuates very strongly and ceases to propagate. The estimate for the fiber critical radius is $R \approx \sqrt{\dfrac{G}{\rho f^{*2}}}$.

REFERENCES

1. L. D. Landau and E. M. Lifshitz, *Theory of Elasticity* (Nauka, Moscow, 1965; Pergamon Press, Oxford, 1986).
2. S. L. Bazhenov, Dokl. Akad. Nauk **383**, 334 (2002) [Dokl. Phys. **47**, 206 (2002)].
3. A. K. Rogozinskiĭ, S. L. Bazhenov, and A. A. Berlin, Dokl. Akad. Nauk **362**, 481 (1998) [Dokl. Phys. **43**, 616 (1998)].
4. V. A. Krasil'nikov and V. V. Krylov, *Introduction to Physical Acoustics* (Nauka, Moscow, 1984).
5. G. N. Watson, *A Treatise on the Bessel Functions* (Cambridge Univ. Press, Cambridge, 1958; Izd. Inostrannoĭ Literatury, Moscow, 1949), Chapt. 1.
6. G. N. Watson, *A Treatise on the Bessel Functions* (Cambridge Univ. Press, Cambridge, 1958; Izd. Inostrannoĭ Literatury, Moscow, 1949), Chapt. 2.
7. G. B. Dwight, *Tables of Integrals and Other Mathematical Data* (Macmillan Co., New York, 1957; Nauka, Moscow, 1973).

Translated by G. Merzon

Doklady Physics, Vol. 47, No. 5, 2002, pp. 360–362. Translated from Doklady Akademii Nauk, Vol. 384, No. 2, 2002, pp. 174–176.

TECHNICAL PHYSICS

Propagation of a Longitudinal Acoustic Wave in a Thin Elastic Strip with a Low-Modulus Coating

S. L. Bazhenov* and Corresponding Member of RAS A. A. Berlin**

Received January 10, 2002

In this work, the problem of the propagation of a longitudinal acoustic wave in a thin elastic strip with a low-modulus coating has been solved theoretically. The coating can give rise to the appearance of frequency bands with anomalous dispersion and forbidden bands wherein the propagation of waves is impossible because of strong attenuation.

The basic parameters determining the propagation of a longitudinal acoustic wave in an elastic rod are the density and elastic modulus of the rod [1]:

$$c_0 = \sqrt{\frac{E}{\rho_0}}, \quad (1)$$

where E is the elastic modulus and ρ_0 is the rod density.

The velocity of a longitudinal supersonic wave in a thin elastic strip decreases if the strip is embedded in a low-modulus elastic matrix [2]. This effect is attributed to the involvement of the boundary layer of the matrix in oscillations.

If the elastic modulus of the coating is negligible compared to the modulus of the substrate, the speed of sound in the coating is negligible according to Eq. (1) and the longitudinal wave propagates through the substrate. The longitudinal oscillations of the strip with allowance for shear stresses induced by interaction with the coating are described by the equation [3, 4]

$$\rho_0 H\frac{\partial^2 u}{\partial t^2} = EH\frac{\partial^2 u}{\partial y^2} + \tau, \quad (2)$$

where u is the displacement of an element of the strip (substrate) from the equilibrium position, H is the strip thickness, τ is the shear stress at the boundary between the strip and coating, and y is the axis along which a longitudinal acoustic wave propagates in the strip.

In order to find the stress τ, we consider the transverse shear oscillations of the coating in the $0 < x < h$ layer (Fig. 1). These oscillations are described by the equation [1]

$$\rho\frac{\partial^2 u}{\partial t^2} = G\frac{\partial^2 u}{\partial x^2}, \quad (3)$$

where ρ and G are the density and shear modulus of the coating, h is the thickness of the low-modulus coating, and x is the axis perpendicular to the strip plane. For bilateral coating (Fig. 1b), the shear stress τ is doubled. In this case, solution of the problem remains the same if H in Eq. (2) is equal to half the substrate thickness.

A solution of Eq. (3) for forced shear oscillations of the coating is sought in the form of the sum of two traveling waves:

$$u = u_0\exp[-i(\omega t - k_\perp x)] + u_1\exp[i(\omega t - k_\perp x)], \quad (4)$$

where ω is the angular frequency of strip oscillations

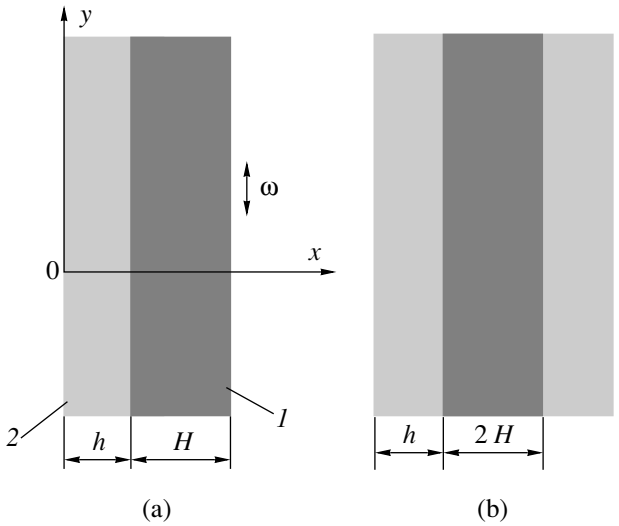

Fig. 1. The model of a composite for (a) unilateral and (b) bilateral coating: (*1*) an elastic rod with thickness H and (*2*) a coating with thickness h.

* *Enikolopov Institute of Synthetic Polymeric Materials, Russian Academy of Sciences, Profsoyuznaya ul. 70, Moscow, 117393 Russia*

** *Semenov Institute of Chemical Physics, Russian Academy of Sciences, ul. Kosygina 4, Moscow, 117977 Russia*

1028-3358/02/4705-0360$22.00

and

$$k_\perp = \omega\sqrt{\frac{\rho}{G}} \quad (5)$$

is the wavenumber describing a transverse wave in the coating. The boundary conditions for solution (4) are determined by the absence of shear stresses at the free boundary of the coating $u'(0) = 0$, and solution (4) takes the form of the standing wave

$$u = A\cos(k_\perp x)\exp(i\omega t), \quad (6)$$

where A is a certain constant.

The shear stress τ at the boundary of the strip and coating is determined as

$$\tau = -G\frac{\partial u}{\partial x} \quad \text{at} \quad x = h$$

and is equal to

$$\tau = AGk_\perp \sin(k_\perp h)\exp(i\omega t). \quad (7)$$

A solution of Eq. (2), which determines longitudinal oscillations of the strip, is sought in the form

$$u = u_0 \exp[i(\omega t - k_\parallel y)], \quad (8)$$

where $k_\parallel$ is the wavenumber describing a longitudinal wave in the rod.

Taking into account that the displacements of the coating and strip are equal to each other at their boundary, we find the constant A entering into Eq. (7):

$$A = \frac{u_0}{\cos(k_\perp h)}.$$

Assuming that the length of the longitudinal wave in the rod is much greater than the length of the transverse wave in the coating, we obtain the dispersion relation

$$\rho_0 H\omega^2 = EHk_\parallel^2 - Gk_\perp \tan(k_\perp h) \quad (9)$$

from Eqs. (2), (7), and (8).

The wavenumber $k_\parallel$ is found from Eq. (9) as

$$k_\parallel = \frac{\omega}{c_0}\sqrt{1 + \frac{Gk_\perp}{\rho_0\omega^2 H}\tan(k_\perp h)}. \quad (10)$$

The wavenumber $k_\parallel$ is imaginary when

$$\rho_0 H\omega^2 + Gk_\perp \tan(k_\perp h) < 0.$$

An imaginary $k_\parallel$ value corresponds to very strong attenuation of the longitudinal wave and to the existence of a forbidden frequency band. This is explained by the reflection of the transverse wave from the free boundary of the coating and by the interaction of the reflected wave with the rod. This interaction is particularly strong when the total path to the free boundary and back is equal to half the wavelength. This condition is generally written in the form

$$h = \frac{\lambda_\perp}{2} + n\lambda_\perp,$$

where n is a positive integer.

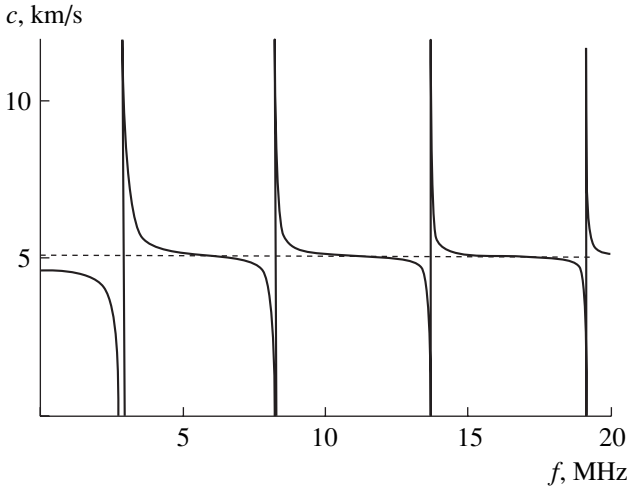

Fig. 2. The velocity of a longitudinal wave vs. the oscillation frequency f for the densities of the coating ρ = 930 kg/m^3 and the substrate ρ_0 = 2600 kg/m^3, shear modulus G = 1 GPa, coating thickness h = 100 μm, substrate thickness H = 50 μm, and speed of sound in the substrate c_0 = 5.1 km/s. The dashed line is the speed of sound in the substrate free of a coating.

The phase velocity $\frac{\omega}{k_\parallel}$ of the transverse wave is equal to

$$c = \frac{c_0}{\sqrt{1 + \frac{Gk_\perp}{\rho_0\omega^2 H}\tan(k_\perp h)}}. \quad (11)$$

A feature of solution (11) is that the phase velocity of an acoustic wave in the rod with a coating for $\tan(k_\perp h) < 0$ exceeds the velocity in the original rod.

For a very thin coating, when $k_\perp h \ll 1$, i.e., $h \ll \lambda_\perp$, by taking into account Eq. (5), we obtain the asymptotic solution

$$c = c_0\sqrt{\frac{m_0}{m_0 + m}}, \quad (12)$$

where $m = \rho h$ and $m_0 = \rho_0 H$ are the masses of the coating and substrate, respectively.

In the limit of small thickness values $h \ll \lambda_\perp$, the coating vibrates with the substrate as an associated mass. Equation (12) follows from classical formula (1)

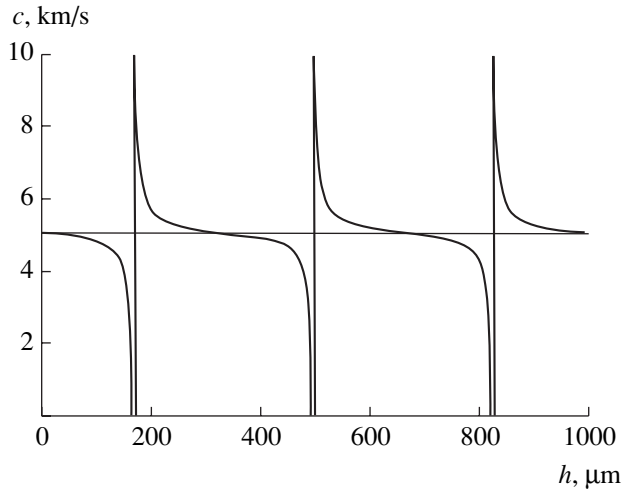

Fig. 3. The same as in Fig. 2, but vs. coating thickness h. The oscillation frequency is $f = 750$ kHz.

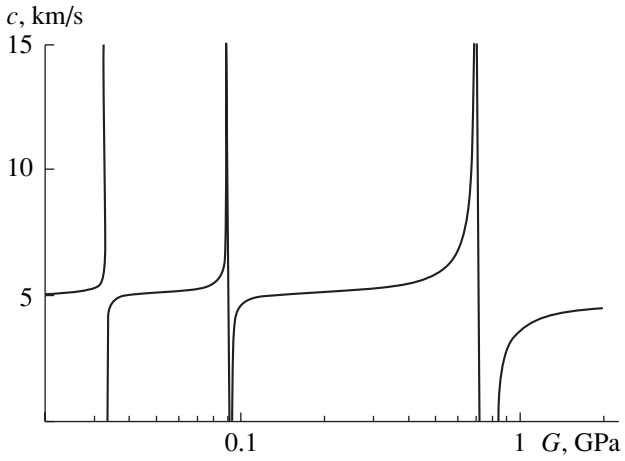

Fig. 4. The same as in Fig. 3, but vs. shear modulus of the coating G.

if the composite rod–coating is treated as a homogeneous material with averaged rigidity and density [5]:

$$\begin{aligned} \rho_c &= V_p\rho + V_o\rho_o, \\ E_c &= V_pE_p + V_oE, \end{aligned} \qquad (13)$$

where V_p and V_o are the bulk fractions of the coating and substrate, respectively.

If the rigidity of the coating is negligible and $V_pE_p \ll V_oE$, Eq. (12) follows from Eqs. (1) and (13). Thus, Eq. (12) is an analog of the so-called mixture rule implying that the rigidity E_c and density ρ_c of a reinforced composite material are determined by averaging the characteristics of reinforcement and matrix [5].

The velocity of an acoustic wave is calculated by Eq. (11) and is shown in Fig. 2 as a function of the frequency of oscillations $f = \omega/2\pi$. The calculations were performed for a 100-μm-thick epoxy coating deposited on a 50-μm aluminum substrate. For low frequencies corresponding to the limit of small coating thickness, the speed of sound is lower in the coating than in the substrate. However, the megahertz region involves the set of periodically repeated forbidden bands and bands where the phase velocity is higher than the velocity of propagation in the original substrate.

The velocity of the wave as a function of coating thickness h is shown in Fig. 3, which is similar to Fig. 2 and exhibits the same set of bands. The speed of sound decreases linearly with increasing thin-coating thickness, which is evident if Eq. (12) is expanded in a series and only the two first terms are retained: $c = c_0\left(1 - \frac{m}{2m_0}\right)$.

Figure 4 shows the velocity of the wave as a function of the shear modulus of the coating G. Forbidden bands appear if the shear modulus of the coating is lower than a certain critical value, which is equal to 0.9 MPa for the parameters used in the calculation. For higher rigidity of the coating, these bands are absent. The general expression for the critical value G^* of the shear modulus of the coating is found from the condition $h = \frac{\lambda_\perp}{2}$:

$$G^* = 4h^2f^2\rho, \qquad (14)$$

where $f = \frac{\omega}{2\pi}$ is the oscillation frequency. Thus, a low-modulus raw-rubber coating applied to a thin strip can give rise to the very surprising appearance of bands with anomalous dispersion and bands where waves strongly attenuate and therefore cannot propagate. Bands with anomalous behavior of the composite appear when the coating thickness is commensurate with the length of the transverse wave in the coating material.

REFERENCES

1. L. D. Landau and E. M. Lifshitz, *Theory of Elasticity* (Nauka, Moscow, 1965; Pergamon Press, Oxford, 1986).
2. S. L. Bazhenov, Dokl. Akad. Nauk **383**, 334 (2002) [Dokl. Phys. **47**, 206 (2002)].
3. A. K. Rogozinskiĭ, S. L. Bazhenov, and A. A. Berlin, Dokl. Akad. Nauk **362**, 481 (1998) [Phys. Dokl. **43**, 623 (1998)].
4. V. A. Krasilnikov and V. V. Krylov, *Introduction to Physical Acoustics* (Nauka, Moscow, 1984).
5. B. W. Rosen, in *Fiber Composite Materials* (ASM, Metals Park (Ohio), 1965), pp. 37–76.

Translated by R. Tyapaev

Doklady Physics, Vol. 47, No. 5, 2002, pp. 363–366. Translated from Doklady Akademii Nauk, Vol. 384, No. 2, 2002, pp. 177–180.

TECHNICAL PHYSICS

Nature of Microplastic Deformation in Polycrystalline Materials

V. A. Pozdnyakov and A. M. Glezer

Presented by Academician O.A. Bannykh December 21, 2001

Received December 26, 2001

The mechanisms of the initial stage of plastic deformation in polycrystals are of principal importance in understanding the general regularities of the mechanical behavior of materials. Investigations of polycrystals in the region of microplastic deformation showed that the deformation curve consists of two parts specified by different hardening coefficients corresponding to the two stages of the microplasticity process [1]. At the first stage of the process, the coefficient of cold hardening is independent of grain size. At the second stage, the coefficient increases with decreasing grain size. A simplified model [1] of this phenomenon assumes that plastic deformation at the first stage occurs in individual grains and the transition to the second stage is caused by the transfer of deformation from grain to grain due to the concentration of stresses at the boundaries of plastically deformed grains.

To determine the mechanisms responsible for the appearance and initial development of plastic flow in polycrystals, it is necessary to consider the results of structure investigations. Numerous experimental data [2–4] indicate that grain boundaries are the main sources of dislocations at the first stage of microplastic deformation in polycrystals. A detailed analysis of the formation and distribution of dislocations in the microplastic region was performed in [4] for polycrystalline copper with a grain size of 18 μm. When the strain reached 10^{-4}, grain-boundary dislocations with a mean density of 8.5×10^4 cm^{-1} appeared inside grain boundaries. The distribution of dislocations over grain boundaries was initially rather nonuniform: there were three to four grain boundaries free of dislocations per grain boundary containing dislocations. When the strain increased to 3×10^{-4}, the density of grain boundary dislocations increased by more than a factor of 3 and their distribution became more uniform. The development of intragrain deformation was observed only when a certain degree of plastic strain was achieved.

In our opinion, the character of evolution of the dislocation structure that was observed in [3, 4] is attributed to the fact that, at the first stage of the process, dislocations are directly generated in grain boundaries and, at the second stage, dislocations are emitted from grain boundaries into the grain bulk in contrast to the simplified model proposed in [1]. Here, this concept is extended and a strict model quantitatively describing the regularities at the initial stage of a microplastic flow of polycrystalline materials, including nanocrystals, is developed.

So far, several mechanisms responsible for the generation of dislocations from grain boundaries have been proposed [2]. For any specific structural mechanism, we introduce the shear stress $\tau_g^{(i)}(T)$ characterizing the generation of a dislocation inside a grain boundary of the *i*th type at temperature *T*. The superscript *i* relates to two unit vectors, namely, the vector of mutual grain misorientation $\boldsymbol{\theta}$ and the normal to the grain-boundary plane $\mathbf{n}$: $i = (\boldsymbol{\theta}, \mathbf{n})$. The stress $\tau_g^{(i)}$ is determined by the structure and state of grain boundaries, the number of impurities, and temperature *T*. When an external shear stress τ_a admissible in the plane of grain boundaries reaches $\tau_g^{(i)}$, the nucleation of dislocations in grain boundaries of the *i*th type becomes energetically possible. Due to the incompatibility of elastic deformations in neighboring grains, a concentration of stresses arises at their boundaries [5] and facilitates the formation of dislocations. The generation of boundary dislocations, which cannot slide in the boundary at low temperatures, leads to uniform relative displacement over the area of a grain face or the facet of the grain boundary.

On the mesoscopic scale, plastic deformation occurs due to the formation and development of domains of grain boundary deformation. The boundaries between such domains are the lines of steps, kinks, and junctions of grain boundaries. Under the action of an external stress on a mesh of grain boundaries in a polycrystal at $q\tau_a > \tau_g$ (q is the concentration coefficient of stresses at grain boundaries due to the incompatibility of elastic

Institute of Metallophysics and Functional Materials, Bardin Central Research Institute for the Iron and Steel Industry, Vtoraya Baumanskaya ul. 9/23, Moscow, 107005 Russia
e-mail: glezer@imph.msk.ru

1028-3358/02/4705-0363$22.00

deformation in anisotropic grains), N domains of grain boundary deformation with volumes Ω_s and proper strain ε_{ik}^{0s} arise, which gives rise to plastic deformation of the sample:

$$\varepsilon_{ik} = \sum_{s=1}^{N} \frac{\varepsilon_{ln}^{0s} m_{il}^s m_{kn}^s \Omega_s}{V}, \quad (1)$$

where V is the sample volume and m_{il}^s are the cosines of the angles between the axes of the coordinate system associated with the sth domain and the coordinate axes of the basis system, one of whose axes coincides with the load axis. When grain boundary deformation is purely shear, the shear $\mathbf{u}^s$ in the sth domain of the boundary with the normal $\mathbf{n}^s$ results in the plastic strain

$$\varepsilon_{ik}^s = (2\delta)^{-1}(u_i^s n_k^s + u_k^s n_i^s) = (m_{ik}^s + m_{ki}^s)\frac{\gamma^s}{2}. \quad (2)$$

Here, each coefficient m_{ik}^s is the product of the two direction cosines of the angles (i) between the normal $\mathbf{n}^s$ to the plane of the sth domain of grain boundary deformation and the kth basis vector and (ii) between the direction of the grain boundary strain $\mathbf{m}^s$ in this plane and the ith basis vector and $\gamma^s = \frac{u^s}{\delta}$, where δ is the thickness of the grain boundary and u^s is the shear averaged over the area S^s.

Let τ_g^* be the stress at which grain boundary deformation arises in a polycrystal and which is averaged over the ensemble of grain boundaries. In the case of uniaxial extension (compression), the first domains of grain boundary deformation appear in the polycrystal at $\frac{\sigma_a}{2} > q^{-1}\tau_g^* \equiv \tau_g$. The planes of these domains are oriented at an angle of approximately 45° to the load axis. Let L be the mean size of the domains of grain boundary deformation. With a further increase in the external stress σ_a, their concentration N and mean size L increase; i.e., the volume fraction $f = \omega\delta L^2 N$ (ω is the numerical coefficient) of these domains also increases. In addition, with increasing σ_a, shear in the domains of grain boundary deformation and, therefore, the energy of these domains also increase, which gives rise to effective cold hardening. The volume fraction of the domains of grain boundary deformation is proportional to the total area of grain boundaries per unit volume and consequently is higher when the grain of the polycrystal is smaller, all other factors being the same. The total strain ε_n is equal to the sum of the elastic ε_y and plastic ε strains, and, in the case of uniaxial extension,

$$\varepsilon_n = \frac{\sigma_a}{E} + \varepsilon. \quad (3)$$

The plastic strain in the direction of the load axis is defined by the volume fraction f and the equilibrium value of the mean shear strain γ in the domains of grain boundary deformation:

$$d\varepsilon = m(fd\gamma + \gamma df), \quad (4)$$

where m is the mean orientation factor. The domains of grain boundary deformation can be considered as planar inclusions with uniform proper strain γ. We assume that a domain of grain boundary deformation has the shape of an oblate ellipsoid with the principal semiaxes $a = b = \frac{L}{2}$, $c = \frac{\delta}{2}$ ($c \ll a$ and $c \ll b$), $\omega = \frac{4\pi}{3}$, and shear deformation is uniform within Ω. The internal shear stress [7] in a domain of grain boundary deformation with the shear strain γ is equal to [6]

$$\tau = -A\frac{\delta}{L}G\gamma. \quad (5)$$

Here, $A = \frac{\pi(2-\nu)}{4(1-\nu)}$, where ν is the Poisson ratio and G is the shear modulus of the material. The plastic strain is related to the external stress as

$$\sigma_a = \sigma_g(\varepsilon) + \frac{AG\delta\varepsilon}{fLm^2}, \quad (6)$$

where $(\sigma_a - \sigma_g)m = \tau_a - \tau_g$.

Dislocations that are formed inside grain boundaries at the first stage of microdeformation can be considered as grain boundary dislocations that are "geometrically necessary" [7] and provide the compatibility of elastic grain deformations. Some of these dislocations participate in the relaxation of internal stresses concentrated at grain boundaries due to the difference in elastic grain deformations. At this stage of microplastic deformation, grain boundary strain ε^* attains the critical value at which the condition of emission of dislocations into the grain bulk is satisfied. At $\varepsilon > \varepsilon^*$, microplastic deformation of the polycrystal passes to the second stage, intragrain plastic deformation. The value ε^* is determined by the mechanisms and conditions for emitting dislocations from the grain boundary: "torch" emission of dislocations from the boundaries of the domains of grain boundary deformation at $\gamma > \gamma^*$ or the uniform egress of dislocations from grain boundaries at $\tau_a \geq \tau_e$. These two conditions determine limiting strain values $\varepsilon_1^* = m f \gamma^*$ and $\varepsilon_2^* = \varepsilon_2^*(\tau_a - \tau_e)$, respectively; $\varepsilon^* = \min\{\varepsilon_1^*, \varepsilon_2^*\}$. At $\varepsilon > \varepsilon^*$, the contribution of internal stresses caused by grain boundary deformation to further cold hardening of the polycrystal decreases. However, another component of hardening from the stress fields of dislocations emitted into the grain bulk appears. The density of dislocations emitted into the grain bulk is proportional to the length of dislocations inside the grain boundary per unit area and to the area of the grain boundary per unit volume S_V. The total area

of grain boundaries per unit volume is $S_v = \frac{q_v}{D}$ (q_v is the numerical coefficient ~3). Some of the dislocations passing to the grain bulk will provide the compatibility of the elastoplastic deformations of grains [7]. Their density equals $\rho_g = \frac{kf(\gamma - \gamma^*)}{bL}$. The stresses caused by dislocations with density ρ are equal to $\sigma_i = \alpha G b \rho^{1/2}$, where $\alpha \approx 1$.

Assuming that the area of grain boundaries per unit volume that are involved in grain boundary deformation at the initial stage of deformation is proportional to S_v, i.e., $\frac{f}{\delta} = hS_v$, plastic strain can be written as $\varepsilon = m\delta h \frac{q}{D}\gamma(\sigma_a)$, where the coefficient h at $\frac{\sigma_a}{2} > \tau_g$ takes a finite value $h_0 = \text{const}$. With a rise in the external stress, the concentration and the mean area of the domains of grain boundary deformation increase and h further increases with increasing σ.

Finally, for microplastic flow of a polycrystal, the plastic strain depends on the external stress as

$$\begin{aligned} \sigma_a &= \sigma_s + \frac{AG(D/L)\varepsilon}{qhm^2}, \quad \varepsilon < \varepsilon^* = mqh\frac{\delta}{D}\gamma^*, \\ \sigma_a &= \sigma_a(\varepsilon^*) + \alpha G\left[\frac{kb(\varepsilon - \varepsilon^*)}{m\zeta D}\right]^{1/2}, \quad \varepsilon > \varepsilon^*, \end{aligned} \tag{7}$$

where $L = \zeta D$ (ζ is a numerical parameter less than unity).

Since $L \sim D$, the behavior of deformation at the first stage of microplastic deformation (at $\varepsilon < \varepsilon^*$) does not depend on the grain size and stress depends linearly on strain. Relationships (3) and (7) describe the behavior of the polycrystal strain $\sigma_a(\varepsilon_n)$ in the range of microplastic deformation. At the first stage (at $\varepsilon < \varepsilon^*$), σ depends linearly on ε. The inclination of the straight line $\sigma(\varepsilon)$ at $\sigma > \sigma_g$ is determined by the so-called relaxed shear modulus of the polycrystal [8]. At the second stage (at $\varepsilon > \varepsilon^*$), σ depends parabolically on ε.

The above analysis reveals the mechanisms determining the yield point of polycrystalline materials in a wide range of grain sizes and anomalies in the dependence of the yield point in a polycrystal on the grain size. The yield point σ_y is defined as a stress corresponding to a given level, e.g., 0.2%, of the plastic strain ε_m. For common polycrystalline materials with grain size $D \approx 10$–100 μm, we have $\varepsilon^* \ll \varepsilon_m$ and $\sigma(\varepsilon^*) \approx \sigma_g$ and Eq. (7) leads to the standard Hall–Petch relationship. The stage of grain boundary deformation is completed much earlier than the level of deformation corresponding to the yield point is achieved, and the dominant part of microdeformation is associated with the development of plastic deformation in individual grains and with the extension of plasticity domains.

For submicrocrystalline materials ($D \approx 0.1$–1 μm), the contributions from both grain boundary deformation and intragrain deformation can be comparable at the stage of microplastic deformation. For nanocrystalline materials ($D \approx 1$–100 nm), the structural mechanism of grain boundary deformation is fundamentally different [9]. The generation and multiplication of dislocations are hindered in them because of significant energy consumption on overcoming the image and linear-tension forces. It is assumed that high shear stresses rearrange the structural elements of grain boundaries in nanocrystals and microdomains of shear transformations form, inducing grain boundary microsliding [9]. However, the grain boundary stage of microplastic deformation as a whole corresponds to the features of plastic flow in nanocrystalline materials. The plastic strain caused by the mechanism of grain boundary microsliding [9] for nanomaterials with $D \sim 10$ nm is equal to $\varepsilon^* \approx 10^{-3}$–$10^{-2}$; i.e., it may exceed the plastic strain corresponding to the yield point. In this case, $\sigma_m(D)$ is determined by the first of Eqs. (7). If $L = \zeta D$, where ζ is a constant, Eq. (6) indicates that the yield point is independent of the grain size and, when accommodation processes occur, the Hall–Petch relation with slightly varying function $\sigma_y(D)$ will be valid, which was observed experimentally in [10]. If either $L \sim D^p$, where the exponent $p < 1$, or L is independent of D, the yield point of nanocrystals, which is determined by the first of Eqs. (7), increases with the grain size in accordance with experimental data [10].

Thus, in different ranges of crystallite sizes, the nature of the yield point of polycrystals can be determined by different structural mechanisms of plastic deformation. The evolution of the dislocation structure and the character of deformation behavior at the stage of microplastic flow in polycrystalline materials depend not only on grain size but also on the type and state of grain boundaries and the state of the crystal lattice of a material. For example, for polycrystals with $\tau_g > \tau_e$, the dislocations that are formed inside grain boundaries and have lattice Burgers vectors will immediately penetrate to the bulk of a grain.

Consequently, the process of microdeformation in polycrystals generally consists of several stages. At the first stage, grain boundary deformation occurs in a nonuniform stress field concentrated at grain boundaries. The second stage corresponds to the emission of dislocations from grain boundaries into the grain bulk. At the final stage of microdeformation, the domains of grain boundary and intragrain plastic deformations are extended and these processes are intensified.

ACKNOWLEDGMENTS

This work was supported by the Russian Foundation for Basic Research, project no. 00-02-16312.

REFERENCES

1. E. F. Dudarev, *Microplastic Strain and Yield Point of Polycrystals* (Tomsk. Gos. Univ., Tomsk, 1988).
2. O. A. Kaĭbyshev and R. Z. Valiev, *Boundaries of Grains and Properties of Metals* (Metallurgiya, Moscow, 1987).
3. L. G. Orlov, in *Proceedings of First All-Union Conference on Structure and Characteristics of Grain Boundaries* (Ufimskiĭ Aviatsionnyĭ Inst., Ufa, 1983), p. 10.
4. T. Malis and K. Tangri, Acta Metall. **27**, 25 (1979).
5. Z. Celinski and K. J. Kurzydlowski, Res. Mech. **5** (2), 89 (1982).
6. T. Mura, *Micromechanics of Defects in Solids* (Martinus Nijhoff Publ., The Hague, 1982).
7. M. F. Ashby, Philos. Mag. **21**, 399 (1970).
8. F. Ghahreman, Int. J. Solids Struct. **16**, 825 (1980).
9. V. A. Pozdnyakov and A. M. Glezer, Fiz. Tverd. Tela **72**, 705 (2002) [Phys. Solid State **44**, 732 (2002)].
10. R. A. Andrievskiĭ and A. M. Glezer, Fiz. Met. Metalloved. **88**, 50 (2000); **89**, 91 (2001).

Translated by Yu. Vishnyakov

Doklady Physics, Vol. 47, No. 5, 2002, pp. 367–369. Translated from Doklady Akademii Nauk, Vol. 384, No. 2, 2002, pp. 181–184.

TECHNICAL PHYSICS

Removal of Dust Particles from Technological Plants

Academician V. E. Fortov, V. I. Vladimirov*, L. V. Deputatova*, A. P. Nefedov, V. A. Rykov, and A. V. Khudyakov****

Received November 19, 2001

The behavior of dust particles in a plasma is currently under active investigation [1, 2]. Crystal and liquid structures, clouds, and voids have been obtained, and the size separation of dust particles has been observed [3, 4]. For practical applications, it is interesting to investigate the conditions under which dusty formations conserving their internal structure move in a plasma under the action of an external electric field and are deposited on certain surfaces. The results of such investigations can provide a basis for a method of disposing of dust particles from a stationary low-temperature plasma. Mastering this technology will make it possible to separate particles by size, to remove them from wall plasma regions and surfaces being worked by plasma etching, and to control processes of forming dusty plasma structures.

Dust particles are a significant factor in processes occurring in prospective power plants. For example, in the photovoltaic electric-power source proposed in [5, 6], the efficiency of the device depends on the possibility of producing and maintaining a stable dusty crystal in a plasma generated by hard ionizers. In lasers with nuclear pumping [7], dust particles produced within a laser-active element can degrade the device parameters. The production of a dusty crystal involving micron-sized fuel particles will make it possible to obtain a uniform energy contribution of nuclear-reaction products to the laser-active medium and conserve its optical transparency.

Micron-sized dust particles are present in magnetic-confinement thermonuclear facilities [8, 9]. These particles are produced due to the interaction of a plasma with a wall surface. The production of dust particles appeared to be a serious safety-engineering problem for the future international thermonuclear experimental reactor (ITER) [10, 11] characterized by high flux densities of plasma particles (in the steady state). The ITER, like most existing large facilities, will have carbon-based wall components (graphite, carbon composites). Implantation of tritium into graphite dust can produce dust particles that each involves two tritium atoms per carbon atom, and the total tritium mass of the dusty component may be as great as a few kilograms. Dust particles can give rise to tritium ejection into the environment in the case of a serious accident. Dust particles are highly mobile and can pollute sizable areas.

In this study, the possibility of removing dust particles from a dusty structure preformed in a nuclear-induced plasma by an external electric field was checked experimentally.

The experiments were conducted in a nuclear-induced plasma with a track structure, which means that the plasma is quasineutral only for volumes containing abundant nuclear-particle tracks, i.e., in the vicinity of a radioactive source. Within the tracks, the quasineutrality is very rapidly violated because the diffusion coefficients of electrons and ions are very different. In an electric field, a track breaks down into moving bunches of electrons and ions. The charge of a dust particle is formed by its interaction with these bunches [12]. Other mechanisms of charging dust particles, e.g., through secondary electron emission, as an ionizing particle passes through a dust particle will be significant for a high-activity radioactive source.

Experiments on removing dust particles from a volume filled with nuclear-induced plasma were conducted on an experimental set similar to that described in [13] and whose layout is shown in Fig. 1. They were carried out in neon at a pressure of 25–100 kPa. A radioactive source, a thin circular ^{252}Cf layer 7 mm in diameter and with an activity of 4×10^6 Bq, was located at the center of the lower ground electrode. To generate electric fields of various patterns, three structures of the upper (high-voltage) electrode were used. The electrodes were spaced about 40 mm apart. Micron-sized polydisperse zinc particles were employed in the experiments. When a voltage of 160 V was applied to the upper continuous electrode (*A* in the right-hand part of Fig. 1) and a gas-dust mixture was injected, the dust particles formed a cloud with well-defined boundaries within a few minutes. The cloud had the shape of a truncated cone whose base was on the upper-electrode plane and whose vertex was close to the radioactive source. When the gas pressure and electrode potentials were constants, the upper part of the cloud, in a few

* *Institute of Thermal Physics of Extremal States, Institute of High Temperatures Scientific Association, Russian Academy of Sciences, Izhorskaya ul. 13/19, Moscow, 127412 Russia*

** *Institute of Physics and Power Engineering, pl. Bondarenko 1, Obninsk, Kaluga oblast, 249020 Russia*

1028-3358/02/4705-0367$22.00 © 2002 MAIK "Nauka/Interperiodica"

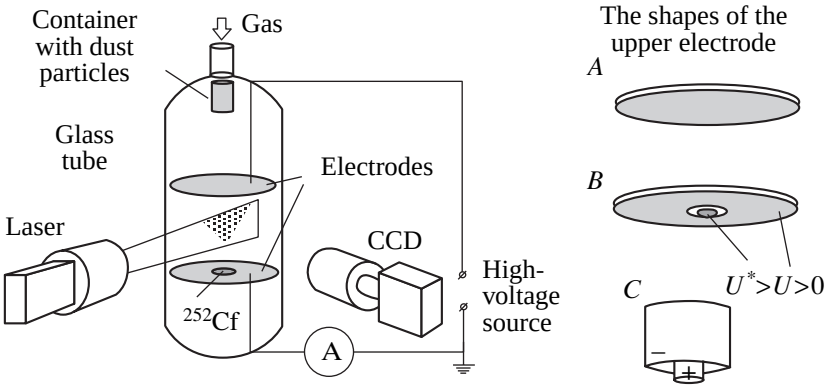

Fig. 1. The layout of the experimental set.

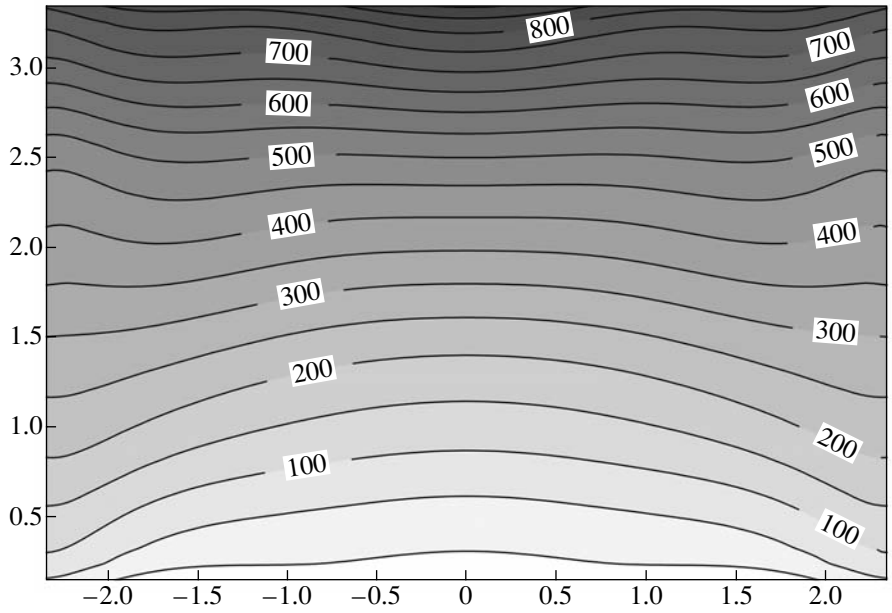

Fig. 2. The charge (in e) of a dust particle 1.4 mm in radius vs. spatial coordinates. The point 0 corresponds to the source center. The potential of the upper continuous electrode is equal to 152 V. The upper and lower electrodes are spaced 3.5 cm apart. The neon pressure is equal to 0.76×10^5 Pa.

minutes, took a streamlined shape close to the spherical one [14]. The radius of the dust particles composing the cloud was calculated by the Stokes formula using the measured velocity of particle fall after the electric-field source had been turned off and appeared to be 1.0–1.4 μm [the particle mass was $(3–8) \times 10^{-11}$ g]. The charge of levitating and slow-moving particles was calculated from the equilibrium condition for a dust particle in the electric field and lay in the range between 400 and 1000 e depending on the particle radius. Figure 2 shows the spatial dependence of the mean dust-particle charge calculated for an experimental cell with a continuous upper electrode by the procedure taken from [12]. The observed values of the dust-particle charge are closely reproduced by the proposed procedure.

When the upper-electrode potential increases above 160 V once the dust-particle cloud has formed, dust particles stream to this electrode. The higher the potential, the higher the velocity of these particles. It is interesting that not all of the structure steams forward when the upper-electrode potential is less than 200 V. One or a few jets are produced in the upper part of the structure. The shape and position of their bases on the electrode are time-variant (Fig. 3a). Near the electrode, the particle velocity within a jet decreases and the jet expands into a funnel shape. There are almost no dust particles outside the cloud and jets.

The employment of an auxiliary hemispherical electrode (B in the right-hand part of Fig. 1B) 3 mm in diameter and insulated from the principal electrode ensured the removal of dust particles from the cloud (Fig. 3b). When the potential of the principal upper electrode is equal to $U \simeq 200$ V and the auxiliary electrode potential is equal to $U \simeq 300$ V, a single dusty jet

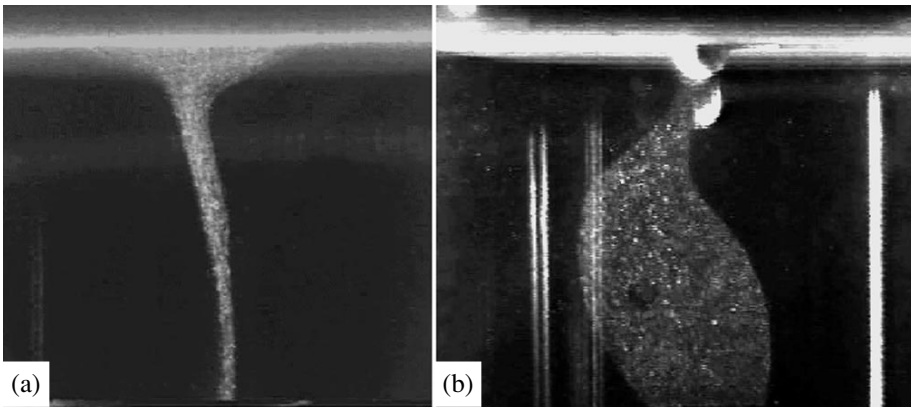

Fig. 3. (a) Dusty jet involving particles moving toward the high-voltage electrode and (b) the drift of dust particles to the auxiliary hemispherical electrode.

directed toward the auxiliary electrode is produced. The dust particles are attracted to the electrode and remain on its surface.

Two thin-walled tubes (*C* in the right-hand part of Fig. 1), which have diameters of 3 and 5 mm and potentials of opposite sign, create an electric field whose configuration is such that negatively charged dust particles from the cloud are collected in the inner tube whose positive potential is equal to 150 V (Fig. 4). In this case, the particles remain on the inner surface of the tube. A potential equal to –200 V was applied to the outer tube. The potentials were measured with respect to the lower ground electrode.

In conclusion, we note that the deposition of dust particles on the collecting probe occurs over a narrow range of electric field strength under the indicated conditions. As the field strength increases, dust particles form stable vortex structures in the vicinity of the probe electrodes [14].

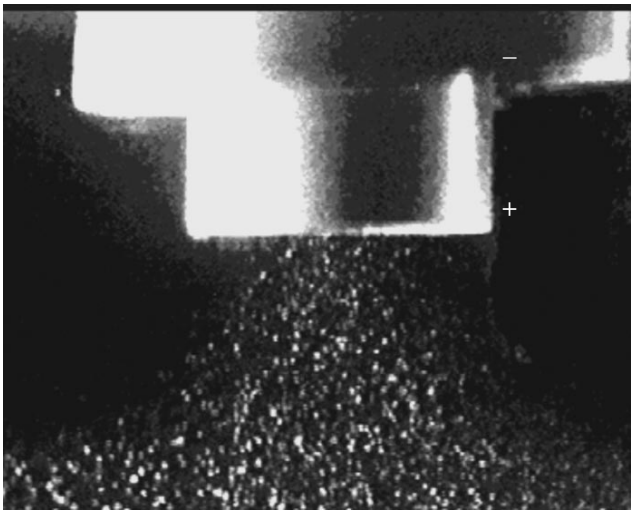

Fig. 4. Removal of particles by means of coaxial sound; the inner and outer tubes are 3 and 5 mm in diameter, respectively.

ACKNOWLEDGMENTS

This work was supported by the Russian Foundation for Basic Research, project no. 00-02-17620.

REFERENCES

1. V. N. Tsytovich, Usp. Fiz. Nauk **167**, 57 (1997) [Phys. Usp. **40**, 53 (1997)].
2. *The Encyclopedia of Low-Temperature Plasma*, Ed. by V. E. Fortov (Nauka, Moscow, 2000), Vol. 3.
3. A. P. Nefedov, O. F. Petrov, V. I. Molotkov, and V. E. Fortov, Pis'ma Zh. Éksp. Teor. Fiz. **72**, 313 (2000) [JETP Lett. **72**, 218 (2000)].
4. H. Thomas, G. E. Morfill, V. Demmel, *et al.*, Phys. Rev. Lett. **73**, 652 (1994).
5. V. Yu. Baranov, I. A. Belov, A. V. Dem'yanov, *et al.*, Preprint No. 6105/6, IAE (Kurchatov Institute of Atomic Energy, 1998).
6. I. A. Belov, A. S. Ivanov, D. A. Ivanov, *et al.*, Pis'ma Zh. Tekh. Fiz. **25**, 89 (1999) [Tech. Phys. Lett. **25**, 630 (1999)].
7. P. P. Dyachenko, Laser Part. Beams **11**, 619 (1993).
8. V. I. Pistunovich, Fiz. Plazmy **17**, 560 (1991) [Sov. J. Plasma Phys. **17**, 328 (1991)].
9. V. N. Tsytovich and J. Winter, Usp. Fiz. Nauk **168**, 899 (1998) [Phys. Usp. **41**, 815 (1998)].
10. C. H. Skinner, C. A. Gentile, J. C. Hosea, *et al.*, Nucl. Fusion **39**, 271 (1999).
11. S. J. Piet, A. Cjstley, G. Federici, *et al.*, in *Proceedings of Seventeenth Symposium of the Inst. of Electronic and Electrical Engineers / National Inst. for Policy and Strategic Studies on Fusion Engineering, San Diego, USA, 1997* (San Diego, 1998), Vol. 1, p. 167.
12. V. E. Fortov, A. P. Nefedov, V. I. Vladimirov, *et al.*, Phys. Lett. A **284**, 118 (2001).
13. V. I. Vladimirov, L. V. Deputatova, V. I. Molotkov, *et al.*, Fiz. Plazmy **27**, 1 (2001) [Plasma Phys. Rep. **27**, 36 (2001)].
14. V. I. Vladimirov, L. V. Deputatova, A. P. Nefedov, *et al.*, Zh. Éksp. Teor. Fiz. **120**, 353 (2001) [JETP **93**, 313 (2001)].

Translated by V. Tsarev

Doklady Physics, Vol. 47, No. 5, 2002, pp. 370–372. Translated from Doklady Akademii Nauk, Vol. 384, No. 2, 2002, pp. 185–187.

ENERGETICS

A Porosity Distribution in Nonuniform Homogeneous Structures

A. P. Mozhaev

Presented by Academician A.I. Leont'ev September 18, 2001

Received August 13, 2001

Porous materials and systems are extensively used in power plants, reactors, and thermal protection elements. To correctly determine the regimes and parameters of heat- and mass-exchange processes proceeding in them, one needs to know the main structural characteristics of a porous medium. The most important characteristics are the mean value $M[\Pi]$, variance $D[\Pi]$, and higher order moments of porosity. The probability density of the porosity distribution over area and volume gives exhaustive information on a nonuniform structure.

Definition. A structure is called nonuniform, homogeneous, and isotropic if the porosity (translucence) probability distribution over area is unique, continuous, and single-modal for any section of a chaotic porous medium.

The simplest and most usual example of a nonuniform homogeneous isotropic porous medium is a disordered packing of identical spherical particles. The theorem given below without any proof (the derivation follows from [1]) defines the unique normal distribution for this packing.

Theorem 1. *Chaotic packings of identical spherical particles* $d_p = \text{const}$ *are nonuniform homogeneous isotropic structures with the following probability density of the porosity distribution* $0 \le \Pi_{\min} \le \Pi \le \Pi_{\max} \le 1$:

$$W(\Pi) = \frac{1}{\sqrt{2\pi}\sigma_1}\exp\left[-\frac{(\Pi-\overline{\Pi})^2}{2\sigma_1^2}\right], \qquad (1)$$

where

$$\sigma_1^2 = D[\Pi] = \frac{(\Pi_{\max}-\overline{\Pi})}{(\Pi_{\max}-\Pi_{\min})}K,$$

$K = \dfrac{\pi d_p^2}{6S}$ *and* $\dfrac{\pi d_p^3}{6V}$ *for area and volume, respectively.*

A simple but important corollary follows from the theorem: the mean value of porosity over the ensemble $\langle\Pi\rangle = M[\Pi]$ is equal to the mean value over area and volume $\overline{\Pi}_V = \overline{\Pi}_S = \langle\Pi\rangle = \overline{\Pi}$.

It is known that the value of the mean porosity of the spherical packings is very stable when it is close to 0.4. Experimental data are given in [2–5]:

$\overline{\Pi}$ = 0.38–0.41 for a spherical packing without additional mechanical actions.

$\overline{\Pi}$ = 0.35–0.39 for a spherical packing with subsequent vibration or shaking.

The physical assumptions for theoretical justification are the following:

(i) $\Pi_{\min} = 0.26$ corresponds to the densest packing (hexagonal, fcc, and some nonlattice structures with the coordination number 12).

(ii) $\Pi_{\max} = 0.476$ and the coordination number 6 correspond to the least dense cubic packing. It is known that the stability limit for systems of chaotically arranged molecules is achieved for the density corresponding to the density of cubic packing [6].

Theorem 2. *In an infinite chaotic spherical packing obtained as a result of a mechanical action* (*mixing, vibration, etc.*) *in the gravitational field, the maximum of the entropy of the porosity probability distribution is achieved for* $\overline{\Pi} = 0.37$.

Proof. The entropy of the probability distribution for random porosity is

$$H = -\int_{-\infty}^{\infty} W(\Pi)\ln W_1(\Pi)d\Pi.$$

For a spherical packing, we have

$$H = \frac{1}{2}\ln(2\pi e\sigma_1^2).$$

Hence, $H_{\max} = \dfrac{1}{2}\ln\dfrac{\pi eK}{2}(\Pi_{\max} - \Pi_{\min})$ for $\overline{\Pi} = \dfrac{\Pi_{\min}+\Pi_{\max}}{2} = 0.37$. In the absence of a mechanical action, $\Pi_{\max}$ and $\overline{\Pi}$ increase slightly owing to the existence of unstable configurational inclusions that are less dense than a cubic packing.

1028-3358/02/4705-0370$22.00

Note that a similar result leading to an entropy maximum for $\overline{\Pi} = \frac{\Pi_{\min} + \Pi_{\max}}{2}$ is also valid for a discrete binomial distribution, which gives rise to a limiting normal distribution in theorem 1.

Theorem 3 (main structural theorem). *A chaotic porous medium is homogeneous and isotropic if and only if the porosity probability distribution density for an arbitrary area S of any section obeys the normal law*:

$$W(\Pi) = \frac{1}{\sqrt{2\pi}\sigma}\exp\left[-\frac{(\Pi - \overline{\Pi})}{2\sigma^2}\right],$$
$$\sigma^2 = D[\Pi] = \overline{\Pi}(1-\overline{\Pi})\frac{S_D}{S}, \quad (2)$$

where S_D is the dispersion area, which is an inherent parameter characterizing the nonuniformity of the porous structure.

Proof. Sufficiency follows from the definition of a homogeneous isotropic porous medium.

In order to prove necessity, we specify uniformly distributed random points N_0 on the section area S_0 (Fig. 1). Some points $N_{0,\Pi}$ are situated in pores, and the average porosity $\overline{\Pi}$ is defined as usual: $\overline{\Pi} = \frac{S_{0,\Pi}}{S_0}$, where $S_{0,\Pi}$ is the pore area in the section. The random quantity $\frac{N_{0,\Pi}}{N_0}$ satisfies the relation

$$\frac{N_{0,\Pi}}{N_0} = \frac{1}{N_0}\sum_{i=1}^{N_0}\xi_i$$

with a uniform distribution for

$$\xi = \begin{pmatrix} 1 & 0 \\ \overline{\Pi} & 1-\overline{\Pi} \end{pmatrix}.$$

The quantity $\frac{N_{0,\Pi}}{N_0}$ for $N_0 \longrightarrow \infty$ is asymptotically normal with the expectation $M\left[\frac{N_{0,\Pi}}{N_0}\right] = \overline{\Pi}$ and variance $D\left[\frac{N_{0,\Pi}}{N_0}\right] = \frac{\overline{\Pi}(1-\overline{\Pi})}{N_0}$. Then, e.g., according to the "rule of three sigma," we obtain

$$P\left(\left|\frac{N_{0,\Pi}}{N_0} - \overline{\Pi}\right| < 3\sqrt{\frac{\overline{\Pi}(1-\overline{\Pi})}{N_0}}\right) = 0.997.$$

This relation substantiates the application of the Monte Carlo method to determine the mean porosity when $N_0 \gg 1$. Let us consider a certain region with the area S, $S < S_0$ in a section; N is the common number of random points, N_Π is the number of random points in pores, and

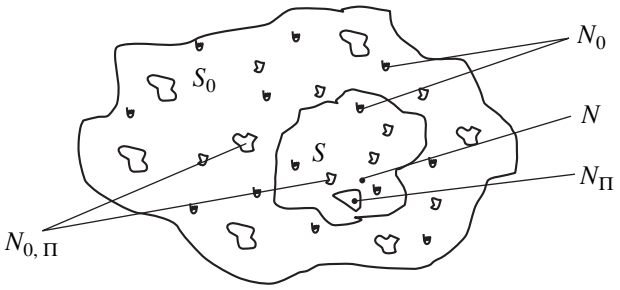

Illustration of the proof of the main structural theorem.

$\Pi = \frac{S_\Pi}{s}$ is the porosity of the region S. Then, it is simple to show that

$$P\left(\left|\frac{N}{N_0} - \frac{S}{S_0}\right| < \frac{3\left[\frac{S}{S_0}\left(1-\frac{S}{S_0}\right)\right]^{\frac{1}{2}}}{\sqrt{N_0}}\right) = 0.997,$$

$$W(N_\Pi) = \frac{C_{N_{0,\Pi}}^{N_\Pi} C_{N_0 - N_{0,\Pi}}^{N - N_\Pi}}{C_{N_0}^{N}}.$$

For $\frac{N}{N_0} \ll 1$, $\frac{N}{N_{0,\Pi}} \ll 1$, and $\frac{N}{N_0 - N_{0,\Pi}} \ll 1$, by applying the De Moivre–Laplace limit theorem and taking into account that $\frac{N_\Pi}{N} = \Pi$ for $N_\Pi, N \gg 1$, we have

$$W(\Pi) = \left[\frac{2\pi\overline{\Pi}(1-\overline{\Pi})}{N}\right]^{-\frac{1}{2}}\exp\left[-\frac{N(\Pi-\overline{\Pi})^2}{2\overline{\Pi}(1-\overline{\Pi})}\right].$$

In this case, $\frac{N}{N_0} = \frac{S}{S_0}$ or $\frac{N_0}{S_0} = \frac{N}{S} = \frac{1}{S_D}$ for any area S. Similarly, it is easy to show that $\frac{N_0}{S} = \frac{N_\Pi}{S_\Pi} = \frac{1}{S_D}$ for the corresponding pore area S_Π. Therefore, S_D is independent of area and porosity and is a characteristic of the structure. The theorem has been proven.

Corollary 1. *If S is a square* ($S = d_S^2$) *or a circle* ($S = \pi d_S^2$),

$$\sigma^2 = D[\Pi] = \overline{\Pi}(1-\overline{\Pi})\frac{d_D}{d_S}, \quad (3)$$

where d_D is the dispersion diameter, which is the main linear characteristic of the nonuniformity of the porous structure: $d_D^2 = S_D$ *and* $d_D^2 = \frac{4}{\pi}S_D$ *for a square and a circle, respectively.*

Corollary 2. *For chaotic homogeneous isotropic porous media, the probability distribution of porosity over volume obeys the normal law. The proof is similar.*

Corollary 3. *Of all continuous distributions, the normal distribution has the largest entropy for a given variance.*

This known result of calculus of variations thermodynamically explains the abundance of homogeneous isotropic porous systems in nature and the normal law of the porosity distribution in them.

Corollary 4. *The dispersion diameter for a spherical packing is defined by the formula*

$$d_D = \sqrt{\frac{4S_D}{\pi}} = \frac{\sigma d_S}{\sqrt{\overline{\Pi}(1-\overline{\Pi})}} = \left[\frac{2(\Pi_{\max}-\overline{\Pi})(\overline{\Pi}-\Pi_{\min})}{3(\Pi_{\max}-\Pi_{\min})(1-\overline{\Pi})\overline{\Pi}}\right]^{\frac{1}{2}} d_p, \quad (4)$$

which follows from Eqs. (1)–(3). *The equivalent diameter is defined by the known formula*

$$d_e = \frac{2\overline{\Pi}d_p}{3(1-\overline{\Pi})}. \quad (5)$$

For $\overline{\Pi} = 0.37$, $\Pi_{\min} = 0.26$, *and* $\Pi_{\max} = 0.476$, *Eqs.* (4) *and* (5) *yield* $d_e = 0.392d_p$ *and* $d_D = 0.394d_p$; *i.e., the equivalent diameter is almost equal to the dispersion diameter*: $d_e \approx d_D$.

This fact is important when using experimental data where d_e is the determining size.

Corollary 5. *The mean value* $\langle\Pi\rangle$ *of porosity over the ensemble is equal to the mean value* $\overline{\Pi}_S$ *of porosity over area and, since* $V_{[a,b]} = \int_a^b S(x)dx$, *to the mean value* $\overline{\Pi}_V$ *over volume. The ergodicity has been proven*:

$$\langle\Pi\rangle = M[\Pi] = \overline{\Pi}_S = \overline{\Pi}_V = \overline{\Pi}.$$

The chaotic deviations of local porosity values from the mean value cause the appearance of macrodispersion flows, which are primarily responsible for the heat- and mass-exchange processes in nonuniform porous structures.

REFERENCES

1. V. M. Polyaev and A. P. Mozhaev, Dokl. Akad. Nauk **343**, 46 (1995) [Phys. Dokl. **40**, 336 (1995)].
2. M. A. Gol'dshtik, *Transfer Processes in a Granular Layer* (Inst. Tepl. Fiz. Sibirsk. Otd. Akad. Nauk SSSR, Novosibirsk, 1984).
3. G. D. Scott, Nature (London) **188**, 908 (1960).
4. J. D. Bernar and J. L. Finney, Nature (London) **214**, 265 (1967).
5. R. J. Greet, J. Appl. Phys. **37**, 4377 (1966).
6. Z. I. Fisher, *Statistical Theory of Liquids* (Fizmatgiz, Moscow, 1961).

Translated by T. Galkina

Doklady Physics, Vol. 47, No. 5, 2002, pp. 373–376. Translated from Doklady Akademii Nauk, Vol. 384, No. 1, 2002, pp. 43–46.

MECHANICS

Control of Quasi-Linear Dynamical Systems with Two Degrees of Freedom

S. V. Volkov

Presented by Academician V.V. Kozlov December 25, 2001

Received January 9, 2002

1. INTRODUCTION

The method of synthesizing dynamical systems that have a given structure of partition in trajectories on a C_1-class plane [1, 2] can be used for the analytical construction of controls that ensure the desired properties of motion of mechanical systems. These systems are described by equations of the form

$$\begin{aligned} a_{11}\ddot{q}_1 + a_{12}\ddot{q}_{12} + b_1\sin q_1 + c_{11}q_1 + c_{12}q_2 &= \mu(f + u_1), \\ a_{21}\ddot{q}_1 + a_{22}\ddot{q}_2 + b_2\sin q_2 + c_{21}q_1 + c_{22}q_2 &= \mu(g + u_2). \end{aligned} \tag{1.1}$$

Here, μ is a small parameter; f and g are nonlinear functions of the variables q_1, q_2, $\dot{q}_1$, $\dot{q}_2$, and t; and u_1, u_2 are the controls. This is illustrated below by solving the matching problem for slowly varying oscillation amplitudes of two coupled pendulums (Fig. 1). This problem is inverse with respect to the problem considered in Section 3, Chapter 5 of [3].

2. FORMULATION OF THE PROBLEM

Let φ and ψ be the angles of deviation from a vertical line for the first and second pendulums with masses m_1 and m_2. Let c, l, and d also be, respectively, the spring rigidity, the pendulum length, and the distance between the pendulum rotation axis and the spring fixation point. We seek the moments U_1 and U_2, which possess the following properties. The system has a stable (in large) biharmonic motion with amplitudes a and b periodically varying under the action of these moments on the first and the second pendulums, respectively. These amplitudes are related to each other by the condition $\omega_0(a, b) = 0$, which corresponds to the stable limiting cycle of the given partition scheme in the trajectories for the first quadrant of the plane (a, b), Fig. 2. Using the equalities

$$\begin{aligned} \omega_1 \equiv a &= 0, \quad \omega_2 \equiv b = 0, \\ \omega_3 \equiv (a-1)^2 + (b-1)^2 &= 0; \end{aligned} \tag{2.1}$$

$$\begin{aligned} \omega_0 \equiv \omega(a, b, 0.9) &= 0, \\ \omega(a, b, \lambda) \equiv -(1-\lambda)\omega_1\omega_2 + \lambda\omega_3 &= 0 \end{aligned} \tag{2.2}$$

we specify other special trajectories contained in this region. Here, $\omega_1 = 0$ and $\omega_2 = 0$ are the separatrix straight lines and $\omega_3 = 0$ is the unstable focus located inside the limiting cycle $\omega_0 = 0$.

3. SOLUTION OF THE PROBLEM

The pendulum system is described by the following equations of motion:

$$\begin{aligned} m_1l^2\ddot{\varphi} + m_1gl\sin\varphi + cd^2\varphi - cd^2\psi &= M_1(\varphi, \dot{\varphi}, \psi, \dot{\psi}, t) + U_1, \\ m_2l^2\ddot{\psi} + m_2gl\sin\psi + cd^2\psi - cd^2\varphi &= M_2(\varphi, \dot{\varphi}, \psi, \dot{\psi}, t) + U_2. \end{aligned} \tag{3.1}$$

Here, M_1, M_2 are the moments of force, which do not

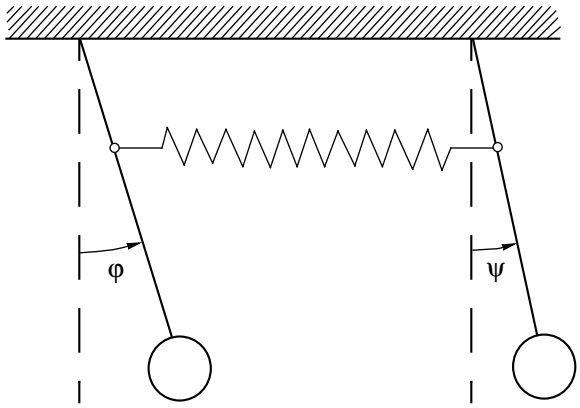

Fig. 1.

Peoples' Friendship University,
ul. Miklukho-Maklaya 6, Moscow, 117198 Russia

1028-3358/02/4705-0373$22.00 © 2002 MAIK "Nauka/Interperiodica"

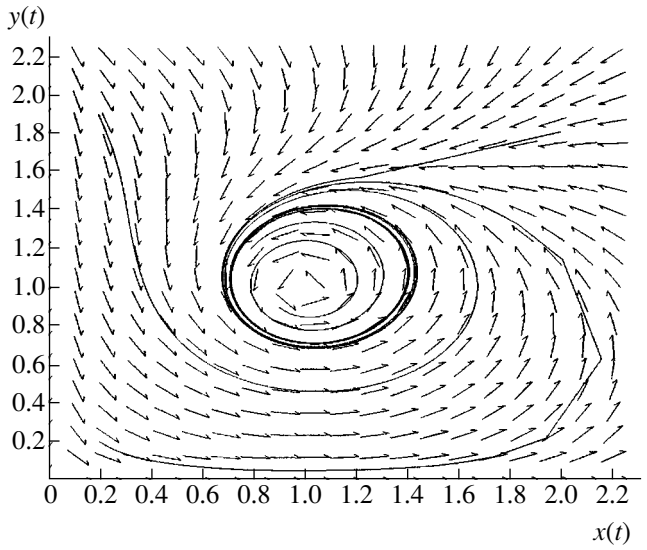

Fig. 2.

enter into the left-hand sides of Eqs. (3.1). We use the following notation:

$$n_1^2 = \frac{g}{l} + \frac{cd^2}{m_1 l^2}, \quad n_2^2 = \frac{g}{l} + \frac{cd^2}{m_2 l^2},$$

$$B_1 = -\frac{cd^2}{m_1 l^2}, \quad B_2 = -\frac{cd^2}{m_2 l^2}.$$

Then system (3.1) can be transformed to the form

$$\begin{aligned} \ddot{\varphi} + B_1\psi + n_1^2\varphi &= \frac{g}{l}(\varphi - \sin\varphi) + \frac{1}{m_1 l^2}(M_1 + U_1), \\ \ddot{\psi} + B_2\varphi + n_2^2\varphi &= \frac{g}{l}(\psi - \sin\psi) + \frac{1}{m_2 l^2}(M_2 + U_2). \end{aligned} \tag{3.2}$$

For reasonably small values of the right-hand sides of Eqs. (3.2), the solution to this system is sought in the form

$$\begin{aligned} \varphi &= a\sin(k_1 t + \beta_1) + b\sin(k_2 t + \beta_2), \\ \psi &= \alpha_1 a\sin(k_1 t + \beta_1) + \alpha_2 b\sin(k_2 t + \beta_2). \end{aligned} \tag{3.3}$$

Here, a, b, β_1, β_2 are slowly varying functions of time and k_1, k_2 are the principal frequencies, which can be found from the frequency equation

$$k^4 - (n_1^2 + n_2^2)k^2 + n_1^2 n_2^2 - B_1 B_2 = 0.$$

We assume that $0 < k_1 < k_2$, and α_1, α_2 are the distribution coefficients:

$$\alpha_1 = \frac{k_1^2 - n_1^2}{B_1} = \frac{B_2}{k_1^2 - n_2^2}, \quad \alpha_2 = \frac{k_2^2 - n_1^2}{B_1} = \frac{B_2}{k_2^2 - n_2^2}. \tag{3.4}$$

We suppose that the first derivatives of φ and ψ with respect to time have the same form as for constant a, b, β_1, β_2. In other words,

$$\begin{aligned} \dot{\varphi} &= ak_1\cos(k_1 t + \beta_1) + bk_2\cos(k_2 t + \beta_2), \\ \dot{\psi} &= a\alpha_1 k_1\cos(k_1 t + \beta_1) + b\alpha_2 k_2\cos(k_2 t + \beta_2). \end{aligned} \tag{3.5}$$

Then, the following additional conditions imposed on the variables a, b, β_1, β_2 can be obtained:

$$\begin{aligned} &\dot{a}\sin(k_1 t + \beta_1) + \dot{b}\sin(k_2 t + \beta_2) \\ &+ a\dot{\beta}_1\cos(k_1 t + \beta_1) + b\dot{\beta}_2\cos(k_2 t + \beta_2) = 0, \\ &\alpha_1\dot{a}\sin(k_1 t + \beta_1) + \alpha_2\dot{b}\sin(k_2 t + \beta_2) \\ &+ \alpha_1 a\dot{\beta}_1\cos(k_1 t + \beta_1) + \alpha_2 b\dot{\beta}_2\cos(k_2 t + \beta_2) = 0. \end{aligned} \tag{3.6}$$

Differentiating derivatives (3.5) with respect to time, we find

$$\begin{aligned} \ddot{\varphi} &= \dot{a}k_1\cos(k_1 t + \beta_1) - ak_1(k_1 + \dot{\beta}_1)\sin(k_1 t + \beta_1) \\ &+ \dot{b}k_2\cos(k_2 t + \beta_2) - bk_2(k_2 + \dot{\beta}_2)\sin(k_2 t + \beta_2), \\ \ddot{\psi} &= \dot{a}\alpha_1 k_1\cos(k_1 t + \beta_1) \\ &- a\alpha_1 k_1(k_1 + \dot{\beta}_1)\sin(k_1 t + \beta_1) \\ &+ \dot{b}\alpha_2 k_2\cos(k_2 t + \beta_2) - b\alpha_2 k_2(k_2 + \dot{\beta}_2)\sin(k_2 t + \beta_2). \end{aligned}$$

We now substitute these expressions for $\ddot{\varphi}$ and $\ddot{\psi}$ into Eqs. (3.2). By taking into account relationships (3.4), the system of equations obtained together with equalities (3.6) can be solved with respect to $\dot{a}$, $\dot{b}$, $a\dot{\beta}_1$, $b\dot{\beta}_2$ [3]:

$$\begin{aligned} \dot{a} &= \frac{1}{k_1(k_1^2 - k_2^2)}\left(\frac{B_2}{\alpha_1}f^* + B_1 g^*\right)\cos\xi, \\ \dot{b} &= -\frac{1}{k_2(k_1^2 - k_2^2)}\left(\frac{B_2}{\alpha_2}f^* + B_1 g^*\right)\cos\eta, \\ a\dot{\beta}_1 &= -\frac{1}{k_1(k_1^2 - k_2^2)}\left(\frac{B_2}{\alpha_1}f^* + B_1 g^*\right)\sin\xi, \\ b\dot{\beta}_2 &= \frac{1}{k_2(k_1^2 - k_2^2)}\left(\frac{B_2}{\alpha_2}f^* + B_1 g^*\right)\sin\eta. \end{aligned} \tag{3.7}$$

Here,

$$\xi = k_1 t + \beta_1, \quad \eta = k_2 t + \beta_2,$$

$$\begin{aligned} f(\varphi, \psi, \dot{\varphi}, \dot{\psi}) &= \frac{g}{l}(\varphi - \sin\varphi) + \frac{1}{m_1 l^2}(M_1 + U_1), \\ g(\varphi, \psi, \dot{\varphi}, \dot{\psi}) &= \frac{g}{l}(\psi - \sin\psi) + \frac{1}{m_2 l^2}(M_2 + U_2), \end{aligned} \tag{3.8}$$

and f^*, g^* denote the same functions in which φ, ψ, $\dot\varphi$, $\dot\psi$ are replaced by their expressions from Eqs. (3.3) and (3.5).

To solve the posed problem, we make up the system of equations

$$\dot a = \mu A(a, b), \quad \dot b = \mu B(a, b), \quad \mu \ge 0, \qquad (3.9)$$

which has a given structure of the partition in trajectories of the region $a > 0$, $b > 0$ (Fig. 2). By equating the right-hand sides of the corresponding equations (3.7) and (3.9), we arrive at

$$\begin{aligned} -\left(\frac{B_2}{\alpha_1 k_1} f^* + \frac{B_1}{k_1} g^*\right)\cos\xi &= \mu_1 A, \\ \left(\frac{B_2}{\alpha_2 k_2} f^* + \frac{B_1}{k_1} g^*\right)\cos\eta &= \mu_1 B, \end{aligned} \qquad (3.10)$$

where $\mu = \dfrac{\mu_1}{k_2^2 - k_1^2}$. Taking $\mu_1 = \mu_2 \cos^2\xi \cos^2\eta$ in Eqs. (3.10), we solve these equations with respect to f^* and g^*:

$$\begin{aligned} f^* &= \frac{\alpha_1\alpha_2\mu_2}{B_2(\alpha_1 - \alpha_2)}(Ak_1\cos\eta + Bk_2\cos\xi)\cos\xi\cos\eta, \\ g^* &= -\frac{\mu_2}{B_1(\alpha_1 - \alpha_2)} \\ &\times (A\alpha_1 k_1\cos\eta + B\alpha_2 k_2\cos\xi)\cos\xi\cos\eta. \end{aligned} \qquad (3.11)$$

After substituting the expressions for f^* and g^* from (3.11) into (3.7), we obtain

$$\begin{aligned} \dot a &= \mu_2 A\cos^2\xi\cos^2\eta, \quad \dot b = \mu_2 B\cos^2\xi\cos^2\eta, \\ a\dot\beta_1 &= -\mu_2 A\cos\xi\sin\xi\cos^2\eta, \\ b\dot\beta_2 &= -\mu_2 B\cos^2\xi\cos\eta\sin\eta. \end{aligned} \qquad (3.12)$$

With allowance for the fact that a, b, β_1, β_2 vary slowly (in the case of a corresponding choice of μ_2), we average the right-hand sides of Eqs. (3.12) over the periods $\dfrac{2\pi}{k_1}$ and $\dfrac{2\pi}{k_2}$. As a result, we arrive at the reduced equations

$$\dot a = \mu_2 A, \quad \dot b = \mu_2 B, \quad \dot\beta_1 = 0, \quad \dot\beta_2 = 0. \qquad (3.13)$$

The system of equations (3.13) has the following solutions: $\beta_1 = 0$, $\beta_2 = 0$, and a, b such that their variations are represented by the given partition in trajectories of the region $a > 0$ and $b > 0$ in the plane (a, b) (Fig. 2).

Using relations (3.3) and (3.5), the variables a, b and functions $\cos\xi$, $\cos\eta$ can be expressed in terms of φ, ψ, $\dot\varphi$, and $\dot\psi$:

$$a = \left[\frac{k_1^2(\alpha_2\varphi - \psi)^2 + (\alpha_2\dot\varphi - \dot\psi)^2}{k_1^2(\alpha_1 - \alpha_2)^2}\right]^{1/2},$$

$$b = \left[\frac{k_2^2(\alpha_1\varphi - \psi)^2 + (\alpha_1\dot\varphi - \dot\psi)^2}{k_2^2(\alpha_1 - \alpha_2)^2}\right]^{1/2},$$

$$\cos\xi = \frac{\alpha_2\varphi - \psi}{k_1(\alpha_1 - \alpha_2)}\left[\frac{k_1^2(\alpha_2\varphi - \psi)^2 + (\alpha_2\dot\varphi - \dot\psi)^2}{k_1^2(\alpha_1 - \alpha_2)^2}\right]^{1/2},$$

$$\cos\eta = \frac{\alpha_1\dot\varphi - \dot\psi}{k_2(\alpha_1 - \alpha_2)}\left[\frac{k_2^2(\alpha_1\varphi - \psi)^2 + (\alpha_1\dot\varphi - \dot\psi)^2}{k_2^2(\alpha_1 - \alpha_2)^2}\right]^{1/2}.$$

Passing to the variables φ, ψ, $\dot\varphi$, and $\dot\psi$ in (3.11), we obtain

$$f_p = \mu_2 F(\varphi, \psi, \dot\varphi, \dot\psi), \quad g_p = \mu_2 G(\varphi, \psi, \dot\varphi, \dot\psi).$$

Finally, equating the right-hand sides of equalities (3.8) to f_p and g_p, respectively, we find the desired controlling moments

$$U_1 = \mu_2 F - \frac{g}{l}(\varphi - \sin\varphi) - M_1,$$

$$U_2 = \mu_2 G - \frac{g}{l}(\psi - \sin\psi) - M_2.$$

Here, the arbitrary nonnegative factor μ_2 is chosen to satisfy the smallness requirement for the right-hand sides of the equations composing system (3.2).

4. CONSTRUCTION OF EQUATIONS FOR PROGRAMMED AMPLITUDE VARIATIONS

In order to construct (by the method of [2]) the vector fields for comparison directions, which correspond to a set of special trajectories defined by Eqs. (2.1), we explicitly express the parameter λ from (2.2):

$$\lambda = -\frac{\omega_1\omega_2}{\omega_3 - \omega_1\omega_2} \equiv \Omega.$$

Then, we calculate the partial derivatives of the function Ω:

$$\frac{\partial\Omega}{\partial a} = \frac{b[(a-1)^2 + (b-1)^2 - 2a(a-1)]}{[(a-1)^2 + (b-1)^2 + ab]^2},$$

$$\frac{\partial\Omega}{\partial b} = \frac{a[(a-1)^2 + (b-1)^2 - 2b(b-1)]}{[(a-1)^2 + (b-1)^2 + ab]^2},$$

where we have taken

$$\begin{aligned} \mathbf{n} &= \{n_a; n_b\}, \quad \boldsymbol{\tau} = \{n_b; -n_a\}, \\ n_a &= b[(a-1)^2 + (b-1)^2 - 2a(a-1)], \\ n_b &= a[(a-1)^2 + (b-1)^2 - 2b(b-1)]. \end{aligned} \qquad (4.1)$$

We now construct functions of the scalar products of these vectors by the vector $\mathbf{P} = \{A, B\}$ for the right-hand sides of the equations of system (3.8) which determine

the partition in trajectories of the region $a > 0, b > 0$ for the given structure (Fig. 2). In particular, the functions

$$F_1 = \mathbf{P} \cdot \mathbf{n} = \xi_1 \omega_0 \omega_1 \omega_2 \omega_3, \quad F_2 = \mathbf{P} \cdot \boldsymbol{\tau} = \xi_2 \omega_3 \tag{4.2}$$

are of this kind, where we take $\xi_1 > 0$, which corresponds to the stable limiting cycle $\omega_0 = 0$, and $\xi_2 > 0$, which corresponds to the motion of the representation points around the point $\omega_2 = 0$ in a counterclockwise direction. The right-hand sides

$$\begin{aligned} A &= \xi_1 \omega_0 \omega_1 \omega_2 \omega_3 b[(a-1)^2 + (b-1)^2 - 2a(a-1)] \\ &\quad + \xi_2 \omega_3 a[(a-1)^2 + (b-1)^2 - 2b(b-1)], \\ B &= \xi_1 \omega_0 \omega_1 \omega_2 \omega_3 a[(a-1)^2 + (b-1)^2 - 2b(b-1)] \\ &\quad + \xi_2 \omega_3 b[(a-1)^2 + (b-1)^2 - 2a(a-1)] \end{aligned} \tag{4.3}$$

of the desired system correspond to the functions F_1 and F_2 from (4.2).

The correctness of the construction of the functions F_1, F_2 from (4.2) and A, B from (4.3) is supported by plotting Figs. 1 and 2 with the help of a computer using the Maple V Release 5 applied software package.

Remark. A method is developed in [1] for synthesizing systems of equations in form (3.8) of the C_1 class which have more complicated structures for the partition in trajectories.

ACKNOWLEDGMENTS

This study was supported by the Ministry of Education of the Russian Federation, project no. 020702-2-075.

REFERENCES

1. S. V. Volkov, *The Construction of Differential Operators of Dynamical Systems* (Izd. Ross. Univ. Druzhby Narodov, Moscow, 1999).
2. S. V. Volkov, *Construction of Sets of Differential Equations by Partitions on a Trajectory of Convex Polygonal Region in R^2*. Available from VINITI, 1984, Moscow, No. 6524-84.
3. N. V. Butenin, Yu. I. Neĭmark, and N. A. Fufaev, *Introduction to the Theory of Nonlinear Oscillations* (Nauka, Moscow, 1987).

Translated by V. Tsarev

Doklady Physics, Vol. 47, No. 5, 2002, pp. 377–381. Translated from Doklady Akademii Nauk, Vol. 384, No. 1, 2002, pp. 47–51.

MECHANICS

Two Classes of Partial Stability Problems: Unification of the Notions and Common Conditions of Solvability

V. I. Vorotnikov

Presented by Academician V.V. Rumyantsev January 8, 2002

Received January 8, 2002

For nonlinear nonautonomous systems of ordinary differential equations, we consider two basic classes of partial stability problems: (i) problems of stability with respect to variables of the zero equilibrium position (Lyapunov–Rumyantsev partial stability problems) and (ii) problems of stability of "partial" equilibrium positions. The corresponding definitions of stability are unified so that the solvability conditions for these two classes of problems are identical in the context of the Lyapunov function method. We present a number of such common stability conditions. The results are illustrated by examples.

1. TWO BASIC CLASSES OF PARTIAL STABILITY PROBLEMS

Since the middle of the 20th century, the theory of partial stability has been actively developing along with conventional investigations in the theory of stability. A special feature of the former theory is analysis of the stability of the processes in dynamic systems with respect to only a fraction of the variables (instead of all the variables) specifying the state of these systems.

The theory of partial stability investigates the following two basic classes of problems.

1. The Lyapunov–Rumyantsev problems [1–10] of stability with respect to the components of a vector $\mathbf{y}$ (problems of $\mathbf{y}$-stability) of the equilibrium position $\mathbf{x} = (\mathbf{y}^T, \mathbf{z}^T)^T = \mathbf{0}$ of the system of ordinary differential equations

$$\dot{\mathbf{y}} = \mathbf{Y}(t, \mathbf{y}, \mathbf{z}), \quad \dot{\mathbf{z}} = \mathbf{Z}(t, \mathbf{y}, \mathbf{z}), \tag{1}$$

under quite general assumptions about the vector functions $\mathbf{Y}$, $\mathbf{Z}$. Hereafter, T means transposition.

In this case, the following conditions occur:

$$\mathbf{Y}(t, \mathbf{0}, \mathbf{0}) \equiv \mathbf{0}, \quad \mathbf{Z}(t, \mathbf{0}, \mathbf{0}) \equiv \mathbf{0}. \tag{2}$$

Nizhniĭ Tagil Technology Institute,
Ural State Technical University, ul. Krasnogvardeĭskaya 59, Nizhniĭ Tagil, 622006 Russia

System (1), (2) is constructed as the system describing a disturbed motion for each particular process whose stability is studied, and the notion of stability is correspondingly formalized mathematically.

Let $\mathbf{x}(t) = \mathbf{x}(t; t_0, \mathbf{x}_0)$ be the solution of system (1) with the initial condition $\mathbf{x}_0 = \mathbf{x}(t_0; t_0, \mathbf{x}_0)$.

Definition 1. The equilibrium position $\mathbf{x} = \mathbf{0}$ of set (1), (2) is

(i) $\mathbf{y}$-stable if, for arbitrary $\varepsilon > 0$ and $t_0 \geq 0$, there is $\delta(\varepsilon, t_0) > 0$ such that $\|\mathbf{y}(t; t_0, \mathbf{x}_0)\| < \varepsilon$ for all $t \geq t_0$ follows from $\|\mathbf{x}_0\| < \delta$;

(ii) uniformly $\mathbf{y}$-stable if δ is independent of t_0;

(iii) asymptotically $\mathbf{y}$-stable if it is $\mathbf{y}$-stable and, for arbitrary $t_0 \geq 0$, there is $\Delta(t_0) > 0$ such that the relationship

$$\lim \|\mathbf{y}(t; t_0, \mathbf{x}_0)\| \longrightarrow 0, \quad t \longrightarrow \infty \tag{3}$$

takes place for any solution $\mathbf{x}(t; t_0, \mathbf{x}_0)$ of system (1), (2), for which $\|\mathbf{x}_0\| < \Delta$;

(iv) uniformly asymptotically $\mathbf{y}$-stable if it is uniformly $\mathbf{y}$-stable, Δ is independent of t_0, and Eq. (3) is satisfied uniformly with respect to t_0, $\mathbf{x}_0$.

2. The problems of stability of partial equilibrium positions [3, 9–11], i.e., the problems of stability (with respect to components of the vector $\mathbf{y}$) of partial equilibrium positions $\mathbf{y} = \mathbf{0}$ of set (1).

In this case, the condition

$$\mathbf{Y}(t, \mathbf{0}, \mathbf{z}) \equiv \mathbf{0} \tag{4}$$

is valid and the position $\mathbf{y} = \mathbf{0}$ is the invariant set of this system if the solution of system (1) is unique.

Definition 2. The partial equilibrium position $\mathbf{y} = \mathbf{0}$ of system (1), (4) is

(i) stable if, for arbitrary $\varepsilon > 0$ and $t_0 \geq 0$, it is possible to find $\delta(\varepsilon, t_0) > 0$ such that $\|\mathbf{y}(t; t_0, \mathbf{x}_0)\| < \varepsilon$ for all $t \geq t_0$ follows from $\|\mathbf{y}_0\| < \delta$ and $\|\mathbf{z}_0\| < \infty$;

(ii) asymptotically stable if it is stable and it is possible to find $\Delta(t_0) > 0$ for arbitrary $t_0 \geq 0$ such that

1028-3358/02/4705-0377$22.00

Eq. (3) is satisfied for any solution $\mathbf{x}(t; t_0, \mathbf{x}_0)$ of set (1), (4) with $\|\mathbf{y}_0\| < \Delta$ and $\|\mathbf{z}_0\| < \infty$.

Similar to definition 1, we introduce the notion of uniform stability (including uniform asymptotic stability).

Remarks. 1°. Under condition (4), set (1) need not have the zero equilibrium position $\mathbf{x} = \mathbf{0}$.

2°. The Lyapunov–Rumyantsev problems of partial stability do not generally reduce [10] to any problems of stability of sets [12, 13], whereas the problems of stability of partial equilibrium positions are problems of the stability of invariant sets. Nevertheless, the indicated problems can be brought together and their solvability conditions can be made identical by a certain mutual modification of the notions of Lyapunov–Rumyantsev partial stability and the stability of partial equilibrium positions.

2. UNIFICATION OF THE NOTION OF PARTIAL STABILITY

To establish the relation between the two types of partial stability problems, we somewhat modify definition 1 of **y**-stability of the equilibrium position $\mathbf{x} = \mathbf{0}$ for system (1), (2).

Definition 3. The equilibrium position $\mathbf{x} = \mathbf{0}$ of system (1), (2) is

(i) **y**-stable for large $\mathbf{z}_0$ if, for arbitrary $\varepsilon > 0$, $t_0 \geq 0$, and $L > 0$, it is possible to find $\delta(\varepsilon, t_0, L) > 0$ such that $\|\mathbf{y}(t; t_0, \mathbf{x}_0)\| < \varepsilon$ for all $t \geq t_0$ follows from $\|\mathbf{y}_0\| < \delta$ and $\|\mathbf{z}_0\| < L$;

(ii) asymptotically **y**-stable for large $\mathbf{z}_0$ if this position is **y**-stable for large $\mathbf{z}_0$ and, for arbitrary $t_0 \geq 0$, it is possible to find $\Delta(t_0, L) > 0$ such that Eq. (3) is satisfied for any solution of system (1), (2) with $\|\mathbf{y}_0\| < \Delta$ and $\|\mathbf{z}_0\| < L$.

Similarly, we introduce the notion of uniform **y**-stability (including uniform asymptotic **y**-stability) for large $\mathbf{z}_0$.

An opposing step for unifying the notions is the corresponding refinement of the notion of stability of partial equilibrium positions.

Definition 4. The partial equilibrium position $\mathbf{y} = \mathbf{0}$ of system (1), (4), is

(i) stable for large $\mathbf{z}_0$ if, for arbitrary $\varepsilon > 0$, $t_0 \geq 0$, and $L > 0$, it is possible to find $\delta(\varepsilon, t_0, L) > 0$ such that $\|\mathbf{y}(t; t_0, \mathbf{x}_0)\| < \varepsilon$ for all $t \geq t_0$ follows from $\|\mathbf{y}_0\| < \delta$ and $\|\mathbf{z}_0\| < L$;

(ii) asymptotically stable for large $\mathbf{z}_0$ if it is stable for large $\mathbf{z}_0$ and it is possible to find $\Delta(t_0, L) > 0$ for arbitrary $t_0 \geq 0$ such that Eq. (3) is satisfied for any solution of system (1), (2) with $\|\mathbf{y}_0\| < \Delta$ and $\|\mathbf{z}_0\| < L$.

The notion of uniform stability (including uniform asymptotic stability) for large $\mathbf{z}_0$ is similarly introduced.

3. COMMON CONDITIONS OF PARTIAL STABILITY IN THE CONTEXT OF THE LYAPUNOV DIRECT METHOD

One of the basic methods of investigating the problems of stability is the Lyapunov function method, also often called the Lyapunov direct method. The modification carried out in Section 2 for the notions makes it possible to give the common solvability conditions for the two classes of problems of partial stability in the context of the LFM.

We introduce the assumptions [1–3], which are conventional for the theory of partial stability, that system (1) is continuous in the region

$$t \geq 0, \quad \|\mathbf{y}\| \leq h, \quad \|\mathbf{z}\| < \infty \tag{5}$$

and its solutions are unique and **z**-continuable. We consider the following functions: (i) $a(r)$, which is continuous and steadily increasing for $r \in [0, h]$ such that $a(0) = 0$, (ii) and the scalar continuous function $V(t, \mathbf{x})$, $V(t, \mathbf{0}) \equiv 0$ and the vector function $\mathbf{W}(t, \mathbf{x})$, $\mathbf{W}(t, \mathbf{0}) \equiv \mathbf{0}$, which is continuously differentiable in region (5).

Theorem 1. *Let there be a scalar function V and a vector function* $\mathbf{W} = \mathbf{W}(t, \mathbf{x})$, $\mathbf{W}(t, \mathbf{0}) \equiv \mathbf{0}$ *such that, in the region*

$$t \geq 0, \quad \|\mathbf{y}\| + \|\mathbf{W}(t, \mathbf{x})\| \leq h, \quad \|\mathbf{z}\| < \infty, \tag{6}$$

the conditions

$$V(t, \mathbf{y}, \mathbf{z}) \geq a(\|\mathbf{y}\| + \|\mathbf{W}(t, \mathbf{x})\|), \quad V(t, \mathbf{0}, \mathbf{z}) \equiv 0, \tag{7}$$

$$\dot{V}(t, \mathbf{x}) \leq 0 \tag{8}$$

are satisfied. In this case, (i) *condition* (4) *is valid for set* (1)*, and the partial equilibrium position* $\mathbf{y} = \mathbf{0}$ *of system* (1), (4) *is stable for large* $\mathbf{z}_0$ (ii) *and the equilibrium position* $\mathbf{x} = \mathbf{0}$ *of system* (1), (2) *is* **y***-stable for large* $\mathbf{z}_0$.

The **proof** of this theorem is divided into two stages.

(i) Let us show that condition (4) is valid if conditions (7) and (8) are satisfied. We consider the solution $\mathbf{x}(t; t_0, \mathbf{0}, \mathbf{z}_0)$ of system (1) for arbitrary $t_0 \geq 0$ and $\mathbf{z}_0$. By virtue of Eqs. (7), $V(t_0, \mathbf{0}, \mathbf{z}_0) \equiv 0$.

On the basis of the equality

$$V(t, \mathbf{x}(t; t_0, \mathbf{x}_0)) = V(t_0, \mathbf{x}_0) + \int_{t_0}^{t} \dot{V}(\tau, \mathbf{x}(\tau; t_0, \mathbf{x}_0))d\tau \tag{9}$$

and the inequalities $V \geq 0$ and $\dot{V} \leq 0$, we obtain that

$$V(t, \mathbf{x}(t; t_0, \mathbf{0}, \mathbf{z}_0)) \equiv 0. \tag{10}$$

In view of the first of Eqs. (7), it follows from Eq. (10) that

$$\mathbf{y}(t; t_0, \mathbf{0}, \mathbf{z}_0) \equiv 0. \tag{11}$$

Let us prove that identities (4) and (11) are equivalent.

We substitute the solution $\mathbf{x}(t; t_0, \mathbf{0}, \mathbf{z}_0)$ into system (1). Taking into account Eq. (11) and the arbitrariness of $t_0 \geq 0$ and $\mathbf{z}_0$, we arrive at identity (4).

Conversely, if identity (4) is satisfied, system (1) admits the equilibrium position $\mathbf{y} = \mathbf{0}$. Taking into account the assumption that the solution of system (1) is unique, we have identity (11) in this case.

(ii) We show that the partial equilibrium position $\mathbf{y} = \mathbf{0}$ of system (1) is $\mathbf{y}$-stable for large $\mathbf{z}_0$ if conditions (7), (8) are satisfied.

By virtue of the conditions $V(t, \mathbf{0}, \mathbf{0}) \equiv V(t, \mathbf{0}, \mathbf{z}) \equiv 0$ for arbitrary $\varepsilon > 0$, $t_0 \geq 0$ and $L > 0$, it is possible to find $\delta(\varepsilon, t_0, L) > 0$ such that $V(t_0, \mathbf{x}_0) < a(\varepsilon)$ follows from $\|\mathbf{y}_0\| < \delta$ and $\|\mathbf{z}_0\| < L$.

Taking into account inequality (8) and Eq. (9), we have

$$\begin{aligned} &a(\|\mathbf{y}(t; t_0, \mathbf{x}_0)\| + \|\mathbf{W}(t, \mathbf{x}(t; t_0, \mathbf{x}_0))\|) \\ &\leq V(t, \mathbf{x}(t; t_0, \mathbf{x}_0)) \leq V(t_0, \mathbf{x}_0) < a(\varepsilon) \end{aligned} \tag{12}$$

for all $t \geq t_0$.

By virtue of the properties of the function $a(r)$, inequalities (12) indicate that $\|\mathbf{y}(t; t_0, \mathbf{x}_0)\| < \varepsilon$ follows from $\|\mathbf{y}_0\| < \delta$ and $\|\mathbf{z}_0\| < L$ for arbitrary $\varepsilon > 0$, $t_0 \geq 0$, and $t \geq t_0$. The theorem has been proven.

Discussion of theorem 1. (i) If conditions (7) are supplemented by the assumption that $V(t, \mathbf{x}) \leq b(\|\mathbf{x}\|)$ [$b(r)$ is a function of the same type as $a(r)$], the stability in theorem 1 is uniform. If conditions (7) are supplemented by the assumption that $V(t, \mathbf{x}) \leq b(\|\mathbf{y}\|)$, the conditions of theorem 1 guarantee the corresponding properties of uniform stability as a whole with respect to $\mathbf{z}_0$ ($L = \infty$ in definitions 2 and 3) [3, 10]. In this connection, we emphasize that the conditions $V(t, \mathbf{0}) \equiv \mathbf{0}$ and $V(t, \mathbf{x}) \leq b(\|\mathbf{x}\|)$ are weaker than the condition $V(t, \mathbf{x}) \leq b(\|\mathbf{y}\|)$.

(ii) If condition (7) is satisfied, the function V is not, generally speaking, $\mathbf{y}$-positive definite in Rumyantsev's sense [2, 3], because the condition $V(t, \mathbf{y}, \mathbf{z}) \geq a(\|\mathbf{y}\|)$ does not have to be valid in region (5) [8].

(iii) As a further unification of definitions 2 and 3, we may introduce a more general notion of $\mathbf{y}$-stability (asymptotic $\mathbf{y}$-stability) of the set $\mathbf{x} = \mathbf{0}$ for large $\mathbf{z}_0$ without the assumption that this set is an equilibrium state of system (1). Such a notion was introduced in [14] in connection with problems of coordinate synchronization of dynamic systems [15] in the context of the theory of partial stability.

Example 1. Let system (1) consist of the equations

$$\begin{aligned} \dot{y}_1 &= y_2^2 z_1, \quad \dot{y}_2 = a y_2 + y_1 y_2^2 z_1, \\ \dot{z}_1 &= b z_1 - 2 y_1 y_2 z_1^2, \end{aligned} \tag{13}$$

where a and b are certain constants.

We consider the auxiliary functions

$$V = [y_1 - (2a + b)^{-1} W_1]^2 + y_2^2 + W_1^2, \quad W_1 = y_2^2 z_1.$$

For $a < 0$, $2a + b < 0$, and $\mathbf{y} = (y_1, y_2)^T$, the following conditions are satisfied in region (6):

$$V(y_1, y_2, z_1) \geq \gamma(y_1^2 + y_2^2 + W_1^2), \quad V(0, 0, z_1) \equiv 0,$$

$$\dot{V} \leq 2[y_2^2 + (2a + b) W_1^2 + y_1 y_2 W_1] \leq 0,$$

for a certain $\gamma = \text{const} > 0$.

On the basis of theorem 1 (with allowance for remark (i) about the uniform character of stability), we conclude that (i) the partial equilibrium position $y_1 = y_2 = 0$ of system (13) is uniformly stable for large z_{10} and (ii) the equilibrium position $y_1 = y_2 = z_1 = 0$ is uniformly stable with respect to y_1 and y_2 for large z_{10}.

4. GENERALIZATION OF COMMON CONDITIONS OF PARTIAL STABILITY

In order to include the stability problem with respect to some of the variables for the partial equilibrium position of system (1), we introduce the designation $\mathbf{y} = (\mathbf{y}_1^T, \mathbf{y}_2^T)^T$.

Let system (1) have the partial equilibrium position $\mathbf{y} = \mathbf{0}$.

Definition 5. The partial equilibrium position $\mathbf{y} = \mathbf{0}$ of system (1), (4) is $\mathbf{y}_1$-stable for large $\mathbf{z}_0$ if, for arbitrary $\varepsilon > 0$, $t_0 \geq 0$, and $L > 0$, it is possible to find $\delta(\varepsilon, t_0, L) > 0$ such that $\|\mathbf{y}_1(t; t_0, \mathbf{x}_0)\| < \varepsilon$ for all $t \geq t_0$ follows from $\|\mathbf{y}_{10}\| < \delta$, $\|\mathbf{y}_{20}\| < \delta$, and $\|\mathbf{z}_0\| < L$.

Theorem 2. *Let there be a scalar function V and a vector function $\mathbf{W} = \mathbf{W}(t, \mathbf{x})$, $\mathbf{W}(t, \mathbf{0}) \equiv \mathbf{0}$ for system* (1) *such that, in the region*

$$t \geq 0, \quad \|\mathbf{y}_1\| + \|\mathbf{W}(t, \mathbf{x})\| \leq h, \quad \|\mathbf{y}_2\| < \infty, \quad \|\mathbf{z}\| < \infty,$$

the conditions

$$V(t, \mathbf{y}_1, \mathbf{y}_2, \mathbf{z}) \geq a(\|\mathbf{y}_1\| + \|\mathbf{W}(t, \mathbf{x})\|),$$

$$V(t, \mathbf{0}, \mathbf{0}, \mathbf{z}) \equiv 0, \quad \dot{V}(t, \mathbf{x}) \leq 0$$

are satisfied. In this case, (i) *the partial equilibrium position $\mathbf{y} = \mathbf{0}$ of system* (1), (4) *is $\mathbf{y}_1$-stable for large $\mathbf{z}_0$*

and (ii) *the equilibrium position* $\mathbf{x} = \mathbf{0}$ *of system* (1), (2) *is* $\mathbf{y}_1$*-stable for large* $\mathbf{z}_0$.

5. COMMON CONDITIONS OF PARTIAL ASYMPTOTIC STABILITY

Along with the previously introduced functions, we also consider (i) the vector function $\mathbf{U}(\mathbf{x})$, $\mathbf{U}(\mathbf{0}) = \mathbf{0}$, which is independent of t and is continuous in region (5), and (ii) the scalar functions a_i ($i = 1, 2, 3$), which are of the $a(r)$ type from Section 3.

Theorem 3. *Let there be a scalar function V and two vector functions* **U** *and* **W** *such that the following conditions are valid in region* (6):

(a) $a_1(\|\mathbf{y}\| + \|\mathbf{W}(t, \mathbf{x})\|) \le V(t, \mathbf{y}, \mathbf{z}) \le a_2(\|\mathbf{y}\| + \|\mathbf{U}(\mathbf{x})\|)$;

(b) $V(t, \mathbf{0}, \mathbf{z}) \equiv 0$;

(c) $\dot{V}(t, \mathbf{x}) \le -a_3(\|\mathbf{y}\| + \|\mathbf{U}(\mathbf{x})\|)$.

In this case, (i) *condition* (4) *is valid for system* (1) *and the partial equilibrium position* $\mathbf{y} = \mathbf{0}$ *of system* (1) (4) *is uniformly asymptotically stable for large* $\mathbf{z}_0$ *and* (ii) *the equilibrium position* $\mathbf{x} = \mathbf{0}$ *of system* (1), (2) *is uniformly asymptotically* **y***-stable for large* $\mathbf{z}_0$.

The **proof** is performed according to [3, 10] with allowance for the proof of theorem 1.

Discussion of theorem 3. (i) If $\mathbf{W} \equiv \mathbf{0}$ and $\mathbf{U} = \mathbf{z}^*$ (the vector $\mathbf{z}^*$ involves some or all of the components of the vector $\mathbf{z}$), conditions (a) and (c) of theorem 3 coincide with the conditions

$$a_1(\|\mathbf{y}\|) \le V(t, \mathbf{y}, \mathbf{z}) \le a_2(\|\mathbf{y}\| + \|\mathbf{z}^*\|), \quad \dot{V} \le -a_3(\|\mathbf{y}\| + \|\mathbf{z}^*\|) \tag{14}$$

of Rumyantsev's theorem [1, 3] on asymptotic stability with respect to some of the variables. However, in the general case, conditions (a) and (c) are more general than (14) even for $\mathbf{W} \equiv \mathbf{0}$.

(ii) If the conditions of theorems 1 and 2 are valid, system (1) does not need to have the equilibrium position $\mathbf{x} = \mathbf{0}$. At the same time, the fulfillment of Eq. (3) is not associated with the presence of either the equilibrium position $\mathbf{x} = \mathbf{0}$ or the partial equilibrium position $\mathbf{y} = \mathbf{0}$ of system (1). Therefore, conditions ensuring the fulfillment of Eq. (3) can be interpreted as conditions of the **y**-attraction of either the equilibrium position $\mathbf{x} = \mathbf{0}$ or the partial equilibrium position $\mathbf{y} = \mathbf{0}$ when either condition (2) or condition (4) is satisfied for system (1), respectively.

Example 2. Let system (1) consist of the equations

$$\dot{y}_1 = ay_1 + by_1^2 z_1, \quad \dot{z}_1 = cy_1 + dz_1 + e, \tag{15}$$

where a, b, c, d, and e are certain constants.

We consider the auxiliary functions

$$V = \frac{1}{2}[y_1^2 + W_1^2], \quad W_1 = U_1 = y_1 z_1. \tag{16}$$

For $a < 0$ and $a(a + d) - \frac{1}{4}e^2 > 0$, the following conditions are valid in region (6):

$$V(y_1, z_1) \le \frac{1}{2}(y_1^2 + U_1^2), \quad V(0, z_1) \equiv 0,$$

$$\dot{V} \le ay_1^2 + ey_1 U_1 + (a + d)U_1^2 + (b + c)y_1^2 U_1 + bU_1^3 \le -\gamma(y_1^2 + U_1^2),$$

for $U_1 = y_1 z_1$ and a certain $\gamma = \text{const} > 0$.

On the basis of theorem 3, the partial equilibrium position $y_1 = 0$ of system (15) is uniformly asymptotically stable for large z_{10}, whereas there is no equilibrium position $y_1 = z_1 = 0$ for this system.

It should be noted that function V (16) does not satisfy conditions (14).

6. CONCLUSION

In this paper, we unified the notions in the two basic classes of problems of partial stability: the problems of stability with respect to some of the variables in the Lyapunov–Rumyantsev sense and the problems of stability of partial equilibrium positions. As a result, in the context of the Lyapunov function method, we obtained the common conditions of such unified partial stability for general nonlinear time-dependent systems of ordinary differential equations.

ACKNOWLEDGMENTS

This work was supported by the Russian Foundation for Basic Research and by the Ministry of Education of the Russian Federation.

REFERENCES

1. V. V. Rumyantsev, Vestn. Mosk. Univ., Ser. Mat., Mekh., Astron., Fiz., Khim., No. 4, 9 (1957).
2. C. Corduneanu, Rev. Roum. Math. Pure Appl. **9**, 229 (1964).
3. V. V. Rumyantsev and A. S. Oziraner, *Stability and Stabilization of Motion in Some Variables* (Nauka, Moscow, 1987).
4. L. Hatvani, Alkalmazott Matematika Lapok **15**, 1 (1991).
5. A. S. Andreev, Prikl. Mat. Mekh. **55**, 539 (1991).
6. V. I. Vorotnikov, *Stability of Dynamic Systems in Some Variables* (Nauka, Moscow, 1991).

7. V. I. Vorotnikov, Avtom. Telemekh., No. 3, 3 (1993).
8. V. I. Vorotnikov, *Partial Stability and Control* (Birkhauser, Boston, 1998).
9. A. L. Fradkov, I. V. Miroshnik, and V. O. Nikiforov, *Nonlinear and Adaptive Control of Complex Systems* (Kluwer, Dordrecht, 1999).
10. V. I. Vorotnikov and V. V. Rumyantsev, *Stability and Control in Some of the Phase-Vector Coordinates of Dynamic Systems: Theory, Methods, and Applications* (Nauchnyĭ Mir, Moscow, 2001).
11. M. M. Khapaev, *Averaging in Stability Theory* (Kluwer, Dordrecht, 1993).
12. V. I. Zubov, *Methods of A. M. Lyapunov and Their Applications* (Noordhoff, Groningen, 1964).
13. A. S. Galiullin, I. A. Mukhametzyanov, R. G. Mukharlyamov, and V. D. Furasov, *Construction of Systems of Programmed Motion* (Nauka, Moscow, 1971).
14. V. I. Vorotnikov, Dokl. Akad. Nauk **375**, 622 (2000) [Dokl. Phys. **46**, 876 (2000)].
15. H. Nijmejer, I. I. Blekhman, A. L. Fradkov, and A. Yu. Pogromsky, Systems Control Lett. **31**, 299 (1997).

Translated by V. Bukhanov

Doklady Physics, Vol. 47, No. 5, 2002, pp. 382–386. Translated from Doklady Akademii Nauk, Vol. 384, No. 1, 2002, pp. 52–56.

MECHANICS

On the Validity of the Property of Asymptotic Rigidity in the Joukowski Sense for the Integral Set of a Nonlinear Differential Equation under Perturbations

O. V. Druzhinina and A. A. Shestakov

Presented by Academician V.V. Rumyantsev December 28, 2001

Received December 29, 2001

The existence and asymptotic stability of integral sets of ordinary differential equations were studied in [1–11]. In this paper, we analyze the validity of the property of asymptotic rigidity in the Joukowski sense for the integral set of an ordinary differential equation under small perturbations.

1. ASYMPTOTIC RIGIDITY IN THE JOUKOWSKI SENSE FOR AN INTEGRAL SET

Let a steady-state differential equation

$$\frac{dx}{dt} = g(x), \quad x \in R^n, \quad g \in C(M, R^n) \tag{1.1}$$

satisfy the Lipshitz condition with a constant $K > 0$ on the set $M ::= \{x \in R^n: |x| < r\}$. Let $\Gamma ::= \{\gamma(t, q), q \in Q\}$ be the set of positive semitrajectories of Eq. (1.1), where Q is a bounded set on R^m, with $m \le n$.

We consider the set of functions

$$\gamma(\varphi(t), q), \quad q \in Q \subset R^m, \tag{1.2}$$

depending on a spatial parameter $q \in Q$, where $\varphi(t)$ is a continuous scalar function strictly increasing on $R^+ = [0, \infty)$.

Definitions 1.1. The set $\Gamma \subset R^n$ is referred to as an integral (invariant) set with respect to Eq. (1.1) if, for each point $p \in \Gamma$, the inclusion $x(t) \in \Gamma$ occurs, where $x(t)$ is the solution to this equation under the initial condition $t = t_0$, $x = p$ for arbitrary values of t within the range of the definition for this solution.

Let Eq. (1.1) under the initial condition $t = t_0$, $x = p$, with $d(p, \Gamma) \le \mu \le \alpha$, have a unique solution $x(t) = x(t, t_0, p)$ belonging to the set M. In addition, let there exist constants $\lambda > 0$, $0 < \alpha < \lambda$, and $r > 0$ such that

$$d(p, \Gamma) < \lambda \Rightarrow |p| < r, \tag{1.3}$$

where $d(\cdot, \Gamma)$ is the distance from a point to the set. The integral set $\Gamma \subset R^n$, generated by the set of solutions $\{\gamma(t, q), q \in Q\}$ of Eq. (1.1), is referred to as *asymptotically* (*or exponentially*) *rigid in the Joukowski sense* if, for every solution $x(t)$ to Eq. (1.1), with $t_0 \ge 0$ and $d(p, \Gamma) \le \alpha$, there exists a strictly increasing continuous function $\varphi: R^+ \longrightarrow R^+$ such that, respectively, either

$$|x(t) - \gamma(\varphi(t), q_0)| \le \psi(\mu)h(t - t_0) \quad \forall t \ge t_0 \tag{1.4}$$

or

$$\begin{aligned} &|x(t) - \gamma(\varphi(t), q_0)| \\ &\le L\mu \exp(-\omega(t - t_0)),\ L \ge 1,\ \omega > 0,\ \forall t \ge t_0. \end{aligned} \tag{1.5}$$

Here, $\gamma(\cdot, q_0)$ is a certain function belonging to set (1.2); the functions $\psi(\cdot)$ and $h(\cdot)$ are positive definite and continuous; $\psi(\mu)$ is a nondecreasing function of $\mu > 0$, with $\mu(0) = 0$; and $h(t)$ is a nonincreasing function of $t > 0$, with $h(0) = 1$ and $h(t) \longrightarrow 0$ as $t \longrightarrow +\infty$.

Comments to Definitions 1.1. (I) If a set Γ is asymptotically (exponentially) rigid and $\varphi(t) = t + \Delta$, $\Delta \in R$, then the set is asymptotically (exponentially) stable with an asymptotic amplitude and phase in the sense of J. Hale [5]. (II) The asymptotic (exponential) rigidity of the set Γ expresses its asymptotic (exponential) stability in the Lyapunov sense under the linear time-reparametrization representing the homeomorphism R^+ in R^+ [10–12].

Theorem 1.1. *If the integral set $\Gamma \subset R^n$ of Eq.* (1.1) *is asymptotically rigid in the Joukowski sense and if the function $\psi(\mu)$ entering into Eq.* (1.4) *is a linear function of the form $\psi(\mu) = C\mu$, then the set Γ is exponentially rigid in the Joukowski sense.*

Russian Open State Technical University of Railway Transport, ul. Chasovaya 22/2, Moscow, 125808 Russia

1028-3358/02/4705-0382$22.00

Proof. Let an integral set $\Gamma \subset R^n$ be asymptotically rigid. We assume that $\psi(\mu) = C\mu$ and $\varphi(t) = t + \Delta_0$. In this case, we have

$$|x(t) - \gamma(t + \Delta_0, q_0)| \le C\mu h(t - t_0) \quad \forall t \ge t_0. \tag{1.6}$$

We choose σ such that $0 < Ch(\sigma) = l < 1$ and assume that $\tau_k = t_0 + k\sigma$, $p_k = x(\tau_k, t_0, p)$, and $d_k = d(p_k, \Gamma)$ for $k \ge 0$. Then, according to the definition and with regard for the equality $x(t, t_0, p) = x(t, \tau_k, p_k)$ for $t \ge \tau_k$, we find that $d_k \le l^{k-1}\mu$. Assuming that $\omega = -\sigma^{-1}\log l$ and $L = Cl^{-2}$, for $t_0 + k\sigma \le t < t_0 + (k+1)\sigma$, we arrive at

$$\begin{aligned} |x(t) - \gamma(t + \Delta_0, q_0)| &= |x(t, \tau_k, p_k) - \gamma(t + \Delta_0, q_0)| \\ &\le Ch(t - \tau_k)d_k \le C\mu l^{k-1} \\ &= Cl^{-2}\mu l^{-\omega(k+1)\sigma} \le L\mu l^{-\omega(t - t_0)}. \end{aligned} \tag{1.7}$$

By virtue of Eq. (1.7), the set Γ is exponentially rigid. Theorem 1.1 is proven.

2. VALIDITY OF THE PROPERTY OF ASYMPTOTIC RIGIDITY FOR AN INTEGRAL SET GENERATED BY A BOUNDED SET OF INITIAL POINTS

We now consider the problem of the existence of a rigid integral set for the perturbed differential equation

$$\frac{dy}{dt} = g(y) + G(t, y), \quad y \in R^n, \tag{2.1}$$

provided that the perturbing vector function $G(t, y)$ satisfies the relationships

$$G(t, y) \le F(t) \quad \forall (t, y) \in R^+ \times M, \tag{2.2}$$

$$\lim_{t \to \infty} \int_t^{t+1} F(t)dt = 0, \tag{2.3}$$

where $F(t)$ is a positive definite continuous function of $t \ge 0$.

For condition (2.3) to be satisfied, it is sufficient that

$$F(t) \longrightarrow \infty, \quad t \longrightarrow +\infty \tag{2.4}$$

or

$$\int_0^\infty F(t)dt < +\infty. \tag{2.5}$$

Lemma 2.1. *Let* (I) *the integral set* Γ *of Eq.* (1.1) *be exponentially rigid in the Joukowski sense and* (II) $x(t, t_0, p)$ *and* $y(t, t_0, q)$ *be solutions to Eqs.* (1.1) *and* (2.1) *under the initial conditions* $x(t_0, t_0, p) = p$ *and* $y(t_0, t_0, q) = q$, *respectively. Then, provided that*

$$t_0 \ge 0, \quad d(q, \Gamma) < \alpha, \tag{2.6}$$

the following estimate is valid:

$$|x(t, t_0, q) - y(t, t_0, p)| \le \exp\{K(t - t_0)\} \int_0^t F(t)dt. \tag{2.7}$$

Lemma 2.1 is proved with the help of the Gronwall–Bellman lemma [3].

Theorem 2.1. *Let* (I) *differential equation* (1.1) *have an exponentially rigid integral set* Γ *generated by a set of solutions* $\gamma(t + \Delta, q)$, *with* $\Delta \in R$ *and* $q \in Q$, *where* Q *is a bounded set on* R^m; (II) *the perturbation vector function* $G(t, y)$ *satisfy conditions* (2.2) *and* (2.3); *and* (III) *for* $t_0 \ge 0$ *and* $q < C$, *Eq.* (2.1) *have a solution* $y(t) = y(t, t_0, q)$, *with* $y(t_0, t_0, q) = q$, *which is defined on an interval to the right of* t_0 *and can be extended as far as* $|y(t)| < r$. *In this case, a constant* $\sigma \ge 0$ *can be found such that, if the initial conditions* $t = t_0$ *and* $y = q$ *satisfy the inequalities*

$$t_0 \ge \sigma, \quad d(q, \Gamma) \le \beta, \quad \beta = \min\left(\alpha, \frac{1}{2}C^{-1}\lambda\right), \tag{2.8}$$

there exists a solution $y(t) = y(t, t_0, q)$ *to Eq.* (2.1) *which is defined for all* $t \ge t_0$ *and converges uniformly with respect to* (t_0, q) *to the integral set* Γ *of Eq.* (1.1) *as* $t \longrightarrow +\infty$; *i.e.*,

$$d(y(t), \Gamma) \longrightarrow 0, \quad t \longrightarrow +\infty. \tag{2.9}$$

Proof. We choose numbers $\delta > 0$, $\beta > 0$, and an integral number a such that the inequalities

$$\begin{aligned} &Ch(r) \le \frac{1}{2}, \quad a\delta\exp(aK) \le \frac{1}{2}\beta, \\ &\int_t^{t+1} F(t)dt < \delta \quad \forall t > \sigma, \end{aligned} \tag{2.10}$$

are satisfied. Let conditions (2.8) be met. Since $\beta < \lambda$ and $|q| < r$, the solution $y(t)$ to Eq. (2.1) is defined on the interval to the right of t_0, on which $|y(t)| < r$. By virtue of the inequality $\beta \le \alpha$, the solution $x(t, t_0, q)$ is defined for all $t \ge t_0$. Let $\gamma(\cdot)$ be a solution belonging to the set $\{\gamma(t + \Delta), q)\}$ to which the solution $x(t, t_0, q)$ corresponds. By virtue of the exponential rigidity, for $t \in [t_0, t_0 + a]$, we have

$$\begin{aligned} |y(t) - \gamma(t)| &\le C\beta h(t - t_0) + \exp(aK) \int_{t_0}^{t_0 + a} F(t)dt \\ &\le C\beta + \exp(aK) \sum_{i=0}^{a-1} \int_{t_0 + i}^{t_0 + i + 1} F(t)dt \\ &\le C\beta + \exp(aK)a\delta \le \frac{\lambda}{2} + \frac{\beta}{2} < \lambda. \end{aligned} \tag{2.11}$$

It follows from (2.11) that the solution $y(t)$ can be extended as far as $\tau_1 = t_0 + a$. Assuming that $y_1 = y(\tau_1, t_0, q)$, we arrive at

$$|y_1 - \gamma(\tau_1)| \le \exp(aK)a\delta + C\beta ha < \frac{\beta}{2} + \frac{\beta}{2} = \beta, \quad (2.12)_1$$

$$d(y_1, \Gamma) \le \beta. \quad (2.12)_2$$

We then find by induction that the solution $y(t)$ can be extended to all values of $t \ge t_0$. In order to prove (2.9), it is sufficient to be convinced that

$$\exists \sigma_1 \ge \sigma \quad \forall \varepsilon > 0 \quad d(y(t), \Gamma) \le \varepsilon \quad \forall t \ge \sigma_1, \quad d(q, \Gamma) \le \beta.$$

Let numbers δ_1, $\sigma_0 \ge \sigma$, and an integer number $a_1 \ge a$ be chosen such that

$$C\beta h(a_1) \le \frac{1}{4}C^{-1}\varepsilon, \quad \exp(Ka_1)a_1\beta \le \frac{1}{4}C^{-1}\varepsilon, \quad (2.13)_1$$

$$\int_t^{t+1} F(t)dt \le \delta_1 \quad \forall t \ge \sigma_0. \quad (2.13)_2$$

If $\tau_i = t_0 + ia$ and $y_i = y(\tau_i, t_0, q)$, then

$$d(y_i, \Gamma) \le \beta \quad \forall t \ge 0, \quad y_0 \equiv q. \quad (2.14)_1$$

It is evident that there exists a smallest integral number b such that $\tau_i = t_0 + ab \ge \sigma_2$. It follows from $(2.14)_1$ that

$$d(y(\tau_i + a_1, t_0, q), \Gamma) \le \frac{1}{2}C^{-1}\varepsilon. \quad (2.14)_2$$

Then,

$$d(y(t), \Gamma) \le \frac{1}{2}\varepsilon + \exp(a_1K)\int_{\tau_i + a_1}^{\tau_i + 2a_1} F(t)dt \le \frac{1}{2}\varepsilon + \exp(a_1K)a_1\delta_1 \le \varepsilon \quad \forall t \in [\tau_i + a_1, \tau_i + 2a_1). \quad (2.15)$$

Since $Ch(a_1) < \frac{1}{2}$ for $a_1 > 0$, then we have

$$d(y(\tau_i + 2a_1, t_0, q), \Gamma) < \frac{1}{2}C^{-1}\varepsilon.$$

Finally, we prove by induction that

$$d(y(t), \Gamma) \le \varepsilon, \quad \forall t \ge \sigma_2 ::= \sigma_2 + a_1 + a. \quad (2.16)$$

Since the choice of σ_1 is independent of (t_0, q), with $t_0 \ge \sigma$, the inequality $d(q, \Gamma) \le \beta$ and relationship (2.9) are valid. Theorem 2.1 is proved.

Theorem 2.2. *Let* (I) *Eq.* (1.1) *have an asymptotically rigid integral set* Γ *generated by a compact set of initial points*; (II) *the vector function* $G(t, y)$ *satisfy Eqs.* (2.2) *and* (2.3); *and* (III) *hypothesis* (III) *of Theorem* 2.1 *be valid. In this case, the conclusion of Theorem* 2.1 *is valid.*

Theorem 2.2 is proved in much the same way as Theorem 2.1.

The Hale and Stokes theorems [5] on asymptotic stability with an asymptotic amplitude and phase for the bounded integral set of an autonomous differential equation follow from Theorems 2.1 and 2.2.

3. VALIDITY OF THE PROPERTY OF ASYMPTOTIC RIGIDITY FOR A PERIODIC INTEGRAL SET

Let Eq. (1.1) have a rigid periodic integral set Γ and its trajectories have the period $\omega(q)$. We now consider the problem of the existence of a rigid integral set for the perturbed differential equation

$$\frac{dy}{dt} = g(y) + G(t, y), \quad (t, y) \in R^+ \times R^n \quad (3.1)$$

under conditions of the validity of (2.2), (2.3), and

$$\int_0^\infty \int_t^\infty F(\tau)d\tau\, dt < +\infty, \quad (3.2)$$

$$\omega(q) \in C^1(q), \quad \gamma(t, q) \in C^2(t, q), \quad (3.3)$$

where $\omega(q)$ is the period of the set $\gamma(t, q)$, $q \in Q$; i.e.,

$$\gamma(t + \omega(q), q) = \gamma(t, q) \quad \forall (t, q) \in R \times Q. \quad (3.4)$$

Theorem 3.1 *Let the period* $\omega(q)$ *of a periodic integral set* Γ *generated by the set* $\gamma(t + \Delta, q)$, *with* $\Delta \in R$ *and* $q \in Q$, *be independent of* q *and the vectors*

$$\left(\frac{\partial\gamma(t, q)}{\partial t}, \frac{\partial\gamma(t, q)}{\partial q^{(i)}}\right), \quad (t, q) \in R \times Q, \quad i = 1, 2, \ldots, m \quad (3.5)$$

be linearly independent of each other for all $(t, q) \in R \times Q$. *Let a perturbation vector function* $G(t, y)$ *satisfy the condition* $|G(t, y)| \le F(t)$, *with* $\forall (t, y) \in R^+ \times M$, *and the function* $F(t)$ *meet condition* (2.5). *In this case, if the conditions*

$$d(q, \Gamma) < \beta, \quad t_0 \ge \sigma \quad (3.6)$$

are satisfied (*with* σ *the same as in Theorem* 2.1), *then* (I) *there exists a point* $q_1 \in Q$ *such that*

$$d(y(t), C(q_1)) \longrightarrow 0, \quad t \longrightarrow \infty, \quad (3.7)$$

where $C(q_1)$ *is a trajectory of Eq.* (1.1); *i.e.*,

$$C(q_1) = \{\gamma(t, q): 0 \le t \le \omega(q_1)\}; \quad (3.8)$$

and (II) *there exists a point* $q_1 \in Q$ *and a number* $\Delta_1 \in R$ *dependent on* (t_0, q) *such that*

$$|y(t) - \gamma(t + \Delta_1, q_1)| \longrightarrow 0, \quad t \longrightarrow \infty. \quad (3.9)$$

Proof. Let conditions (3.6) be met. Then, according to Theorem 2.1, the solution $y(t)$ to Eq. (3.1) is defined for all $t \geq t_0$ and satisfies condition (2.9). We choose sequences $\tau_k \subset R$, $q_k \subset R^n$, and $\Delta_k \subset R$ and, after that, $y_k = y(\tau_k, t_0, q)$ and $\gamma_k = \gamma(\Delta_k, q_k)$, such that

$$\begin{gathered} y_k \longrightarrow \gamma(\Delta_1, q_1) \in \Gamma, \quad \tau_k \longrightarrow +\infty, \\ |y_k - \gamma_k| \longrightarrow 0, \quad k \longrightarrow +\infty. \end{gathered} \tag{3.10}$$

We now prove that

$$\begin{gathered} |y(t) - \gamma(t - \tau_k + \Delta_1, q_1)| \longrightarrow 0, \\ t \in [\tau_k, \tau_{k+1}], \quad k \longrightarrow +\infty. \end{gathered} \tag{3.11}$$

Since Q is a bounded set and the period $\omega(q)$ is a continuous function of q, there exist constants π_1 and π_2 such that

$$0 < \pi_1 \leq \omega(q) \leq \pi_2 \quad \forall q \in Q. \tag{3.12}$$

We choose an integral number a such that $ch(a\pi_1) \leq \frac{1}{2}$. Let a point (t_0, q) be given and the function $\gamma_0(t)$ corresponding to a function $x(t, t_0, q)$ belong to the set Γ. In this case, $\gamma_0(t)$ is a periodic function with the period $\omega_0 \in [\pi_1, \pi_2]$. Let $\tau_1 = t_0 + a\omega_0$, $y_1 = y(\tau_1, t_0, q)$, $\gamma_0 = \gamma_0(t_0) = \gamma_0(\tau_1)$, and $d_0 = d(q, \Gamma)$. Then, we have

$$\begin{aligned} |y_1 - \gamma_0| &\leq cd_0 h(a\omega_0) + \exp(a\omega_0 K)\int_{t_0}^{\tau_1} F(t)dt \\ &\leq cd_0 h(a\omega_0) + \exp(a\omega_0 K)\int_{t_0}^{\tau_1} F(t)dt \\ &\leq \frac{1}{2}d_0 + c_1\int_{t_0}^{\tau_1} F(t)dt, \quad c_1 ::= \exp(a\pi_2 K). \end{aligned} \tag{3.13}$$

Introducing the notation

$$\Omega_1 ::= \frac{1}{2}d_0 + c_1\int_{t_0}^{\tau_1} F(t)dt, \tag{3.14}_1$$

we arrive at the inequality

$$|y_1 - q| \leq |y_1 - \gamma_0(\tau_1)| + |\gamma_0(t_0) - q| \leq cd_0 + \Omega_1.$$

It follows from the inequality $|y_1 - \gamma_0| \leq \Omega_1$, with $\gamma_0 \in \Gamma$, that $\Omega_1 \geq d_1$, where $d_1 = d(y_1, \Gamma)$.

Let the function $\gamma_1(t)$ with a period ω_1 belong to the set Γ and correspond to $x(t, \tau_1, y_1)$. Let $\tau_2 = \tau_1 + a\omega_1$, $y_2 = y(\tau_2, t_0, q)$, and $\gamma_1 = \gamma_1(\tau_1) = \gamma_1(\tau_2)$.

In this case,

$$|y_2 - \gamma_1| \leq \frac{1}{2}d_1 + c_1\int_{\tau_1}^{\tau_2} F(t)dt.$$

Denoting

$$\Omega_2 ::= \frac{1}{2}d_1 + c_1\int_{\tau_1}^{\tau_2} F(t)dt, \tag{3.14}_2$$

we have

$$|y_2 - y_1| \leq cd_1 + \Omega_2 \leq \Omega_2 + c\Omega_1.$$

Proving by induction, we find for all $k \geq 0$ that $d_k ::= d(y_k, \Gamma)$, $d_k \leq \Omega_k$, $\tau_{k+1} = \tau_k + a\omega_k$, $y_{k+1} = y(\tau_{k+1}, t_0, q)$, and $\gamma_k = \gamma_k(\tau_k) = \gamma_k(\tau_{k+1})$, where the functions $\gamma_k(t)$ belong to set (1.2) and have the period ω_k. It is evident that

$$|y_{k+1} - \gamma_k| \leq \Omega_{k+1}, \tag{3.15}_k$$

where

$$\Omega_{k+1} ::= \frac{1}{2}d_k + c_1\int_{\tau_k}^{\tau_{k+1}} F(t)dt. \tag{3.14}_{k+1}$$

Then,

$$|y_{k+1} - y_k| \leq cd_k + \Omega_{k+1} \leq \Omega_{k+1} + c\Omega_k. \tag{3.15}$$

Since $d_k \leq \Omega_k$,

$$\Omega_{k+1} \leq \frac{1}{2}\Omega_k + c_1\int_{\tau_k}^{\tau_{k+1}} F(t)dt.$$

By induction, we find for all integral numbers $i > 0$ that

$$\Omega_{k+i} \leq 2^{-i}d_k + c_1\sum_{j=0}^{i-1} 2^{j-i+1}\int_{\tau_{k+j}}^{\tau_{k+j+1}} F(t)dt.$$

Using (3.15), we obtain the inequality

$$\sum_{i=1}^{s}\Omega_{k+i} \leq d_k + 2c_1\int_{\tau_k}^{\tau_k+s} F(t)dt \quad \forall s > 0. \tag{3.16}$$

In addition, we have

$$\begin{aligned} |y_{k+s} - y_k| &\leq \sum_{i=0}^{s-1}|y_{k+i+1} - y_{k+1}| \\ &\leq cd_k + (c+1)\sum_{i=1}^{s}\Omega_{k+i}. \end{aligned}$$

It follows from estimates (2.5) and (3.16) that

$$|y_{k+s} - y_k| \leq (1+2c)d_k + 2c_1(c+1)\int_{\tau_k}^{\infty} F(t)dt. \tag{3.17}$$

Hence, y_k is a Cauchy sequence in R^n and the right-hand side of inequality (3.17) approaches zero as

$k \longrightarrow \infty$. Therefore, $y_k \longrightarrow \bar{y} \in \bar{\Gamma}$. As far as the sets $[0, \pi_2]$ and Q are compact and $\Gamma = \{\gamma(t, q)\colon 0 \le t \le \pi_2, q \in Q\}$, the set Γ is also compact. Thus, $\Gamma = \bar{\Gamma}$ and $\bar{y} = \gamma(\Delta_1, q_1)$ for certain values of $\Delta_1 \in R$ and $q_1 \in Q$. Since $|y_{k+1} - \gamma_k| \longrightarrow 0$ as $k \longrightarrow \infty$, then $\gamma_k \longrightarrow \gamma(\Delta_1, q_1)$ as $k \longrightarrow \infty$. From Eqs. (3.15) and (3.16), we have

$$|\gamma_{k+s} - \gamma_k| \le (1 + 2c)d_k + 2c_1(1 + c)\int_{\tau_k}^{\tau_{k+s}} F(t)dt. \quad (3.18)$$

It follows from (3.18) that $d(y(t), c(q_1)) \longrightarrow 0$ as $k \longrightarrow \infty$. Since the period $\omega(q)$ is constant, we find that $\omega(q) = \omega$, with $\forall q \in Q$, and therefore $\tau_k = t_0 + ka\omega \equiv t_0 (\mathrm{mod}\,\omega)$ and $\gamma((t - \tau_k) + \Delta_1, q_1) = \gamma(t - t_0 + \Delta_1, q_1)\ \forall k$, $\forall t$. For $\Delta^* = \Delta_1 - t_0$, we have $|y(t) - \gamma(t + \Delta^*, q_1)| \longrightarrow 0$ as $t \longrightarrow \infty$. Theorem 3.1 is proven.

Theorem 3.2. *Let the period $\omega(q)$ of a periodic integral set Γ generated by the set $\{\gamma(t + \Delta, q), \Delta \in R, q \in Q\}$ depend on q and vectors* (3.5) *be linearly independent of each other for all $(t, q) \in R \times Q$. Let the perturbing vector function $G(t, y)$ satisfy conditions (*3.2) *and* (3.3) *in addition to the hypotheses of Theorem* 3.1. *In this case, the integral set $\Gamma \subset R^n$ of Eq.* (3.1) *is asymptotically rigid in the Joukowski sense.*

The proof of Theorem 3.2 is based on Theorem 3.1.

The theorems of M. Urabe [4] on asymptotic stability with the asymptotic amplitude and phase of the periodic integral set of Eq. (1.1) follow from Theorems 3.1 and 3.2.

ACKNOWLEDGMENTS

The authors are grateful to Academician V.V. Rumyantsev for his attention to this work.

The study is performed under financial support of the Ministry of Education of Russian Federation, project no. 02-07-02-075.

REFERENCES

1. N. M. Krylov and N. N. Bogolyubov, *Application of Methods of Nonlinear Mechanics to the Theory of Steady-State Vibrations* (Izd. Akad. Nauk SSSR, Kiev, 1934).
2. N. M. Krylov and N. N. Bogolyubov, *New Methods in Nonlinear Mechanics* (Gos. Tekh. Teor. Izd., Moscow, 1934).
3. V. V. Nemytskiĭ and V. V. Stepanov, *Qualitative Theory of Differential Equations* (Gostekhizdat, Moscow, 1949).
4. M. Urabe, Funkcialaj Ekvacioj, Serio Internacia **1**, 1 (1958).
5. J. K. Hale and A. P. Stokes, Arch. Ration. Mech. Anal. **6**, 133 (1960).
6. Yu. A. Mitropol'skiĭ and O. B. Lykova, *Integral Manifolds in Nonlinear Mechanics* (Nauka, Moscow, 1973).
7. V. V. Rumyantsev and A. S. Oziraner, *Stability and Stabilization of Motion with Respect to Part of the Variables* (Nauka, Moscow, 1987).
8. V. A. Pliss, *Integral Sets of Periodic Systems of Differential Equations* (Nauka, Moscow, 1977).
9. A. M. Samoĭlenko, *Elements of Mathematical Theory of Multifrequency Oscillations* (Nauka, Moscow, 1987).
10. O. V. Druzhinina and A. A. Shestakov, Dokl. Akad. Nauk **351**, 48 (1996) [Phys. Dokl. **41**, 536 (1996)].
11. O. V. Druzhinina and A. A. Shestakov, Dokl. Akad. Nauk **351**, 332 (1996) [Phys. Dokl. **41**, 559 (1996)].
12. O. V. Druzhinina and A. A. Shestakov, *The Rigidity of Motion for Mechanical Systems* (RUDN-PAIMS, Moscow, 1996).

Translated by V. Chechin

Doklady Physics, Vol. 47, No. 5, 2002, pp. 387–391. Translated from Doklady Akademii Nauk, Vol. 384, No. 1, 2002, pp. 57–61.

MECHANICS

Characteristic Relations for the Velocities of Displacements in the Three-Dimensional Problem of the Full Limit Equilibrium of a Soil Continuum

D. D. Ivlev*, Academician A. Yu. Ishlinskiĭ, and R. I. Nepershin*****

Received January 11, 2002

Characteristic relations for the velocities of displacements in the three-dimensional problem of the full limit equilibrium of a Coulomb soil continuum are obtained. The corresponding relations for the plane and axisymmetric problems follow from the relations for the three-dimensional problem. As an example, compatible fields of slip lines and displacement velocities are constructed for the problem of the pressure of a smooth flat elliptic die on the soil half-space.

Analytical methods of constructing slip-line fields and determining the critical load exist for the plane [1] and axisymmetric [2] problems of the limit equilibrium of a Coulomb soil continuum. The three-dimensional problem is statically determinate and hyperbolic when the soil continuum is at full limit equilibrium, which corresponds to the edges of the Coulomb pyramid in the space of the principal stresses [3, 4]. For the three-dimensional problem of the full limit equilibrium of a soil continuum, the characteristic relations for stresses and calculations of slip surfaces were presented in [5].

In this paper, we derive characteristic relations for the velocities of displacements along slip lines for the three-dimensional problem of the full limit equilibrium of the Coulomb soil continuum. The compatible fields of these lines and displacement velocities are constructed for the problem of the pressure of a smooth elliptic die on the half-space.

At the three-dimensional full limit equilibrium of the Coulomb soil continuum, the principal stresses satisfy the relations [5]

$$\sigma_1 = \sigma_2 = \sigma(1 - \lambda\sin\rho) - h,$$
$$\sigma_3 = \sigma(1 + \lambda\sin\rho) - h. \quad (1)$$

Here, $\lambda = +1$ (-1) for $\sigma_3 > \sigma_1$ $(\sigma_3 < \sigma_1)$ and σ is the reduced average pressure calculated as [1]

$$\sigma = \frac{1}{2}(\sigma_1 + \sigma_3) + h, \quad h = k\cot\rho, \quad (2)$$

where k is the cohesion and ρ is the angle of internal friction. Hereafter, compressive normal stresses are considered to be positive.

The axis of the characteristic cone coincides with the direction of the stress σ_3. Slip surfaces are tangent to the characteristic cone and form the angle

$$\mu = \frac{\pi}{4} - \frac{\rho}{2} \quad (3)$$

with the stress σ_3. In the Cartesian coordinates $\{x, y, z\}$, the direction of σ_3 is specified by the unit vector $\mathbf{n}$ with the components

$$\mathbf{n}_1 = \cos\varphi, \quad \mathbf{n} = \sin\varphi\sin\theta, \quad \mathbf{n} = \sin\varphi\cos\theta, \quad (4)$$

where φ and θ are the angles between the x-axis and the vector $\mathbf{n}$ and between the z-axis and the projection of the vector $\mathbf{n}$ onto the plane $\{y, z\}$, respectively. In turn, the unit vectors $\mathbf{l}$ and $\mathbf{m}$ specify the directions of the stresses σ_1 and σ_2, respectively.

We introduce the orthogonal curvilinear coordinate system $\{1, 2, 3\}$ connected with a surface orthogonal to the vector $\mathbf{m}$. Line *3* is directed along the unit vector $\mathbf{m}$, line *2* is opposite to the principal normal to the line *3*, and the principal normals to lines *1* and *2* are directed along the vector $-\mathbf{m}$ (Fig. 1).

In many important practical problems, the surface $\{1, 2\}$ is plane or approximately plane. In this case, the three-dimensional problem can be solved as a sequence of two-dimensional problems formulated at the known surfaces $\{1, 2\}$, where boundary conditions for stresses are used to determine slip surfaces and the field of stresses in the region of the limit equilibrium [5].

To determine the field of displacement velocities, we use the isotropy condition and the generalized associated rule of a plastic flow for the edges of the Coulomb pyramid. The condition and the rule ensure the maximum flow freedom for both a perfectly plastic

* *Chuvash State Pedagogical University, pr. Karla Marksa 38, Cheboksary, 428000 Russia*
** *Institute for Problems in Mechanics, Russian Academy of Sciences, pr. Vernadskogo 101, Moscow, 117526 Russia*
*** *Moscow State Academy for Instrumentation Engineering and Computer Sciences, ul. Stromynka 20, Moscow, 107846 Russia*

1028-3358/02/4705-0387$22.00 © 2002 MAIK “Nauka/Interperiodica”

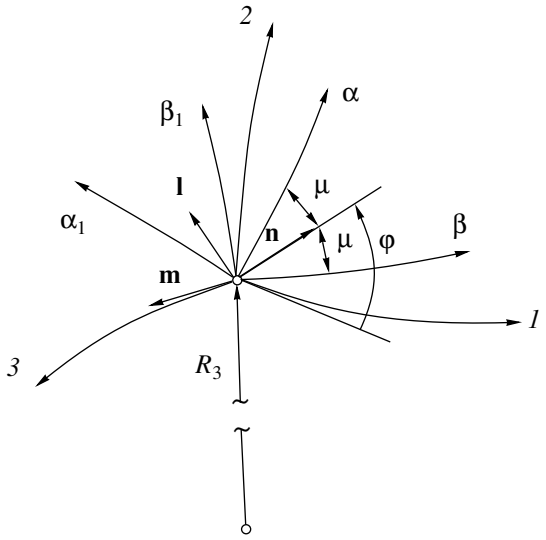

Fig. 1. Curvilinear coordinates and slip lines in the surface orthogonal to the stress σ_2.

body and the Coulomb soil continuum at the limit equilibrium [6–8]. The generalized associated flow rule leads to the following expression for strain rates:

$$\varepsilon_1 + \varepsilon_2 + \varepsilon_3 = (\varepsilon_1 + \varepsilon_2 - \varepsilon_3)\sin\rho. \quad (5)$$

The dissipative function D for compressive principal stresses has the form

$$D = (\varepsilon_1 + \varepsilon_2 - \varepsilon_3)k\cos\rho \geq 0, \quad (6)$$

and the principal strain rates satisfy the inequality

$$\varepsilon_1 + \varepsilon_2 - \varepsilon_3 \geq 0. \quad (7)$$

The right-hand side of Eq. (5) determines the variation rate for the medium density ω:

$$\frac{d}{dt}(\ln\omega) = [\varepsilon_3 - (\varepsilon_1 + \varepsilon_2)]\sin\rho. \quad (8)$$

Relations (7) and (8) indicate that deformation of the soil continuum in the region of the limit equilibrium decreases its density.

According to the isotropy condition, the principal strain rates ε_1, ε_2, and ε_3 are directed along the unit vectors **l**, **m**, and **n** of the principal stresses, respectively. The strain rates along the slip lines α and β, as well as along the directions α_1 and β_1 orthogonal to these lines, are related to ε_1 and ε_3 by the formulas

$$\varepsilon_\alpha = \varepsilon_\beta = \varepsilon_1\sin^2\mu + \varepsilon_3\cos^2\mu, \quad (9)$$

$$\varepsilon_{\alpha 1} = \varepsilon_{\beta 1} = \varepsilon_1\sin^2\mu + \varepsilon_3\cos^2\mu, \quad (10)$$

which lead to the invariant relations

$$\varepsilon_\alpha + \varepsilon_{\alpha 1} = \varepsilon_\beta + \varepsilon_{\beta 1} = \varepsilon_1 + \varepsilon_3. \quad (11)$$

Expressions (3), (9), and (11) yield

$$\varepsilon_\alpha - \varepsilon_{\alpha 1} = \varepsilon_\beta - \varepsilon_{\beta 1} = (\varepsilon_3 - \varepsilon_1)\sin\rho, \quad (12)$$

and Eqs. (5), (11), and (12) lead to

$$\varepsilon_\alpha = \varepsilon_\beta = -\frac{-\varepsilon_2(1 - \sin\rho)}{2}. \quad (13)$$

According to the isotropy condition, the shear rates along the normal to the surface $\{1, 2\}$ are equal to zero. The displacement-velocity vector lying in the plane tangent to the surface $\{1, 2\}$ satisfies this condition. Its projections onto the slip lines are denoted as V_α and V_β.

The strain rates ε_α, ε_β, and ε_2 are found by differentiating the velocity vector in the orthogonal curvilinear coordinates $\{\alpha, \alpha_1, 3\}$ and $\{\beta, \beta_1, 3\}$, where the rotation angles φ_α, φ_β, and φ_3 of tangents to the coordinate lines α, β, and *3*, respectively, are considered as independent variables. Then, in terms of the coordinates $\{\alpha, \alpha_1, 3\}$,

$$\varepsilon_\alpha = \frac{\partial}{\partial S_\alpha}(V_\alpha + V_\beta\sin\rho) - V_\beta\cos\rho\frac{\partial\ln R_\alpha}{\partial S_{\alpha 1}}, \quad (14)$$

$$\varepsilon_2 = (V_\alpha + V_\beta\sin\rho)\frac{\partial\ln R_3}{\partial S_\alpha} - V_\beta\cos\rho\frac{\partial\ln R_3}{\partial S_{\alpha 1}}, \quad (15)$$

whereas, in terms of the coordinates $\{\alpha, \alpha_1, 3\}$,

$$\varepsilon_\beta = \frac{\partial}{\partial S_\beta}(V_\beta + V_\alpha\sin\rho) + V_\alpha\cos\rho\frac{\partial\ln R_\beta}{\partial S_{\beta 1}}, \quad (16)$$

$$\varepsilon_2 = (V_\beta + V_\alpha\sin\rho)\frac{\partial\ln R_3}{\partial S_\beta} + V_\alpha\cos\rho\frac{\partial\ln R_3}{\partial S_{\beta 1}}. \quad (17)$$

If the surface $\{1, 2\}$ is of low curvature, the touching planes of the curves α, α_1, β, and β_1 are close to the plane tangent to the surface $\{1, 2\}$. Then, variations of the curvature radii of the slip lines satisfy the relations (Fig. 1)

$$\begin{aligned} dR_\alpha &= -dS_{\alpha 1} = dS_\beta\cos\rho, \\ dR_\beta &= -dS_{\beta 1} = -dS_\alpha\cos\rho. \end{aligned} \quad (18)$$

Differentials of the curvature radius R_3 satisfy the relations

$$\begin{aligned} dR_3 &= dS_\alpha\sin(\varphi + \mu) \text{ in } \alpha, \\ dR_3 &= -dS_\beta\cos\rho\cos(\varphi + \mu) \text{ in } \alpha_1, \end{aligned} \quad (19)$$

$$\begin{aligned} dR_3 &= dS_\beta\sin(\varphi - \mu) \text{ in } \beta, \\ dR_3 &= dS_\alpha\cos\rho\cos(\varphi - \mu) \text{ in } \beta_1, \end{aligned} \quad (20)$$

where φ is the angle between the direction of the stress σ_3 and the coordinate line *1* on the surface $\{1, 2\}$.

Expressions (13)–(20) provide the following differential relations for the velocities V_α and V_β:

$$d(V_\alpha + \sin\rho V_\beta) + \cos\rho V_\beta d\varphi + (1 - \sin\rho)\frac{V_2}{2R_3}dS_\alpha = 0 \text{ along } \alpha, \quad (21)$$

$$d(V_\beta + \sin\rho V_\alpha) - \cos\rho V_\alpha d\varphi + (1 - \sin\rho)\frac{V_2}{2R_3}dS_\beta = 0 \text{ along } \beta. \quad (22)$$

Here, $d\varphi$ is the angle of rotation of a tangent to the slip lines along the arcs dS_α and dS_β and the velocity component V_2 along the coordinate line *2* is expressed as

$$V_2 = (V_\alpha + \sin\rho V_\beta)\sin(\varphi + \mu) - \cos\rho V_\beta\cos(\varphi + \mu) \text{ in } \alpha, \quad (23)$$

$$V_2 = (V_\beta + \sin\rho V_\alpha)\sin(\varphi - \mu) + \cos\rho V_\alpha\cos(\varphi - \mu) \text{ in } \beta. \quad (24)$$

If the surface $\{1, 2\}$ is plane and $\frac{1}{R_3} = 0$, Eqs. (21) and (22) describe flow kinematics in the plane limit equilibrium of the Coulomb soil continuum. If all the planes $\{1, 2\}$ intersect each other along the line *1*, Eqs. (21)–(24) describe flow kinematics in the axisymmetric full limit equilibrium of the soil continuum. When $\rho = 0$, where $\frac{1}{R_3} = 0$ and $\frac{1}{R_3} > 0$, Eqs. (21) and (22) go over into Geiringer's equations of plane deformation and into the relations for velocities of axisymmetric shear of a perfectly plastic body, respectively [9].

For the plane limit equilibrium of a soil continuum, the homogeneous differential relations (21) and (22) admit velocity discontinuities $[V]_\alpha = \text{const}$ and $[V]_\beta = \text{const}$ when the velocity components V_β and V_α are continuous along the slip lines α and β, respectively. For $\frac{1}{R_3} > 0$, Eqs. (21)–(24) complemented by the equations $dS_\alpha\sin(\varphi + \mu) = dR_3$ and $dS_\beta\sin(\varphi - \mu) = dR_3$ along the α and β lines, respectively, lead to the following differential relations for the velocity discontinuities:

$$d[V]_\alpha = -(1 - \sin\rho)[V]_\alpha\frac{dR_3}{2R_3} \text{ along } \alpha, \quad (25)$$

$$d[V]_\beta = -(1 - \sin\rho)[V]_\beta\frac{dR_3}{2R_3} \text{ along } \beta. \quad (26)$$

The integration of Eqs. (25) and (26) for a given discontinuity $[V]^0_{\alpha,\beta}$ at the point R_3^0 of line *2* determines the variation of velocity discontinuity along the slip lines α and β as follows:

$$[V]_{\alpha,\beta} = [V]^0_{\alpha,\beta}\sqrt{\frac{R_3^0}{R_3}} \text{ at } R_3, R_3^0 > 0. \quad (27)$$

Below, we consider the problem of constructing compatible fields of slip lines and velocities at the full limit equilibrium of the half-space $x \geq 0$ when a die that is flat, smooth, and elliptic in plan presses on this half-space.

The surfaces $\{1, 2\}$ are assumed to be plane and orthogonal to the ellipse contour. In the plane $\{1, 2\}$, we specify the Cartesian coordinate system $\{x_1, x_2\}$ with the origin at the point of intersection of this plane with the ellipse axis. The x_1-axis is parallel to the x-axis of the basic coordinate system $\{x, y, z\}$, and the x_2-axis is normal to the ellipse.

In the plane $x = 0$ of the coordinate system $\{x, y, z\}$, the ellipse is parametrically specified as

$$z_0 = \cos\xi, \quad y_0 = b\sin\xi, \quad 0 \leq \xi \leq \frac{\pi}{2}. \quad (28)$$

The minor semiaxis of the ellipse is directed along the z-axis and has a length considered to be the characteristic dimension of the problem, and b is the length of the major semiaxis. The ellipse curvature radius R and the angle θ between the z-axis and the plane $\{1, 2\}$ passing through the point z_0, y_0 are determined by the expressions

$$R = \frac{1}{b}(\sin^2\xi + b^2\cos^2\xi)^{3/2}, \quad \tan\theta = \frac{\tan\xi}{b}. \quad (29)$$

The plane $\{1, 2\}$ intersects the y-axis at the following distance d from the die boundary:

$$d = \frac{1}{b}\sqrt{\sin^2\xi + b^2\cos^2\xi}. \quad (30)$$

The curvature radius of the coordinate line *3* normal to the plane $\{1, 2\}$ is determined by the expression

$$R_3 = R - d + x_2. \quad (31)$$

Based on the static boundary conditions of the problem and taking body force into account, we calculated slip surfaces in [5]. Figure 2 shows the field of slip lines in the plane $\theta = \text{const}$ under the assumption that, upon reaching the limit equilibrium, the material can slip along the smooth die boundary *OA*. The boundary *AB* is free of shear stresses and is subject to a given pressure p. The quantity $\gamma H = 1$ is considered to be the characteristic stress, where γ is the volume weight of the medium and H is the length of the minor semiaxis of the ellipse. The die is forced into the half-space with velocity $V = 1$ along the x-axis.

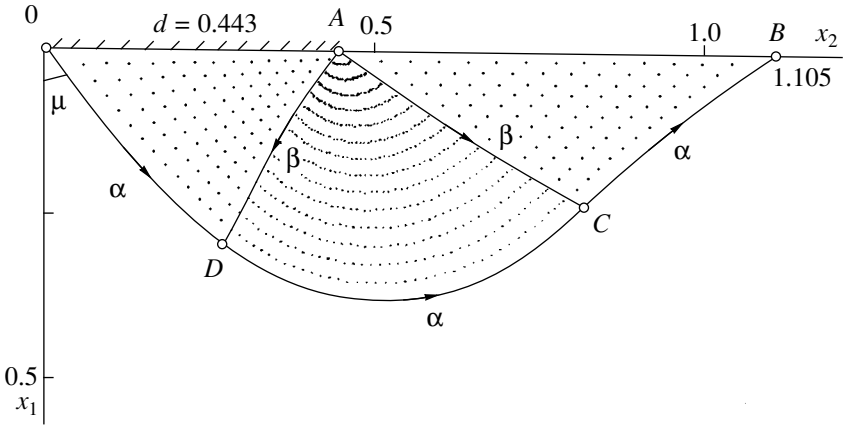

Fig. 2. Slip lines caused by penetration of a smooth elliptic die into the half-space in the plane θ = 0.798 at $b = 3$ and $p = 0.1$.

The velocity components along the x_1- and x_2-axes are related to V_α and V_β as

$$\begin{aligned} V_{x1} &= V_\alpha \cos(\varphi + \mu) + V_\beta \cos(\varphi - \mu), \\ V_{x2} &= V_\alpha \sin(\varphi + \mu) + V_\beta \sin(\varphi - \mu), \end{aligned} \tag{32}$$

which can be inverted as

$$\begin{aligned} V_\alpha &= \frac{V_{x2}\cos(\varphi - \mu) - V_{x1}\sin(\varphi - \mu)}{\cos\rho}, \\ V_\beta &= \frac{V_{x1}\sin(\varphi + \mu) - V_{x2}\cos(\varphi + \mu)}{\cos\rho}. \end{aligned} \tag{33}$$

The half-space below the boundary *ODCB* is stationary. At the point *O*, the die velocity $V_x = 1$ causes a velocity gap along a tangent to the slip line α,

$$[V]_\alpha^0 = \frac{1}{\cos\mu} \quad \text{at} \quad x_2 = 0. \tag{34}$$

This gap varies along the boundary *ODCB* according to Eq. (27), where R_3^0 and R_3 are defined by Eq. (31) at $x_2 \geq 0$. Since the velocity component normal to the α line *ODCB* is continuous, $V_\beta = 0$. Thus, at the boundary *ODCB*, boundary conditions for velocities are determined by the expressions

$$V_a = \frac{1}{\cos\mu}\sqrt{\frac{R-d}{R-d+x_2}}, \quad V_\beta = 0 \text{ at } ODCB. \tag{35}$$

At a smooth die boundary *OA*, φ = 0. The continuity of the velocity component normal to this boundary and the first of Eqs. (32) yield the boundary condition

$$V_\alpha + V_\beta = \frac{1}{\cos\mu} \quad \text{at} \quad OA. \tag{36}$$

The calculation of the slip-line field on the basis of the static boundary conditions of the problem provides the coordinates of the slip-line points and the angles φ in the region of the limit equilibrium. The field of the displacement velocities V_α and V_β is found by integrating differential relations (21)–(24) with boundary conditions (35) and (36). In the region *OAD*, we solve the mixed problem with conditions (35) specified in *OD* and relations (22), (24), and (36) applied in *OA*. In the regions *ADC* and *ACB*, we solve the Goursat problem with conditions (35) specified in *DC* and *CB*, respectively, and using velocities found in *AD* and *AC*, respectively.

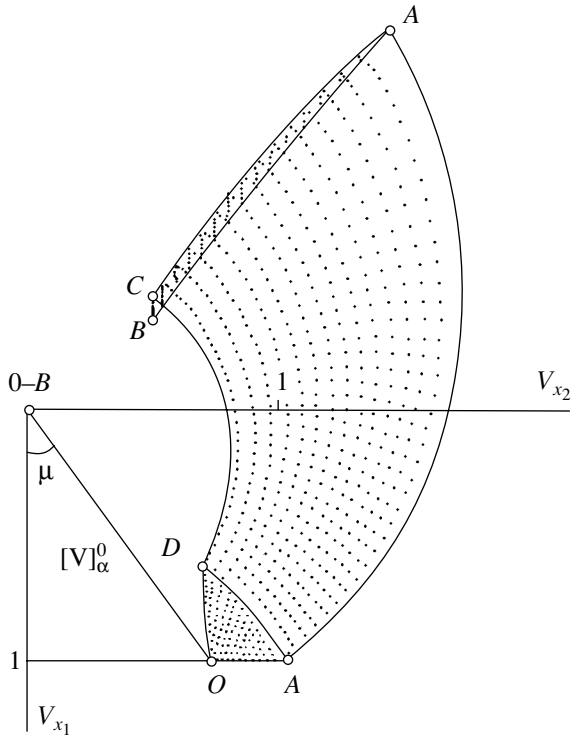

Fig. 3. Hodograph of displacement velocities in the region of the limit equilibrium for the slip-line field shown in Fig. 2.

Relations (21)–(24) are integrated numerically via approximating velocity differentials by finite differences and variable functions by their average values between nodes of the slip lines. As a result, these relations lead to the system of two linear equations for V_α and V_β at the nodes of the slip-line network. In the coordinates $\{x_1, x_2\}$, the velocity is found from Eqs. (32). In the coordinates $\{x, y, z\}$, the velocity vector is expressed as

$$U = V_{x1}, \quad V = V_{x2}\sin\theta, \quad W = V_{x2}\cos\theta, \quad (37)$$

$$x = x_1, \quad y = y_0 + (x_2 - d)\sin\theta, \quad z = x_2\cos\theta, \quad (38)$$

where y_0, θ, and d are determined by Eqs. (28)–(30).

To calculate the fields of slip lines and displacement velocities when the elliptic die presses on the half-space, we have written a computer program. Figure 3 shows the field of displacement velocities in the hodograph plane $\{V_{x1}, V_{x2}\}$. The field was calculated for the slip-line field in the plain $\theta = 0.798$ that is shown in Fig. 2. Figures 2 and 3 demonstrate that strain rates in the region of the limit equilibrium satisfy the inequalities $\varepsilon_1 > 0$, $\varepsilon_2 > 0$, and $\varepsilon_3 < 0$. Dissipative function (6) is positive, and the rate of variation of medium density (8) is negative. The penetration of the die into the half-space decreases the density in the region of the limit equilibrium. In this case, the maximum decrease occurs near the die edge.

REFERENCES

1. V. V. Sokolovskiĭ, *Statics of a Soil Continuum* (Gos. Izd. Tekh. Teor. Lit., Moscow, 1954).
2. V. G. Berezantsev, *Axisymmetric Problem in the Theory of Limit Equilibrium of a Soil Continuum* (Gos. Izd. Tekh. Teor. Lit., Moscow, 1952).
3. D. D. Ivlev, Prikl. Mat. Mekh. **22**, 90 (1958).
4. D. D. Ivlev, *Mechanics of Plastic Media* (Fizmatlit, Moscow, 2001), Vol. 1, pp. 5–14 and 34–37.
5. D. D. Ivlev, A. Yu. Ishlinskiĭ, and R. I. Nepershin, Dokl. Akad. Nauk **383**, 638 (2002) [Dokl. Phys. **47** (2002)] (in press).
6. A. Yu. Ishlinskiĭ, Izv. Akad. Nauk SSSR, Otd. Tekh. Nauk, No. 3, 250 (1945).
7. A. Yu. Ishlinskiĭ, *Applied Problems of Mechanics* (Nauka, Moscow, 1986), Vol. 1, pp. 62–83.
8. D. D. Ivlev, Prikl. Mat. Mekh. **36**, 957 (1972).
9. D. D. Ivlev, *Theory of Ideal Plasticity* (Nauka, Moscow, 1966).

Translated by Yu. Verevochkin

Doklady Physics, Vol. 47, No. 5, 2002, pp. 392–396. Translated from Doklady Akademii Nauk, Vol. 384, No. 2, 2002, pp. 188–192.

MECHANICS

On the Stability in the Joukowski Sense for Trajectories of Certain Celestial Systems

O. V. Druzhinina

Presented by Academician V.V. Rumyantsev December 28, 2001

Received December 29, 2001

Basic results related to the stability of motion and rigidity of trajectories were established in classic studies [1, 2]. The theory of the stability of motion has been developed in papers of both Russian and foreign authors (see, e.g., [4–7]).

In this paper, we establish the principle of reducing the problem on stability in the Joukowski sense for trajectories of a differential equation describing certain celestial-mechanics systems to a problem on stability in the Lyapunov sense for a linear time-dependent second-order differential equation. We apply the results to the analysis of stability in the Joukowski sense for trajectories of certain Keplerian motions.

We consider a conservative system with two degrees of freedom described by the set of equations

$$\begin{aligned} \ddot{x}_1 &= 2a(x_1, x_2)\dot{x}_2 + U_{x_1}(x_1, x_2), \\ \ddot{x}_2 &= -2a(x_1, x_2)\dot{x}_1 + U_{x_2}(x_1, x_2), \end{aligned} \tag{1}$$

where $a(x_1, x_2)$ and $U(x_1, x_2)$ are given functions of x_1 and x_2. Here, U_{x_i} is the partial derivative of U with respect to x_i, $i = 1, 2$. It is well known [8, 9] that for any conservative system with two degrees of freedom, set (1) represents a canonical form with respect to the properly chosen coordinate system (x_1, x_2).

A variety of problems of celestial mechanics are reduced to equations taking the form of Eqs. (1). These are the classic problem of two spherical bodies, the problem of two fixed and one mobile material points, the restricted circular three-body problem, the problem of a point moving under the action of several material rings and of two points circling around their center of inertia, the restricted circular three-body problem in a gravitating medium, the problem of a point inside a gravitating ring similar to Saturn's rings, etc. [10–12].

For a series of celestial-mechanics problems, the condition of stability in the Lyapunov sense turns out to be too rigorous and it is not satisfied in a number of important cases. Thus, the analysis of a less rigorous characteristic, namely, the stability of trajectories in the Joukowski sense, is of interest [13, 14].

Let $x_i = \varphi_i(t)$ $(i = 1, 2)$ be a solution to Eqs. (1) which does not correspond to the equilibrium state. The Jacobi equations of system (1), which determine a perturbation $y(t) = (y_1(t), y_2(t))$ of the solution $x_i = \varphi_i(t)$, take the form

$$\begin{aligned} \ddot{y}_1 - 2a[t]\dot{y}_2 &= \sum_{i=1}^{2} A_i(t)y_i, \\ \ddot{y}_2 + 2a[t]\dot{y}_1 &= \sum_{i=1}^{2} B_i(t)y_i, \end{aligned} \tag{2}$$

where $a[t] ::= a(\varphi_1(t), \varphi_2(t))$. The coefficients $A_i(t)$ and $B_i(t)$ are determined by the relationships

$$\begin{aligned} A_1(t) &= U_{x_1x_1}[t] + 2a_{x_1}[t]\dot{\varphi}_2, \\ A_2(t) &= U_{x_1x_2}[t] + 2a_{x_2}[t]\dot{\varphi}_2, \\ B_1(t) &= U_{x_2x_1}[t] - 2a_{x_1}[t]\dot{\varphi}_1, \\ B_2(t) &= U_{x_2x_2}[t] - 2a_{x_2}[t]\dot{\varphi}_1, \end{aligned}$$

where the argument $[t]$ of the functions implies that this function is evaluated for $x_1 = \varphi_1(t)$ and $x_2 = \varphi_2(t)$.

The set of linear Jacobi equations (2) has a first integral of the form

$$\begin{aligned} \dot{\varphi}_1(t)\dot{y}_1 + \dot{\varphi}_2(t)\dot{y}_2 - U_{x_1}[t]y_1 - U_{x_2}[t]y_2 \\ = h = \text{const}. \end{aligned} \tag{3}$$

It is evident that the expressions

$$x_i = \varphi_i(t) + y_i \tag{4}$$

belong to the solutions to Eqs. (1) with an accuracy to the second order in y_1 and y_2 if and only if the functions y_i are solutions to Jacobi equations (2). Therefore, $y_i =$

Russian Open State Technical University of Railway Communication,
ul. Chasovaya 22/2, Moscow, 125808 Russia

1028-3358/02/4705-0392$22.00

δx_i and integral (3) of Eqs. (2) can formally be derived from the kinetic-energy integral for system (1)

$$\frac{1}{2}(\dot{x}_1^2 + \dot{x}_2^2) - U(x_1, x_2) = c_1 \tag{5}$$

on condition that $h = \delta c_1$.

We assume that

$$\begin{aligned}&\dot{\varphi}_1(t)\dot{y}_1(t) + \dot{\varphi}_2(t)\dot{y}_2(t)\\ &- U_x[t]y_1(t) - U_y[t]y_2(t) = 0 \quad \forall t.\end{aligned} \tag{6}$$

Identity (6) implies that the integration constant h entering into Eq. (3) and determined by the four initial values of the solution $y(t) = (y_1(t), y_2(t))$ to Eqs. (2) is zero.

After substituting the solution $x = \varphi(t)$ into (1) and (5) and differentiating the results of the substitution with respect to t, we arrive at (2) and (6), where y_i are replaced by $\dot{\varphi}_i(t)$, i.e.,

$$y_i = \dot{\varphi}_i(t), \quad i = 1, 2. \tag{7}$$

Thus, the quantities $y(t)$ are isoenergetic perturbations of the quantities $\varphi_i(t)$, $i = 1, 2$. Since the solution $x_i = \varphi_i(t)$ to set (1) does not correspond to an equilibrium state, solution (7) to Jacobi equations (2) is not identically equal to zero. Therefore, the origin $t = 0$ of the t-axis can always be chosen such that for the solution $x_i = \varphi_i(t)$ under consideration, we have

$$\varphi_i(0) \neq 0, \quad \dot{\varphi}_i(0) \neq 0, \quad i = 1, 2. \tag{8}$$

Since expression (3) is an integral of Eqs. (2), the perturbation determined by the four initial values

$$y_i(0), \quad \dot{y}_i(0), \quad i = 1, 2 \tag{9}$$

is an isoenergetic perturbation if and only if the condition

$$\begin{aligned}&\dot{\varphi}_1(0)y_1(0) + \dot{\varphi}_2(0)\dot{y}_2(0)\\ &- U_{x_1}[0]y_1(0) - U_{x_2}[0]y_2(0) = 0\end{aligned} \tag{10}$$

is satisfied. It follows from Eqs. (8) and (10) that the set of isoenergetic perturbations of the solution $\varphi(t)$ depends only on the three constants entering into (9).

For a fixed value of t, the projection $z(t)$ of the perturbation $y(t) = (y_1(t), y_2(t))$ along the directed normal to the trajectory of the solution $x_i = \varphi_i(t)$ is determined by the formula

$$z(t) = \frac{-\dot{\varphi}_2(t)}{\dot{\varphi}_1^2(t) + \dot{\varphi}_2^2(t)}y_1(t) + \frac{\dot{\varphi}_1(t)}{\sqrt{\dot{\varphi}_1^2(t) + \dot{\varphi}_2^2(t)}}y_2(t). \tag{11}$$

Definition 1. The scalar function $z = z(t)$ is referred to as a normal perturbation of the solution $x_i = \varphi_i(t)$ to conservative system (1) with two degrees of freedom if there exists at least one solution $y_i = y_i(t)$ to Jacobi equations (2) such that the function $z(t)$ can be presented in form (11).

We consider the function

$$u = u(t) ::= \dot{\varphi}_1(t)y_2(t) - \dot{\varphi}_2(t)y_1(t) \tag{12}$$

related to the function $z = z(t)$ by the expression

$$u = (\dot{\varphi}_1^2 + \dot{\varphi}_2^2)^{1/2}z, \quad \dot{\varphi}_1 = \dot{\varphi}_1(t), \quad \dot{\varphi}_2 = \dot{\varphi}_2(t). \tag{13}$$

Theorem 1. *Any normal perturbation* $z(t) = (\dot{\varphi}_1^2 + \dot{\varphi}_2^2)^{-1/2}u(t)$ *of a solution* $(\varphi_1(t), \varphi_2(t))$ *to a conservative system with two degrees of freedom is a solution to the following linear second-order differential equation*:

$$A(t)\ddot{u} + B(t)\dot{u} + C(t)u = 0. \tag{14}$$

Conversely, any solution $u(t)$ *to Eq.* (14) *is a normal perturbation of the solution* $(\varphi_1(t), \varphi_2(t))$ *to conservative system* (1) *with two degrees of freedom. In this case, the coefficients* $A(t)$, $B(t)$, *and* $C(t)$ *of Eq.* (14) *are determined by the formulas*

$$A(t) ::= -\frac{1}{2}(\dot{\varphi}_1^2(t) + \dot{\varphi}_2^2(t)), \tag{15}_1$$

$$B(t) ::= \dot{\varphi}_1(t)\ddot{\varphi}_1(t) + \dot{\varphi}_2(t)\ddot{\varphi}_2(t), \tag{15}_2$$

$$\begin{aligned}C(t) ::= {}& 2a[t](\dot{\varphi}_1(t)\ddot{\varphi}_2(t) - \dot{\varphi}_2(t)\ddot{\varphi}_1(t))\\ &- (\ddot{\varphi}_1^2(t) + \dot{\varphi}_2^2(t)) + \frac{1}{2}(\dot{\varphi}_1^2(t) + \dot{\varphi}_2^2(t))\\ &\times [-4a^2[t] + U_{x_1x_1}[t] + U_{x_2x_2}[t]\\ &- (\dot{\varphi}_1(t)a_{x_2}[t] - \dot{\varphi}_2(t)a_{x_1}[t])].\end{aligned} \tag{15}_3$$

Remark. Substituting (13) into Eq. (14), we arrive at the equation

$$\ddot{z} + D(t)z = 0, \tag{16}$$

where the coefficient $D(t)$ is unambiguously determined by set (1), by its solution $x_i = \varphi_i(t)$, and by the relationship

$$D(t) = D_1(t) + D_2(t), \tag{17}$$

where

$$D_1(t) = v^{-2}(\ddot{v}v - 2\dot{v}^2), \tag{18}_1$$

$$v = \sqrt{2(U[t] + h)},$$

$$\begin{aligned}D_2(t) = {}& 2v^{-2}(U_{x_1}^2[t] + U_{x_2}^2[t])\\ &+ 4v^{-2}a[t](U_{x_1}[t]\dot{\varphi}_2 - U_{x_2}[t]\dot{\varphi}_1)\\ &- 4a^2[t] + U_{x_1x_1}[t] + U_{x_2x_2}[t].\end{aligned} \tag{18}_2$$

Proof. Let $y = y(t)$ be the solution to Jacobi equations (2) such that condition (6) is satisfied. By virtue of

Eqs. (1), we have

$$U_{x_1}[t] = \ddot{\varphi}_1(t) - 2a[t]\dot{\varphi}_2(t),$$
$$U_{x_2}[t] = \ddot{\varphi}_2(t) - 2a[t]\dot{\varphi}_1(t). \quad (19)$$

Thus, it follows from Eq. (6) that

$$\dot{\varphi}_1(t)\dot{y}_1 + \dot{\varphi}_2(t)\dot{y}_2 - (\ddot{\varphi}_1(t) - 2a[t])y_1 - (\ddot{\varphi}_2(t) + 2a[t]\dot{\varphi}_1(t))y_2 = 0. \quad (20)$$

Taking into account Eq. (12), we arrive at

$$\ddot{u} + 2[\dot{y}_1\ddot{\varphi}_2(t) - \dot{y}_2\varphi_1(t)] = y_2\dddot{\varphi}_1(t) - y_1\dddot{\varphi}_2(t) + \ddot{y}_2\dot{\varphi}_1(t) - \ddot{y}_1\dot{\varphi}_2(t). \quad (21)$$

It follows from Eqs. (3) and (19) that

$$\ddot{\varphi}_1(t) = 2a[t]\ddot{\varphi}_2(t) + (U_{x_1x_1}[t] + 2a_{x_1}[t]\varphi_2(t))\dot{\varphi}_1(t) + (U_{x_1x_2}[t] + 2a_{x_2}[t]\dot{\varphi}_2(t))\dot{\varphi}_2(t), \quad (22)_1$$

$$\ddot{\varphi}_2(t) = -2a[t]\ddot{\varphi}_1(t) + (U_{x_2x_2}[t] - 2a_{x_2}[t]\varphi_1(t))\dot{\varphi}_2(t), \quad (22)_2$$

$$\ddot{y}_2 = -2a[t]\dot{y}_1 + (U_{x_2x_1}[t] - 2a_{x_1}[t]\dot{\varphi}_1(t))y_1 + [U_{x_2x_2}[t] - 2a_{x_2}[t]\dot{\varphi}_1(t)]y_2, \quad (22)_3$$

$$\ddot{y}_1 = 2a[t]\ddot{y}_2 + (U_{x_1x_1}[t] + 2a_{x_1}[t]\dot{\varphi}_2(t))y_1 + [U_{x_1x_2}[t] + 2a_{x_2}[t]\dot{\varphi}_2(t)]y_2. \quad (22)_4$$

Multiplying Eqs. $(22)_1$–$(22)_4$ by y_2, $-y_1$ and $\dot{\varphi}_1(t) - \dot{\varphi}_2(t)$, respectively, and summing the products obtained, we have

$$y_2\dddot{\varphi}_1(t) - y_1\dddot{\varphi}_2(t) + \ddot{y}_2\dot{\varphi}_1(t) - \ddot{y}_1\dot{\varphi}_2(t) = 2a[t]\{\ddot{\varphi}_1(t)y_1 + \ddot{\varphi}_2(t)y_2 - \dot{\varphi}_1(t)\dot{y}_1 + \dot{\varphi}_2(t)\dot{y}_2\} + \{U_{x_1x_1}[t] + U_{x_2x_2}[t] - 2[\dot{\varphi}_1(t)a_{x_2}[t] - \dot{\varphi}_2(t)a_{x_1}[t]]\}(\dot{\varphi}_1(t)y_2 - \dot{\varphi}_2(t)y_1). \quad (23)$$

Introducing the notation

$$H(t) ::= -4a^2[t] + U_{x_1x_1}[t] + U_{x_2x_2}[t] - [\dot{\varphi}_1(t)a_{x_2}[t] - \dot{\varphi}_2(t)a_{x_1}[t]],$$

we find from Eqs. (12) and (20)

$$\ddot{u} - H(t)u + 2(\dot{y}_1\ddot{\varphi}_2(t) - \dot{y}_2\ddot{\varphi}_2(t)) = 0. \quad (24)$$

We then use Eqs. (19) and (24) and the algebraic identity [8]

$$(\dot{\varphi}_1(t)\ddot{\varphi}_1(t) + \dot{\varphi}_2(t)\ddot{\varphi}_2(t))u - (\dot{\varphi}_1^2(t) + \ddot{\varphi}_2^2(t))u = \{\dot{y}_1\dot{\varphi}_1(t) + \dot{y}_2\dot{\varphi}_2(t) - y_1\ddot{\varphi}_1(t) - \dot{y}_2\ddot{\varphi}_2(t)\} \times \{\dot{y}_1(t)\ddot{\varphi}_2(t) - \dot{y}_2(t)\ddot{\varphi}_1(t)\} - (\dot{y}_1\ddot{\varphi}_2(t) - \dot{y}_2\ddot{\varphi}_1(t))(\dot{y}_1^2(t) + \dot{y}_2^2(t)). \quad (25)$$

As a result, we have

$$(\dot{\varphi}_1(t)\ddot{\varphi}_1(t) + \dot{\varphi}_2(t)\ddot{\varphi}_2(t))\dot{u} + 2a[t](\dot{\varphi}_1(t)\ddot{\varphi}_2(t) - \dot{\varphi}_2(t)\ddot{\varphi}_1(t))u + \frac{1}{2}(-\ddot{u} + H(t))(\dot{\varphi}_1^2(t) + \dot{\varphi}_2^2(t)) - (\ddot{\varphi}_1^2(t) + \dot{\varphi}_2^2(t))u = 0. \quad (26)$$

It is easy to prove that Eq. (14), with its coefficients determined from formulas $(15)_1$–$(15)_3$, follows from Eq. (26).

Now, we prove that for an arbitrary solution $u = u(t)$ to Eq. (14), there exists at least one solution $\{y_1(t), y_2(t)\}$ such that the three functions $u(t)$, $y_1(t)$, and $y_2(t)$ satisfy conditions (6) and (12).

Let the initial conditions for the solution $u(t)$ to Eq. (14) be given by the values

$$u(0), \quad \dot{u}(0). \quad (27)$$

We specify the four initial values in (9) as follows. One of them, for example, $y_1(0)$, is chosen arbitrarily, and the three remaining values, $y_2(0)$, $\dot{y}_1(0)$, and $\dot{y}_2(0)$, are chosen in such a way that they satisfy the set of algebraic equations

$$-u(0) - \dot{\varphi}_2(0)y_1(0) + \dot{\varphi}_1(0)y_2(0) = 0, \quad (28)_1$$

$$-\dot{u}(0) - \dot{x}_2(0)y_1(0) + \ddot{\varphi}_1(0)y_2(0) - \dot{\varphi}_2(0)\dot{y}_1(0) + \dot{\varphi}_1(0)\dot{y}_2(0) = 0, \quad (28)_2$$

$$-U_{x_1}[0]y_1(0) - U_{x_2}[0]y_2(0) + \dot{\varphi}_1(0)\dot{y}_1(0) + \dot{\varphi}_2(0)\dot{y}_2(0) = 0. \quad (28)_3$$

Since the determinant of set $(28)_1$–$(28)_3$ is not zero, the quantities $y_2(0)$, $\dot{y}_1(0)$, and $\dot{y}_2(0)$ are uniquely determined by this set. We denote the solution to Eq. (2) under initial conditions (9) as

$$y_1 = \psi_1(t), \quad y_2 = \psi_2(t). \quad (29)$$

By virtue of Eq. $(28)_3$, the integration constant c for solution (29) is equal to zero; therefore, the function

$$\alpha(t) ::= \dot{\varphi}_1(t)\psi_2(t) - \dot{\varphi}_2(t)\psi_1(t) \quad (30)$$

is a solution to Eq. (14).

It follows from Eqs. $(28)_1$, $(28)_2$, and (30) that

$$u(0) = \alpha(0), \quad \dot{u}(0) = \dot{\alpha}(0). \quad (31)$$

Therefore, the given solution $u(t)$ to Eq. (14) has the same initial values as solution (30). Hence, $u(t) \equiv \alpha(t)$ and an arbitrarily given solution $u(t)$ can be represented using the isoenergetic perturbation $(y_1(t), y_2(t))$ determined by Eqs. (2). This perturbation is responsible for the normal displacement $z(t)$ and depends on three arbitrary constants. At the same time, the general solution to Eq. (14) depends only on two arbitrary constants provided that $A(t)$, $B(t)$, and $C(t)$ are given. This is explained by the fact that the trivial solution $u \equiv 0$ to Eq. (14) corresponds not only to the trivial solution $y_1(t) = y_2(t) = 0$ of Eqs. (24) but also to the isoenergetic perturbation $y_1 = c\dot{\varphi}_1(t)$ and $y_2 = c\dot{\varphi}_2(t)$, with c = const, $c \neq 0$. The constant c is just the missing third arbitrary constant. In fact, the functions $\dot{\varphi}_1(t)$ and $\dot{\varphi}_2(t)$ cannot be identically equal to zero or represent the trivial solution $y_1 = y_2 \equiv 0$, because otherwise the solution $x_i = \varphi_i(t)$ would degenerate into the equilibrium state, which is excluded by the definition of the theorem. Thus, Theorem 1 is proved.

Definition 2. The solution $x_i = \varphi_i(t)$ $(i = 1, 2)$ to conservative system (1) with two degrees of freedom is referred to as (I) a stable solution in the Joukowski sense if for an arbitrary number $\varepsilon > 0$, there exists a number $\delta = \delta(\varepsilon)$ such that

$$|z(t_0)| < \delta \Rightarrow |z(t)| < \varepsilon \ \forall t \geq t_0, \tag{32}$$

where $z(t)$ is a normal perturbation of the solution $x_i = \varphi_i(t)$ $(i = 1, 2)$ to conservative system (1) or as (II) a asymptotically stable solution in the Joukowski sense if this solution is stable in the Joukowski sense and, in addition,

$$|z(t)| \longrightarrow 0, \text{ as } t \longrightarrow +\infty. \tag{33}$$

Remark. The notion of stability for the solution $(y_1(t), y_2(t))$, which was formulated above using the normal perturbation $z(t)$, is equivalent to the notion of stability in the Lyapunov sense for the reparameterized solution $(\varphi_1(t), \varphi_2(t))$ [13, 14].

Theorem 2. *For the conservative system with two degrees of freedom, the motion corresponding to the solution* $x_i = \varphi_i(t)$ $(i = 1, 2)$ *to Eqs.* (1) *is stable* (*asymptotically stable*) *in the Joukowski sense if the solution* $u(t)$ *to second-order equation* (14) *is stable* (*asymptotically stable) in the Lyapunov sense.*

Theorem 2 is a corollary of Theorem 1 and the definitions of both stability (asymptotic stability) in the Lyapunov sense and stability (asymptotic stability) in the Joukowski sense.

Example 1. Let $U(x_1, x_2)$ = const (Coriolis force field). For $a = 2\omega$ = const, we are dealing with a potential motion with respect to a coordinate system uniformly rotating with angular velocity ω. In this case, the system of equations (1) takes the form

$$\ddot{x}_1 - 2\omega\dot{x}_2 = 0, \quad \ddot{x}_2 + 2\omega\dot{x}_1 = 0, \tag{34}$$

where $U = 2\omega$ and $D(t) = 32\omega^2$. All trajectories of Eq. (34) are stable in the Joukowski sense.

Example 2. Let $U(x_1, x_2) = \frac{1}{2}[\omega^2(x_1^2 + x_2^2) + h]$ (inertial motion with respect to a uniformly rotating coordinate system). In this case,

$$\ddot{x}_1 - 2\omega\dot{x}_2 - \omega^2 x_1 = 0, \quad \ddot{x}_2 + 2\omega\dot{x}_1 - \omega^2 x_2 = 0, \tag{35}$$

where $U_{x_1} = \omega^2 x_1$, $U_{x_2} = \omega^2 x_2$, $U_{x_1x_1} = \omega^2$, $U_{x_1x_2} = 0$, $U_{x_2x_2} = \omega^2$, and $D(t) = (\varphi_1^2 + \varphi_2^2)\omega$. For $h > 0$, all trajectories of Eq. (35) are stable in the Joukowski sense.

Example 3. Let $\omega = 0$, $U = r^{-1} + \frac{1}{2}h$, and $r^2 = x_1^2 + x_2^2$ (Keplerian motion with respect to a fixed coordinate system). In this case, Eqs. (1) take the form

$$\ddot{x}_1 = U_{x_1}, \quad \ddot{x}_2 = U_{x_2}, \tag{36}$$

where $U_{x_1} = -r^{-3}x_1$, $U_{x_2} = -r^{-3}x_2$, $U_{x_1x_1} = -r^{-3} + 3r^{-5}x_1^2$, $U_{x_1x_2} = 3r^{-5}x_1x_2$, and $U_{x_2x_2} = -r^{-3} + 3r^{-5}x_2^2$. The function $D(t)$ corresponding to Eq. (17) is

$$D(t) = \frac{\omega^2(\dot{\varphi}_1^2 + \dot{\varphi}_2^2 + \varphi_1\ddot{\varphi}_1 + \ddot{\varphi}_2) - 4\omega^3(\varphi_1\dot{\varphi}_2 - \varphi_2\dot{\varphi}_1) - 6\omega^2 h}{\omega^2(\varphi_1^2 + \varphi_2^2) + 3h} - \frac{3\omega^4(\varphi_1\dot{\varphi}_1^2 + \dot{\varphi}_2^2 + \varphi_1\ddot{\varphi}_1 + \ddot{\varphi}_2)}{\omega^2((\varphi_1^2 + \varphi_2^2) + 3h)^2}.$$

Example 4. Let $\omega \neq 0$ and $U = \frac{1}{r} + \frac{\omega^2}{2}r^2 + \frac{h}{2}$ (Keplerian motion with respect to a uniformly rotating coordinate system). In this case,

$$U_{x_1} = -r^{-3}x_1 + \omega^2 x_1, \quad U_{x_2} = -r^{-3}x_2 + \omega^2 x_2,$$

$$U_{x_1x_1} = -r^{-3} + 3r^{-5}x_1^2 + \omega^2, \quad U_{x_1x_2} = 3r^{-5}x_1x_2,$$

$$U_{x_2x_2} = -r^{-3} + 3r^{-5}x_2^2 + \omega^2.$$

For simplicity, we consider only those phase-space points whose projections onto the (x_1, x_2) plane coincide with one of the libration points. In this case, $U_{x_1} = U_{x_2} = 0$ in the libration points and the equations of motion take the form

$$\ddot{x}_1 - 2\dot{x}_2 = U_{x_1}, \quad \ddot{x}_2 + 2\dot{x}_1 = U_{x_2}. \tag{37}$$

The function corresponding to Eq. (17) is

$$D(t) = 2[-r^{-3}\varphi_1 - r^{-3}\varphi_2]$$
$$+ 2[-2r^{-3} + 3r^{-5}(\varphi_1^2 - r^{-3}\varphi_2^2)]$$
$$+ (\ddot{v}[t]v[t] - 2\dot{v}^2[t])v^2[t].$$

If

$$D(t) = b^2(t) \text{ and } \dot{b}(t) \cdot b^{-1}(t) \geq 0 \ \forall t \in R^+, \quad (38)$$

then the motion corresponding to the solution $z_i = z_i(t)$ to Eq.(16) is stable in the Lyapunov sense [15]. Therefore, in the cases considered in Examples 3 and 4, the Keplerian trajectory that corresponds to the solutions $x_i = \varphi_i(t)$ to Eqs. (36) and (37) will be stable in the Joukowski sense if condition (38) is satisfied.

ACKNOWLEDGMENTS

The author is grateful to Academician V.V. Rumyantsev and Professor A.A. Shestakov for their attention to this work.

The study is performed under financial support of the Ministry of Education of Russian Federation, project no. 020702-075.

REFERENCES

1. A. M. Lyapunov, *General Problem on the Stability of Motion. Consideration* (Izd. Khar'kov. Mat. Obshchestva, Khar'kov, 1892).
2. N. E. Zhukovskiĭ, Uchenye Zapiski Mosk. Gos. Univ., Otd. Fiz. Mat., No. 4, 1 (1882).
3. N. G. Chetaev, *Stability of Motion* (Gos. Izd. Tekh. Teor. Lit., Moscow, 1955).
4. V. V. Rumyantsev, Differ. Uravn. Ikh Primen. **19**, 739 (1983).
5. V. V. Rumyantsev and A. S. Oziraner, *Stability and Stabilization of Motion with Respect to Part of the Variables* (Nauka, Moscow, 1987).
6. A. A. Shestakov, *Generalized Direct Lyapunov Method for Systems with Distributed Parameters* (Nauka, Moscow, 1990).
7. V. M. Matrosov, *Method of Lyapunov Vector Functions: Analysis of Dynamic Properties of Nonlinear Systems* (Fizmatlit, Moscow, 2001).
8. D. Birkhoff, Trans. Am. Math. Soc. **18** (1917).
9. V. V. Stepanov, Astron. Zh. **13**, 435 (1936).
10. N. D. Moiseev, Trudy Gos. Astronom. Inst. im. Shternberga **7**, 129 (1936).
11. G. N. Duboshin, *Celestial Mechanics: Analytical and Qualitative Methods* (Nauka, Moscow, 1964).
12. E. A. Grebenikov and Yu. A. Ryabov, *New Qualitative Methods in Celestial Mechanics* (Nauka, Moscow, 1971).
13. O. V. Druzhinina, Dokl. Akad. Nauk **362**, 198 (1998).
14. O. V. Druzhinina, Dokl. Akad. Nauk **379**, 473 (2001) [Dokl. Phys. **46**, 566 (2001)].
15. P. Bellman, *Theory of Stability for Solutions to Differential Equations* (Inostr. Lit., Moscow, 1954).

Translated by V. Chechin

Doklady Physics, Vol. 47, No. 5, 2002, pp. 397–400. Translated from Doklady Akademii Nauk, Vol. 384, No. 2, 2002, pp. 193–196.

MECHANICS

Reduction of Equations of Motion of an Elastic Medium to One Independent and Two Coupled Equations

G. Ya. Popov

Presented by Academician A.Yu. Ishlinskiĭ January 21, 2002

Received January 23, 2002

1. The system of three equations under consideration has the vector form [1]

$$\mu\Delta\mathbf{u} + (\lambda + \mu)\mathrm{grad}(\mathrm{div}\mathbf{u}) = \rho\frac{\partial^2\mathbf{u}}{\partial t^2} - \mathbf{P}, \qquad (1)$$

where $\mathbf{u}$ is the desired displacement vector, $\mathbf{P}$ is the given body force, μ and λ are the Lamé constants, ρ is the material density, and Δ is the Laplace operator. System (1) can be written in any orthogonal coordinate system [1, 2]. I investigated the problem of reducing this system to one independent and two coupled equations and demonstrated that this reduction is possible only in Cartesian, circular cylindrical, and spherical coordinate systems. Below, the reduction will be represented in these coordinate systems.

Equation (1) is preliminarily rewritten as follows. The symbol μ will denote the Poisson ratio, and the shear modulus G will be used instead of the Lamé constant μ. Then, in terms of the notation

$$2G\mathbf{u} = \mathbf{u}^*, \qquad (2)$$

Eq. (1) can be written as

$$\Delta\mathbf{u}^* + \frac{\mathrm{grad}(\mathrm{div}\mathbf{u}^*)}{1-2\mu} = \frac{1}{c_2^2}\frac{\partial^2\mathbf{u}^*}{\partial t^2} - 2\mathbf{P}, \qquad (3)$$

where $c_2 = G^{1/2}\rho^{-1/2}$ is the velocity of an elastic shear wave.

First, system (3) is considered in the Cartesian coordinate system. Notation (2) is presented in the form

$$2G(u_x, u_y, u_z) = u, v, w. \qquad (4)$$

In addition, the partial derivatives of a function $f(x, y, z)$ with respect to the first, second, and third variables are denoted as this function with a prime, a dot, and a comma, respectively, i.e.,

$$\frac{\partial f}{\partial x} = f', \quad \frac{\partial f}{\partial y} = f^{\cdot}, \quad \frac{\partial f}{\partial z} = f'. \qquad (5)$$

For further transformations, the functions

$$Z = u' + v^{\cdot}, \quad Z^* = v' - u^{\cdot} \qquad (6)$$

are introduced. As a result, Eq. (3) takes the scalar form

$$\begin{aligned}
\Delta u + \frac{(Z + w')'}{1-2\mu} &= \frac{1}{c_2^2}\frac{\partial^2 u}{\partial t^2} - 2P_x,\\
\Delta v + \frac{(Z + w')^{\cdot}}{1-2\mu} &= \frac{1}{c_2^2}\frac{\partial^2 v}{\partial t^2} - 2P_y,\\
\Delta w + \frac{(Z + w')'}{1-2\mu} &= \frac{1}{c_2^2}\frac{\partial^2 w}{\partial t^2} - 2P_z.
\end{aligned} \qquad (7)$$

The first and second of Eqs. (7) are differentiated with respect to x and y, respectively, and the results are added. The resulting equation and the third of Eqs. (7) form the system of coupled equations

$$\begin{aligned}
\Delta Z + \frac{\nabla_{xy}(Z + w')}{1-2\mu} &= \frac{1}{c_2^2}\frac{\partial^2 Z}{\partial t^2} - 2(P'_x + P'_y),\\
\Delta w + \frac{(Z + w')'}{1-2\mu} &= \frac{1}{c_2^2}\frac{\partial^2 w}{\partial t^2} - 2P_z,\\
\nabla_{xy} f &= f'' + f^{\cdot\cdot}.
\end{aligned} \qquad (8)$$

The second and first of Eqs. (7) are differentiated with respect to x and y, respectively, and the results are subtracted from each other. The resulting equation, with allowance for the second of Eqs. (6), takes the form

$$\Delta Z^* = \frac{1}{c_2^2}\frac{\partial^2 Z^*}{\partial t^2} + 2(P^{\cdot}_x - P'_y). \qquad (9)$$

When the functions w and Z have been found from system (8) and the function Z^* has been found from Eq. (9), the displacements u and v should be sought by solving the Poisson equation

$$\nabla_{xy}\begin{Vmatrix} u \\ v \end{Vmatrix} = \begin{Vmatrix} Z' - Z^{*\cdot} \\ Z^{\cdot} - Z^{*\prime} \end{Vmatrix}. \qquad (10)$$

Mechnikov Odessa State University,
ul. Dvoryanskaya 2, Odessa, 65100 Ukraine

1028-3358/02/4705-0397$22.00 © 2002 MAIK “Nauka/Interperiodica”

In order to obtain the first of Eqs. (10), one should differentiate the first and second of Eqs. (6) with respect to x and y, respectively, and subtract the results from each other. The second of Eqs. (10) is obtained similarly.

It is convenient to formulate boundary conditions for system (8) in terms of the following combinations of shear stresses:

$$\left\| \begin{array}{c} \tau \\ \tau^* \end{array} \right\| = \left\| \begin{array}{c} \tau'_{zx} + \tau^{\cdot}_{zy} \\ \tau'_{zy} - \tau^{\cdot}_{zx} \end{array} \right\|,$$

which are similar to Eqs. (6). These combinations satisfy the equations

$$2\tau = \nabla_{xy} w + Z', \quad 2\tau^{\cdot} = Z^{*\prime}.$$

In addition, it can be shown that

$$(1-2\mu)\sigma_z = \mu Z + (1-\mu)w'.$$

The above transformation is valid for the equations of decoupled thermoelasticity and for problems of statics.

2. Let us write Eq. (3) in the cylindrical coordinates r, φ, z and introduce the notation

$$\begin{gathered} 2G\|u_r, u_\varphi, u_z\| = \|u, v, w\|, \\ \frac{\partial f(r,\varphi,z)}{\partial r} \equiv f', \quad \frac{\partial f}{\partial \varphi} \equiv f^{\cdot}, \quad \frac{\partial f}{\partial z} \equiv f', \end{gathered} \tag{11}$$

which is similar to Eqs. (4) and (5), and take

$$\left\| \begin{array}{c} Z \\ Z^* \end{array} \right\| = \frac{1}{r}\left\{ \left\| \begin{array}{c} ru \\ rv \end{array} \right\|' \pm \left\| \begin{array}{c} v \\ u \end{array} \right\|^{\cdot} \right\} \tag{12}$$

instead of Eq. (6). Then, the scalar form of Eq. (3) is [1]

$$\begin{gathered} \Delta u - \frac{u + 2v^{\cdot}}{r^2} + \frac{(Z + w')'}{1-2\mu} = \frac{1}{c_2^2}\frac{\partial^2 u}{\partial t^2} - 2P_r, \\ \Delta v - \frac{v - 2u^{\cdot}}{r^2} + \frac{(Z^{\cdot} + w')^{\cdot}}{1-2\mu} = \frac{1}{c_2^2}\frac{\partial^2 v}{\partial t^2} - 2P_\varphi, \\ \Delta w + \frac{(Z + w')'}{1-2\mu} = \frac{1}{c_2^2}\frac{\partial^2 w}{\partial t^2} - 2P_z, \end{gathered} \tag{13}$$

where Δ is the Laplace operator in the cylindrical coordinate system [1].

The first of Eqs. (13) is multiplied by r, differentiated with respect to this variable, and divided by it. The second of Eqs. (13) is differentiated with respect to φ and divided by r. The results are added and, after some manipulations with allowance for Eqs. (12), yield an equation which, together with the third of Eqs. (13), forms the system of two equations

$$\begin{gathered} \Delta Z + \frac{\nabla_{r\varphi}(Z + w')}{1-2\mu} = \frac{1}{c_2^2}\frac{\partial^2 Z}{\partial t^2} - \frac{2}{r}((rP_r)' + P^{\cdot}_\varphi), \\ \Delta w + \frac{(Z + w')^{\cdot}}{1-2\mu} = \frac{1}{c_2^2}\frac{\partial^2 w}{\partial t^2} - 2P_z, \end{gathered} \tag{14}$$

where

$$\nabla_{r\varphi} f(r,\varphi,z) \equiv \nabla_{r\varphi} f = \frac{(rf')'}{r} + \frac{f^{\cdot\cdot}}{r^2}.$$

The second of Eqs. (13) is multiplied by r, differentiated with respect to this variable, and divided by it. The first equation is differentiated with respect to φ and divided by r. Subtraction of the results and certain transformations with allowance for Eqs. (12) lead to the equation

$$\Delta Z^* = \frac{1}{c_2^2}\frac{\partial^2 Z^*}{\partial t^2} + \frac{2}{r}(P^{\cdot}_r - (rP_\varphi)'). \tag{15}$$

When the functions w and Z have been found from system (14) and the function Z^* has been found from (15), the unknown displacements u and v should be determined by solving the equations

$$\nabla_{r\varphi}\left\| \begin{array}{c} ru \\ rv \end{array} \right\| = \left\| \begin{array}{c} r^{-1}(r^2 Z)' - Z^{*\cdot} \\ r^{-1}(r^2 Z^*)' + Z^{\cdot} \end{array} \right\|. \tag{16}$$

Here, the first of Eqs. (16) is derived as follows. The first of Eqs. (12) is multiplied by r, and the product is differentiated with respect to this variable. The second of Eqs. (12) is differentiated with respect to φ. The results are subtracted from each other. The second of Eqs. (16) is obtained similarly by interchanging the above manipulations with the first and second of Eqs. (12).

It is convenient to formulate boundary conditions for system (14) in terms of the following combinations of shear stresses:

$$\left\| \begin{array}{c} \tau \\ \tau^* \end{array} \right\| = \frac{1}{r}\left\{ \left\| \begin{array}{c} (r\tau_{zr})' \\ (r\tau_{z\varphi})' \end{array} \right\| \pm \left\| \begin{array}{c} \tau_{z\varphi} \\ \tau_{zr} \end{array} \right\|^{\cdot} \right\},$$

which are similar to Eqs. (12). These combinations can be expressed in terms of functions satisfying Eqs. (14) and (15) as follows:

$$2\tau = \nabla_{r\varphi} w + Z', \quad 2\tau^* = Z^{*\prime}.$$

The normal stress σ_z satisfies the formula

$$(1-2\mu)\sigma_z = \mu Z + (1-\mu)w'.$$

As in the case of Cartesian coordinates, the reduction of Eqs. (13) to system (14) and Eq. (15), which are

independent of each other, is valid for the equations of decoupled thermoelasticity and the static equations of elasticity theory.

3. We now present Eq. (3) in the spherical coordinate system (r, θ, φ) and introduce the notation

$$2G\|u_r, u_\theta, u_\varphi\| = \|u, v, w\|,$$
$$\frac{\partial f(r,\theta,\varphi)}{\partial r} \equiv f', \quad \frac{\partial f}{\partial \theta} \equiv f^{\cdot}, \quad \frac{\partial f}{\partial \varphi} \equiv f'. \tag{17}$$

Then, with the use of auxiliary functions Z and Z^*, which, instead of Eqs. (12), are defined by the formulas

$$\left\| \begin{array}{c} Z(r,\theta,\varphi) \\ Z^*(r,\theta,\varphi) \end{array} \right\| = \frac{1}{\sin\theta}\left\{ \left\| \begin{array}{c} v\sin\theta \\ w\sin\theta \end{array} \right\|^{\cdot} \pm \left\| \begin{array}{c} w \\ v \end{array} \right\|' \right\}, \tag{18}$$

vector equation (3) can be represented in the scalar form [1]:

$$\Delta^0 u - 2(u+Z) + \frac{r^2}{1-2\mu}\left[\frac{1}{r^2}(r^2u)' + \frac{Z}{r}\right]' = \frac{r^2}{c_2^2}\frac{\partial^2 u}{\partial t^2} - 2r^2 P_r, \quad \Delta^0 u = r^2 \Delta u, \tag{19}$$

$$\Delta^0 v + 2\left(u^{\cdot} - \frac{\cot\theta}{\sin\theta}w'\right) - \frac{v}{\sin^2\theta} + \frac{r}{1-2\mu}\left[\frac{1}{r^2}(r^2u)' + \frac{Z}{r}\right]^{\cdot} = \frac{r^2}{c_2^2}\frac{\partial^2 v}{\partial t^2} - r^2 P_\theta, \tag{20}$$

$$\Delta^0 w + \frac{2}{\sin\theta}(u' + \cot\theta\, v') - \frac{w}{\sin^2\theta} + \frac{r}{(1-2\mu)\sin\theta}\left[\frac{1}{r^2}(r^2u)' + \frac{Z}{r}\right]' = \frac{r^2}{c_2^2}\frac{\partial^2 w}{\partial t^2} - r^2 P_\varphi. \tag{21}$$

Here, Δ is the Laplace operator in the spherical coordinate system and the operator Δ^0 can be represented as

$$\Delta^0 u = (r^2u')' + \nabla_{\theta\varphi} u, \tag{22}$$

where

$$\nabla_{\theta\varphi} u = \frac{(\sin\theta u^{\cdot})^{\cdot}}{\sin\theta} + \frac{u''}{\sin^2\theta}.$$

Both sides of Eq. (20) are multiplied by $\sin\theta$, differentiated with respect to the variable θ, and divided by $\sin\theta$. Equation (21) is differentiated with respect to φ and divided by $\sin\theta$. Summation of the results and subsequent transformations with allowance for Eqs. (17) and (18) yield an equation which, together with Eq. (19), forms the system of two coupled equations

$$\Delta^0 u - 2(u+Z) + \frac{1}{1-2\mu}\left[(r^2u')' + r^2\left(\frac{Z}{r}\right)'\right] = \frac{r^2}{c_2^2}\frac{\partial^2 u}{\partial t^2} - r^2 P_r,$$
$$\Delta^0 Z + 2\nabla_{\theta\varphi} u + \frac{1}{1-2\mu}\nabla_{\theta\varphi}\left[\frac{1}{r}(r^2u)' + Z\right] = \frac{r^2}{c_2^2}\frac{\partial^2 Z}{\partial t^2} - \frac{r^2}{\sin\theta}[(\sin\theta P_\theta)^{\cdot} + P'_\varphi]. \tag{23}$$

Equation (20) is multiplied by $\sin\theta$, differentiated with respect to the variable θ, and divided by $\sin\theta$. Equation (21) is differentiated with respect to φ and divided by $\sin\theta$. Subtraction of the derived equations and subsequent transformations with allowance for Eqs. (18) and (22) lead to the equation

$$\Delta^0 Z^* = \frac{r^2}{c_2^2}\frac{\partial^2 Z^*}{\partial t^2} + \frac{r^2}{\sin\theta}[P'_\theta - (\sin\theta P_\varphi)^{\cdot}]. \tag{24}$$

When the functions u and Z have been found from system (23) and the function Z^* has been found from Eqs. (24), the displacements v and w should be determined by solving the equations

$$\nabla_{\theta\varphi}\left(\sin\theta \left\| \begin{array}{c} v' \\ w' \end{array} \right\|\right) = \frac{1}{\sin\theta}\left(\sin^2\theta \left\| \begin{array}{c} Z \\ Z^* \end{array} \right\|\right)^{\cdot} \mp \left\| \begin{array}{c} Z^* \\ Z \end{array} \right\|', \tag{25}$$

The first of Eqs. (25) is derived as follows. The first of Eqs. (18) is multiplied by $\sin^2\theta$, differentiated with respect to the variable θ, and divided by $\sin\theta$. The second of Eqs. (18) is multiplied by $\sin^2\theta$, differentiated with respect to the variable φ, and divided by $\sin^2\theta$. The equations obtained are subtracted from each other. To derive the second of Eqs. (25), the above manipulations with the first of Eqs. (18) should be applied to the second of them and vice versa. The results should be added.

It is convenient to formulate boundary conditions for the system of Eqs. (23) and (24) in terms of the following combinations of shear stresses:

$$\left\| \begin{array}{c} \tau \\ \tau^* \end{array} \right\| = \frac{1}{\sin\theta}\left\{ \left\| \begin{array}{c} \sin\theta\tau_{r\theta} \\ \sin\theta\tau_{r\varphi} \end{array} \right\|^{\cdot} \pm \left\| \begin{array}{c} \tau_{r\varphi} \\ \tau_{r\theta} \end{array} \right\|' \right\},$$

which are similar to Eqs. (18). These combinations can be expressed in terms of solutions of the above

equations as follows:

$$2\tau = \frac{\nabla_{\theta\varphi} u}{r} + r\left(\frac{Z}{r}\right)', \quad 2\tau^* = r\left(\frac{Z^*}{r}\right)'.$$

In addition, the normal stress σ_r satisfies the formula

$$(1-2\mu)r\sigma_r = 2\mu u + (1-\mu)ru' + \mu Z. \qquad (26)$$

As in the coordinate systems considered above, the reduction of Eqs. (19)–(21) to system (23) and Eq. (24), which are independent of each other, is valid for the equations of decoupled thermoelasticity and the static equations of elasticity theory. This conclusion was demonstrated in [3], where particular problems of thermoelasticity were solved and the efficiency of applying analogs to Eqs. (23)–(25) to obtain exact solutions to certain problems of thermoelasticity was shown.

REFERENCES

1. V. Nowacki, *Theoria sprężystości* (PWN, Warsawa, 1970; Mir, Moscow, 1975).
2. N. E. Kochin, *Vector Calculus and Elements of Tensor Calculus* (Gostekhteorizdat, Leningrad, 1937).
3. G. Ya. Popov, Dokl. Akad. Nauk **380**, 349 (2001) [Dokl. Phys. **46**, 904 (2001)].

Translated by Yu. Verevochkin

Doklady Physics, Vol. 47, No. 5, 2002, pp. 401–404. Translated from Doklady Akademii Nauk, Vol. 384, No. 2, 2002, pp. 197–201.

MECHANICS

Stabilization of a Hypersonic Boundary Layer by Ultrasound-Absorbing Coatings

Corresponding Member of the RAS V. M. Fomin*, A. V. Fedorov, A. N. Shiplyuk*, A. A. Maslov*, E. V. Burov*, and N. D. Malmuth*****

Received January 14, 2002

INTRODUCTION

For small disturbances of a free flow, the laminar–turbulent transition in a boundary layer on a smooth surface of an aircraft occurs due to amplification of various unstable modes [1]. Both stability theory and experimental data imply the dominance of the first and second disturbance modes in a hypersonic boundary layer.

The first mode corresponds to Tollmien–Schlichting waves whose instability at low Mach numbers is due to viscous effects. These disturbances can be stabilized by cooling the corresponding surface, by suction, or by choosing a favorable pressure gradient. On the basis of the theoretical investigations from [2, 3], it was shown in [4] that the amplification of Tollmien–Schlichting waves can be considerably reduced using a thin penetrable coating (perforated sheet) arranged above a longitudinal cavity. These conclusions have not yet been corroborated experimentally, because the realization of this method is associated with a number of difficulties discussed in [4].

The second mode is the result of inviscid instability and belongs to the family of acoustic disturbances [1]. For a thermally insulated surface, the growth rates of the second mode exceed those of the first mode for Mach numbers M > 4 [1, 5]. For cooled surfaces, the second mode begins to dominate at even lower values of M. In contrast to the first mode, cooling destabilizes the second mode. Since the temperature of the surface of a typical hypersonic vehicle is substantially lower than that of a thermally insulated wall ($T_w < 0.2T_{ad}$), the first mode is suppressed naturally, whereas the second mode becomes more stable and can initiate an early transition. In order to increase the length of a laminar flow, it is necessary to stabilize the second mode.

The second mode is associated with high-frequency acoustic disturbances. Therefore, the assumption was made in [6] that ultrasound-absorbing coatings (UAC) can efficiently stabilize this type of instability. This hypothesis was verified in the framework of linear stability theory in the inviscid [6] and viscous [7] approximations. In [7], a perforated surface with cylindrical blind microholes was analyzed. It was shown that a relatively thin porous coating can induce a dramatic decrease in the second mode growth rate. Qualitative corroboration of these results was obtained in the experiments in [8] performed in the GALCIT T-5 shock tube at M = 5–6. The transition locus was measured for a model of an acute cone with a vertex semiangle of 5°. Half of the cone surface (between generatrices) was covered with a perforated (approximately 100 cylindrical holes per mm^2) sheet 0.5 mm thick, whereas the other half was continuous. The experiments showed that the flow in the boundary layer was laminar on the porous surface, up to the cone base. At the same time, on the continuous surface, a transition was observed in the middle cross section of the cone. The results of the experiments [8] were rather impressive; however, they did not answer the question as to what occurs with the disturbances in the boundary layer and whether the second mode is really suppressed.

Many materials that can efficiently absorb acoustic disturbances have a random porosity. For practical use, UAC should be compatible with heat-resistant coatings that also have a chaotic microstructure. The interaction of unstable disturbances with such coatings has still not been investigated.

The lack of direct experimental corroboration of the theory and the practical advantages of materials with random porosity have initiated a number of theoretical and experimental studies of the stability of a boundary layer on a porous surface with a random microstructure. The main objective of this study were the following: to directly measure the disturbances in the boundary layer on porous and continuous surfaces; to develop a theoretical model corresponding to available experimental

* *Institute of Theoretical and Applied Mechanics, Siberian Division, Russian Academy of Sciences, ul. Institutskaya 4/1, Novosibirsk, 630090 Russia*

** *Faculty of Aeromechanics and Aircraft Engineering, Moscow Institute of Physics and Technology, ul. Gagarina 16, Zhukovskiĭ, Moscow oblast, 140180 Russia*

*** *Rockwell Scientific Company, 1049 Camino Dos Rios, Thousand Oaks, CA 91360, USA*

1028-3358/02/4705-0401$22.00

data; and to directly compare them with results of theoretical calculations.

POROUS COATING

We chose a felt metal as a UAC prototype. Its porous layer consisted of thin wires connected to each other and to a substrate in a random fashion. The wires were made of stainless steel 30 μm in diameter. The layer thickness was 0.75 mm. To ensure continuity of the coating, the felt-metal layer was deposited onto a solid base, namely, a stainless steel sheet 0.245 mm thick. The average porosity of the coating was $\phi \approx 0.75$; the average pore diameter was approximately 100 μm, so that there were about 20 pores per disturbance wavelength in the boundary layer.

EXPERIMENTAL METHOD

The experiments were carried out in the T-326 wind tunnel of the Institute of Theoretical and Applied Mechanics, Siberian Division, Russian Academy of Sciences. The following parameters of the unperturbed flow were chosen: the Mach number of the incoming flow was $M_\infty = 5.92$, the stagnation temperature was $T_0^* = 390$ K, the unit Reynolds number was $\mathrm{Re}_{1\infty} = 12.0 \times 10^6$ 1/m, and the surface temperature was $T_w^* = 0.82\,T_0^*$.

We used an acute cone with a vertex semiangle of 7° and a height of 0.5 m as a model. The cone was installed in the flow at the zero angle of attack. The half of the cone surface between generatrices was covered with the UAC, whereas the other half was continuous. The leading edge of the coating was located 186 mm from the cone vertex. A source of artificial disturbances was placed at a distance of 69 mm. The disturbances were introduced into the flow by means of a high-voltage periodic electric discharge initiated in a miniature chamber placed inside the model. The disturbances penetrated into the boundary layer through a hole 0.4 mm in diameter in the cone surface. Spatial distributions of pulsations of the mass flow were measured by a hot-wire anemometer and were subjected to Fourier analysis, which made it possible to obtain the wave characteristics of the pulsations. This technique was successfully used for investigating wave packets propagating in the hypersonic boundary layers [9].

These measurements showed that the flow was laminar on both continuous and porous surfaces. The average flow characteristics in the boundary layer (the flow-velocity profile, the boundary-layer thickness, etc.) turned out to be close to each other and were consistent with calculations based on the boundary-layer theory.

The spectra of natural disturbances were measured in various cross sections along the longitudinal (*X*) and normal (*Y*) coordinate axes. In Fig. 1, we show examples of the amplitude–frequency spectra of mass flow pulsations. The spectra were measured at the *Y*-level corresponding to maximal disturbances and in the cross section $X = 293$ mm on the continuous (*1*) and porous (*2*) surfaces. The arrows in Fig. 1 show the direction of variations in the spectrum pulsation amplitudes as the surface changed from solid to porous. For the solid surface, we obtained the typical disturbance spectrum of [5]. On the porous surface, we observed destabilization of the first mode (low-frequency disturbances within the 100- to 200-kHz band) and strong stabiliza-

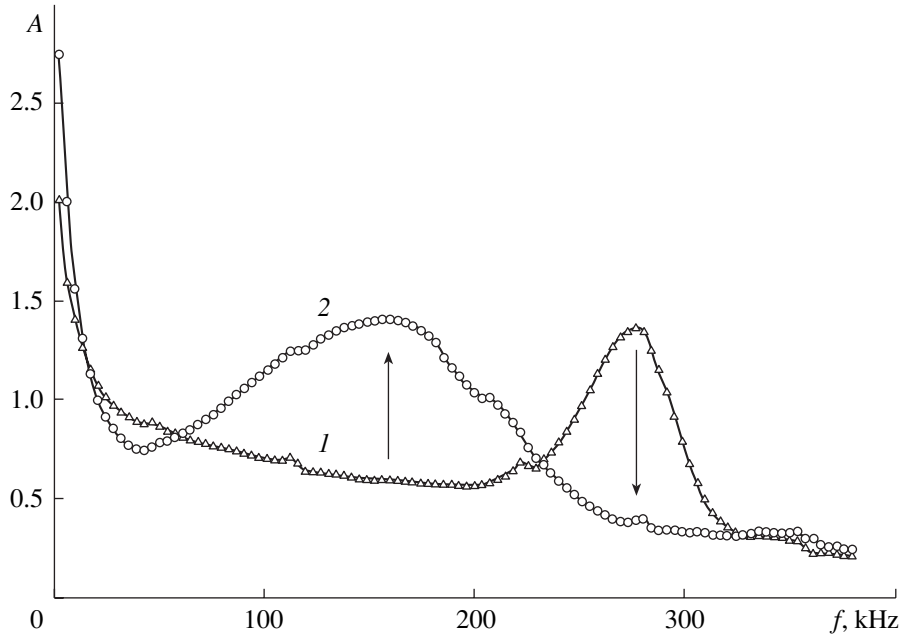

Fig. 1. Amplitude–frequency spectra for the mass flow pulsations on (*1*) solid and (*2*) porous surfaces. $X = 293$ mm.

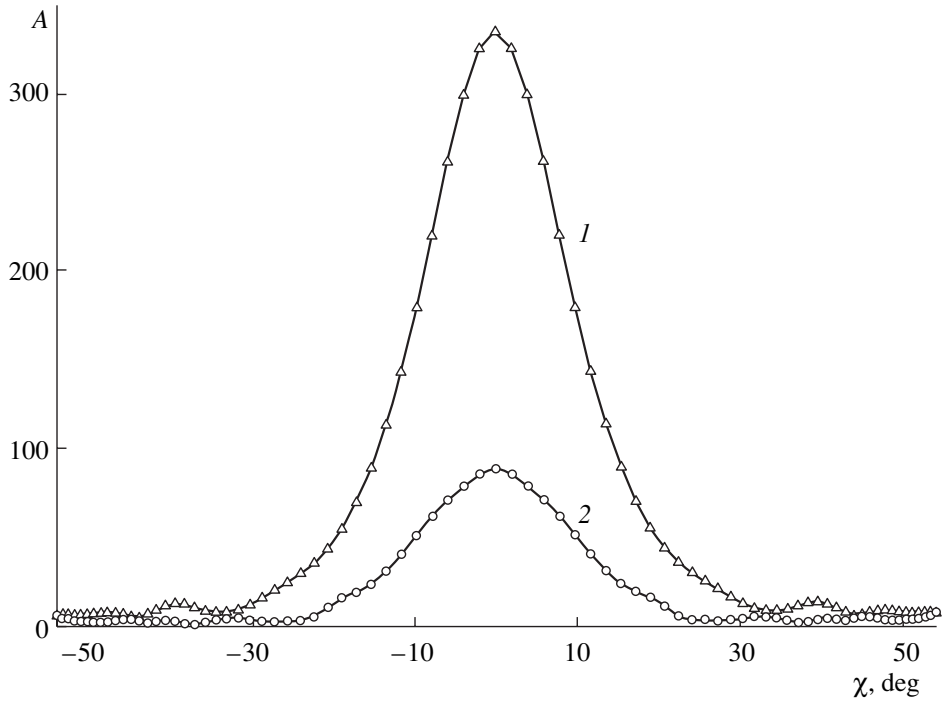

Fig. 2. Distribution of the mass flow pulsations in a wave packet as a function of the wave-vector inclination angle: (*1*) solid surface and (*2*) porous surface; $X = 293$ mm and $f = 280$ kHz.

tion of the second mode (high-frequency disturbances within the 225- to 350-kHz band). This confirms the concept of stabilizing the second mode with ultrasound-absorbing coatings.

Artificial wave packets were introduced into the boundary layer at a frequency $f = 280$ kHz, which corresponded to the most intense disturbances of the second mode. The initial amplitudes of the disturbances in the boundary layers on the solid and porous surfaces were adjusted to be equal. The distributions for mass flow pulsations of the A were measured in the boundary layer and were subjected to Fourier analysis. From the wave spectra, we determined the wave amplitudes for various inclination angles χ of the wave vector to the flow. Examples of the dependences obtained for solid (*1*) and porous (*2*) surfaces are shown in Fig. 2. The maximum at $\chi = 0$ shows that two-dimensional disturbances dominate in both cases, which is typical of the second mode. It can be seen that the UAC strongly stabilizes the disturbances within a wide range of inclination angles χ.

STABILITY ANALYSIS AND COMPARISON WITH EXPERIMENTAL DATA

The stability of a hypersonic boundary layer on a solid surface was analyzed on the basis of the classical approach [1]. The boundary value problem for searching for eigenvalues is formulated using a linear set of stability equations for three-dimensional disturbances. These equations are derived from the complete Navier–Stokes equations and are complemented by zero boundary conditions for disturbances of the velocity and temperature both on the surface and outside the boundary layer. The problem was numerically integrated with allowance for the effects of nonparallel flow streamlines in the boundary layer [10]. The averaged flow was calculated for a compressible boundary layer at an acute cone for a zero angle of attack.

The formulation of the problem on a porous surface differs from the classical problem in the boundary conditions for $Y = 0$. The disturbances of the velocity and temperature are generally proportional to pressure disturbances with corresponding coefficients that characterize the acoustic admittance of a porous medium. The parametric calculations showed that a reasonably good approximation can be obtained if the admittance coefficient is taken into account only for disturbances of the normal velocity component, while the remaining coefficients can be set equal to zero. In this case, the approximated boundary conditions have the form

$$y = 0: \quad u = w = \theta = 0, \quad v = A_y p.$$

Here, u, w, and v are disturbances of the longitudinal, transverse, and normal velocity components; θ is the temperature disturbance; and p is the pressure disturbance. They are made dimensionless with respect to the flow characteristics U_e^*, T_e^*, and $\rho_e^* U_e^{*2}$ at the upper boundary-layer edge, respectively. It was found in [8] that the admittance coefficient is

$$A_y = \frac{\phi \tanh(\Lambda h)}{Z_0},$$

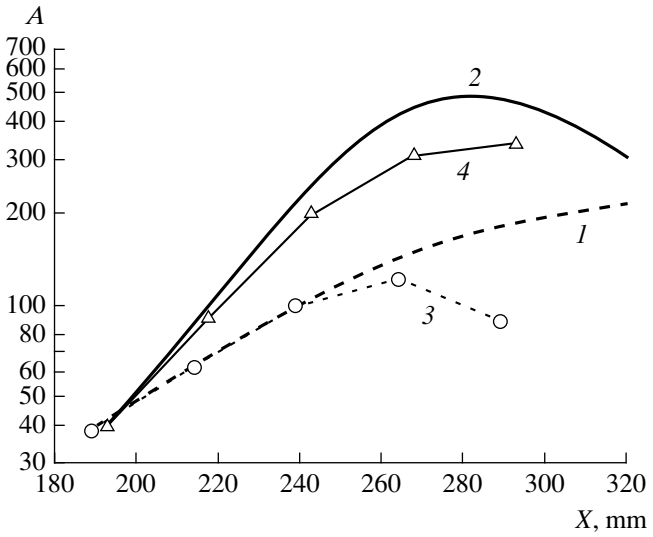

Fig. 3. Growth curves in the mass-flow disturbances for two-dimensional waves, $\chi = 0$, $f = 280$ kHz: (*1*) and (*2*), theoretical predictions; (*3*) and (*4*), experimental data; (*1*) and (*3*), porous surface; (*2*) and (*4*), solid surface.

where $h = \frac{h^*}{\delta^*}$ is the porous-layer thickness (δ^* is the boundary-layer displacement thickness), $Z_0 = -\frac{\sqrt{\bar{\rho}/\bar{C}}}{M_e\sqrt{T_w}}$ is the characteristic impedance, and $\Lambda = \frac{i\omega M_e\sqrt{\bar{\rho}\bar{C}}}{\sqrt{T_w}}$ is the propagation constant or the complex wave number $\left(\omega = \frac{\omega^*\delta^*}{U_e^*}\right.$ is the angular frequency of the disturbance, and $T_w = \frac{T_w^*}{T_e^*}$ is the dimensionless temperature of the surface$\left.\right)$. The dynamic density $\bar{\rho}$ and the dynamic compressibility $\bar{C}$, which were normalized to the average values of the density and pressure on the surface, were calculated using the semiempirical relationships from [11]. These relationships describe sound propagation in a porous material with a solid structure. The parameters involved in these relationships were determined from the data of laboratory measurements related to the reflection of sound from samples of felt metal.

Stability calculations were performed for the conditions of the wind-tunnel experiment: the local Mach number was $M_e = 5.3$; the local temperature was $T_e^* = 59.3$ K; the specific heat ratio was $\gamma = 1.4$; the Prandtl number and the local unit Reynolds number were Pr = 0.708 and $\mathrm{Re}_1 = \frac{U_e^*}{\nu_e^*} = 15.5 \times 10^6$ 1/m, respectively; and the surface temperature was $T_w^* = 5.5\,T_e^*$. The last value is close to the temperature of a heat-insulated wall. The data presented in Fig. 3 allow us to compare the theoretical curves for the mass-flow growth (lines) with the experimental data (symbols) for two-dimensional disturbances ($\chi = 0$) at a frequency $f = 280$ kHz. Good agreement between the theoretical and experimental results is observed. It should be noted that the theoretical values of the growth rates for disturbances (or the slope of the growth curves) are very close to the experimental data within the range $190 < X < 260$ mm, especially for the porous surface.

The results of the present study lead to the following conclusions. If the three-dimensional effects of the mean flow are minimized (which helps to avoid crossflow instability), the surface roughness is made acceptable (to avoid bypass), and the second mode is stabilized using a thin porous coating, then it seems to be possible to retain the laminar flow around the greater part of a hypersonic vehicle surface. This leads to both a considerable decrease in heat flows and an increase in the lift–drag ratio, which is an important factor in developing hypersonic vehicles of new generation.

ACKNOWLEDGMENTS

This work was supported by the Rockwell Scientific Company, contracts B1S438293 and B1S438296.

REFERENCES

1. L. M. Mack, Advisory Group for Aerospace Research, Rep. No. 709, 3 (1984).
2. S. A. Gaponov, Prikl. Mekh. Tekh. Fiz., No. 1, 121 (1975).
3. S. A. Gaponov, Izv. Akad. Nauk SSSR, Ser. Mekh. Zhidk. Gaza, No. 1, 41 (1977).
4. P. W. Carpenter and L. J. Porter, AIAA J. **39**, 597 (2001).
5. R. Kimmel, A. Demetriades, and J. Donaldson, Am. Inst. of Aeronautics and Astronautics, Paper No. 95-2292 (1995).
6. N. D. Malmuth, A. V. Fedorov, V. Shalaev, J. Cole, and A. Khokhlov, AIAA Papers, No. 98-2995 (1998).
7. A. V. Fedorov and N. D. Malmuth, AIAA J. **39**, 605 (2001).
8. A. Rasheed, H. G. Hornung, A. V. Fedorov, and N. D. Malmuth, Am. Inst. of Aeronautics and Astronautics, Paper No. 2001-0274 (2001).
9. A. A. Maslov, A. N. Shiplyuk, A. A. Sidorenko, and D. Arnal, J. Fluid Mech. **426**, 73 (2001).
10. V. N. Zhigulev and A. M. Tumin, *Occurrence of Turbulence* (Nauka, Novosibirsk, 1987).
11. J.-F. Allard and Y. Champoux, J. Acoust. Soc. Am. **91**, 3346 (1992).

Translated by V. Bukhanov

Doklady Physics, Vol. 47, No. 5, 2002, pp. 405–409. Translated from Doklady Akademii Nauk, Vol. 384, No. 3, 2002, pp. 341–345.

MECHANICS

Reorientation of a Rigid Body under Conditions of Uncertainty

V. I. Vorotnikov

Presented by Academician V.V. Rumyantsev February 4, 2002

Received February 6, 2002

The nonlinear game problem of the reorientation of an asymmetric rigid body in the presence of uncontrolled noise and inaccurately specified inertial characteristics is considered. Certain geometric restrictions are imposed on controlling moments and noise. A method of solving this problem [1–4] is developed on the basis of the equivalent linearization of nonlinear conflict-controlled systems and by using the methods of linear game theory [5]. The admissible range of noise was found as a function of the constraints imposed on the controlling moments and the original position of the body, as well as of the constraints on the inertial characteristics of the body.

1. Formulation of the problem. We consider three equations, one of which has the form

$$J_1\dot{x}_1 - J_{12}\dot{x}_2 - J_{13}\dot{x}_3 + (J_3 - J_2)x_2x_3 + J_{23}(x_3^2 - x_2^2) + (J_{12}x_3 - J_{13}x_2)x_1 = u_1 + \nu_1 \ (123), \tag{1.1}$$

where x_i are the projections of the angular velocity $\mathbf{x}$ of the body onto the axes of the *Oxyz* system, u_i are the controls (the projections of the controlling moment $\mathbf{u}$ onto the same axes), J_i are the axial moments of inertia and J_{ij} are the centrifugal moments of inertia of the body, ν_i characterize external forces and uncontrolled disturbances and are treated as the components of a vector $\boldsymbol{\nu}$, and (123) means that the other two equations are obtained by cyclic permutation of the subscripts $1 \longrightarrow 2 \longrightarrow 3$. These equations describe the rotational (angular) motion of a rigid body with respect to the Cartesian coordinate system *Oxyz* associated with the body.

In most applied problems, the inertial characteristics of a body are specified with uncertainties. Tolerances for the parameters of system (1.1) are defined as

$$A_i^- \le J_i \le A_i^+, \quad \max(|J_{12}|, |J_{13}|, |J_{23}|) \le \gamma, \tag{1.2}$$

where A_i^-, A_i^+, and γ are given positive numbers.

Nizhniĭ Tagil Technology Institute,
Ural State Technical University,
ul. Krasnogvardeĭskaya 59, Nizhniĭ Tagil, 622031 Russia
e-mail: vorot@ntiustu.ru

Along with Eqs. (1.1), we consider the following kinematic equations in the Rodrigues–Hamilton variables (hereafter, summation with respect to the subscript i is performed from 1 to 3) [6]:

$$2\dot{\lambda}_0 = -\sum(x_i\lambda_i),$$
$$2\dot{\lambda}_1 = x_1\lambda_0 + x_3\lambda_2 - x_2\lambda_3 \ (123), \tag{1.3}$$

which determine the orientation of the body. The variables λ_0 and λ_i forming the vector $\boldsymbol{\lambda}$ are related to each other as

$$\lambda_0^2 + \sum\lambda_i^2 = 1. \tag{1.4}$$

The controls $u_i \in K$ are taken in the class K of the piecewise continuous functions $u_i = u_i(\mathbf{x}, \boldsymbol{\lambda}, \mathbf{x}^0, \boldsymbol{\lambda}^0)$, where $\mathbf{x}^0$ and $\boldsymbol{\lambda}^0$ are the original values of $\mathbf{x}$ and $\boldsymbol{\lambda}$, respectively, and satisfy the constraints

$$\|\mathbf{u}\| = \left(\sum u_i^2\right)^{1/2} \le \alpha = \text{const} > 0 \tag{1.5}$$

corresponding to a pair of vernier (rotary) engines, which generate controlling moments u_i with respect to the axes of the *Oxyz* system [7].

Noise $\nu_i \in K_1$ can be realized in the form of arbitrary piecewise continuous functions $\nu_i[t]$ satisfying the constraint

$$|\nu_i| \le \beta_i = \text{const} > 0. \tag{1.6}$$

In this case, the probability characteristics of realizing noise within the limits imposed by inequalities (1.6) are unknown.

Problem 1. For all $\nu_i \in K_1$ and all inertial characteristics satisfying conditions (1.2), it is necessary to find the controls $u_i \in K$ transferring a body from the initial state $\boldsymbol{\lambda}(t_0) = \boldsymbol{\lambda}^0$ to a given state $\boldsymbol{\lambda}(t_1) = \boldsymbol{\lambda}^1$ in a finite time. Both states are rest states: $\mathbf{x}(t_0) = \mathbf{x}^0 = \mathbf{x}(t_1) = \mathbf{x}^1 = \mathbf{0}$. The time $t_1 > t_0$ is not fixed.

Remarks. (i) Below, we take $\boldsymbol{\lambda}^1 = (1, 0, 0, 0)$ without loss of generality.

(ii) A further solution of problem 1 is valid for all J_i, J_{12}, J_{13}, and J_{23} values satisfying conditions (1.2),

1028-3358/02/4705-0405$22.00 © 2002 MAIK “Nauka/Interperiodica”

although the inertial characteristics of an actual body satisfy additional relations [8].

2. Auxiliary linear conflict-controlled system. By solving Eqs. (1.1) with respect to $\dot{x}_i$, we arrive at the expressions

$$\begin{aligned}\dot{x}_1 &= F_1(\mathbf{x}, \mathbf{u}, \mathbf{v}) = \Delta^{-1}(P_1\Lambda_1 + Q_1\Lambda_2 + R_1\Lambda_3),\\ P_1 &= J_2J_3 - J_{23}^2, \quad Q_1 = J_3J_{12} + J_{13}J_{23},\\ R_1 &= J_2J_{13} + J_{12}J_{23},\\ g_1 &= (J_2 - J_3)x_2x_3 + J_{23}(x_2^2 - x_3^2)\\ &\quad + (J_{13}x_2 - J_{12}x_3)x_1 \ (123),\\ \Lambda_i &= g_i + u_i + v_i.\end{aligned} \tag{2.1}$$

Here, $\Delta = \det(J)$, where J is the matrix of the inertia tensor of the body.

Following [2–4], we differentiate both sides of each of Eqs. (1.3) for $\dot{\lambda}_i$ with respect to time and substitute $\dot{x}_i$ from Eqs. (2.1), where F_i are represented in the form

$$F_1 = J_1^{-1}u_1 + \Delta^{-1}(P_1^*u_1 + Q_1u_2 + R_1u_3) + F_1^*(\mathbf{x}, \mathbf{v}),$$

$$P_1^* = J_1^{-1}(J_2J_{13}^2 + J_3J_{12}^2 + 2J_{12}J_{13}J_{23}) \ (123),$$

where F_i^* are free of terms dependent on u_i.

After transformations, we obtain the equations

$$\begin{aligned}\ddot{\lambda}_i &= f_i(\boldsymbol{\lambda}, \mathbf{u}) + \varphi_i(\boldsymbol{\lambda}, \mathbf{v}, \mathbf{x}),\\ f_1 &= \frac{1}{2}[\lambda_0J_1^{-1}u_1 + \lambda_2J_3^{-1}u_2 - \lambda_3J_2^{-1}u_3] + f_1^0,\\ f_1^0 &= \frac{1}{2}\Delta^{-1}(\lambda_0P_1^*u_1 + \lambda_2Q_1u_2 - \lambda_3R_1u_3),\\ \varphi_1 &= \frac{1}{2}\Delta^{-1}(\lambda_0P_1\Lambda_1^* + \lambda_2Q_1\Lambda_2^* - \lambda_3R_1\Lambda_3^*)\\ &\quad - \frac{1}{4}\lambda_1\sum x_i^2 \ (123), \quad \Lambda_i^* = g_i + v_i.\end{aligned} \tag{2.2}$$

If, following [1–3], f_i and φ_i are treated as auxiliary controls and noise, respectively, the initial controls u_i depend explicitly on the matrix components of the inertia tensor of the body. In case (1.2) under consideration, this leads to uncertainty in the realization of u_i.

In the method of equivalent linearization, this uncertainty can be overcome as follows. According to estimates (1.2), we have $J_i = A_i^- + \delta_iA_i^-$, where δ_i is any number from the given range $\delta_i \in [0, \delta_i^+]$, where $\delta_i^+ = (A_i^+)(A_i^-)^{-1} - 1$.

Let us use the equalities

$$\begin{aligned}J_i^{-1} &= [A_i^-(1 + \delta_i)]^{-1} = (A_i^-)^{-1}(1 - \delta_i^*),\\ \delta_i^* &= \delta_i(1 + \delta_i)^{-1},\end{aligned} \tag{2.3}$$

which can be directly verified. With allowance for Eq. (2.3), Eqs. (2.2) are represented in the form

$$\begin{aligned}\ddot{\lambda}_i &= f_i^*(\boldsymbol{\lambda}, \mathbf{u}) + \varphi_i^*(\boldsymbol{\lambda}, \mathbf{u}, \mathbf{v}, \mathbf{x}),\\ \varphi_1^* &= \varphi_1 - \frac{1}{2}[\lambda_0\delta_1^*u_1(A_1^-)^{-1} + \lambda_2\delta_3^*u_3(A_3^-)^{-1}\\ &\quad - \lambda_3\delta_2^*u_2(A_2^-)^{-1}] + f_1^0 \ (123)\end{aligned} \tag{2.4}$$

and expressions for f_i^* are obtained from the expressions for φ_i^* at $\varphi_i = f_i^0 = 0$ and $\delta_1^* = \delta_2^* = \delta_3^* = -1$.

We treat f_i^* and φ_i^* as auxiliary controls u_i^* and noise v_i^* and Eqs. (2.4) as a conflict-controlled system:

$$\ddot{\lambda}_i = u_i^* + v_i^*. \tag{2.5}$$

In this case, the initial controls have the form

$$\begin{aligned}u_1 &= \frac{2A_1^-}{\lambda_0}[(\lambda_0^2 + \lambda_1^2)u_1^* + (\lambda_1\lambda_2 + \lambda_0\lambda_3)u_2^*\\ &\quad + (\lambda_1\lambda_3 - \lambda_0\lambda_3)u_3^*] \ (123)\end{aligned} \tag{2.6}$$

and are free of inaccurately specified inertial characteristics.

Then, the solution of original nonlinear problem 1 is constructed on the basis of the corresponding game problems for linear system (2.5). As a result, Eqs. (2.6) can be treated as the general form of controls in problem 1.

In order to estimate auxiliary noise v_i^*, we propose the principle of specification and further verification of its levels on the set of states of linear system (2.5).

3. Auxiliary linear game problem and algorithm for solving problem 1. Let us solve the game problem of the fastest transfer (for any admissible v_i^*) of system (2.5) to the position

$$\lambda_i = \dot{\lambda}_i = 0. \tag{3.1}$$

In order for this problem to be solvable, the admissible levels u_i^* must be higher than the levels v_i^*. The corresponding constraints are taken in the form

$$|u_i^*| \le \alpha_i^*, \quad |v_i^*| \le \beta_i^* = \rho_i\alpha_i^*, \quad 0 < \rho_i < 1.$$

For fixed α_i^* and β_i^* values such as $\alpha_i^* > \beta_i^*$, the game problem indicated above for system (2.5) reduces

to the problem of the optimal speed for the system [5]

$$\ddot{\lambda}_i = (1-\rho_i)u_i^*, \quad |u_i^*| \le \alpha_i^*. \tag{3.2}$$

The boundary conditions are the same as for system (2.5). System (3.2) follows from Eqs. (2.5) at $v_i^* = -\rho_i u_i^*$. These "worst" v_i^* values are optimal controls of an "opponent."

The solution of the speed problem for system (3.2) has the form [9]

$$u_i^*(\lambda_i, \dot{\lambda}_i) = \begin{cases} \alpha_i^* \operatorname{sgn}\psi_i(\lambda_i, \dot{\lambda}_i), & \psi_i \ne 0 \\ \alpha_i^* \operatorname{sgn}\lambda_i = -\alpha_i^* \operatorname{sgn}\dot{\lambda}_i, & \psi_i = 0, \end{cases} \tag{3.3}$$

where $\psi_i = -\dot{\lambda}_i - [2\alpha_i^*(1-\rho_i)]^{-1}\dot{\lambda}_i|\dot{\lambda}_i|$ are the switch functions.

Since $\dot{\lambda}_i^0 = \dot{\lambda}_i^1 = 0$ due to $\mathbf{x}^0 = \mathbf{x}^1 = \mathbf{0}$, the quantity

$$\tau = \max(\tau_i), \quad \tau_i = 2\{|\lambda_i^0|[\alpha_i^*(1-\rho_i)]^{-1}\}^{1/2} \tag{3.4}$$

determines the minimum guaranteed time of control in the linear game problem for system (2.5). In this case, the quantity τ determines the guaranteed time of reorientation in problem 1.

An iteration algorithm for solving problem 1 includes the following stages [2–4]:

(i) Specification of β_i^* and preliminary choice of the value $\tau = \tau_i$. This condition determines the values α_i^* and ρ_i in Eqs. (3.3).

(ii) Verification of actual fulfillment of inequalities $|v_i^*| \le \beta_i^*$ and constraint (1.5) on the set of states of the system specified by Eqs. (2.5) and (3.3).

The algorithm will be described in Section 5.

Remarks. (i) Form (2.6) of the controls formally leads to a singularity arising at $\lambda_0 = 0$. However, $|\lambda_0| \in [|\lambda_0^0|, 1]$ in the control process and this singularity does not arise.

(ii) Let $\boldsymbol{\lambda}^1 \ne (1, 0, 0, 0)$. In this case, in order to avoid a singularity, it is sufficient to pass to controls obtained from Eqs. (2.6) by rearranging subscripts (or to the combination of these controls).

4. Estimation of the admissible region of uncontrolled noise. Let us find the sufficient condition on α, β_i, λ_0^0, δ_i, and γ that determines the possibility of solving problem 1 in the approach proposed above.

Let $\delta^* = \max(\delta_i^*)$, $A_* = \min(A_i^-)$, and $A^* = \max(A_i^-)$; B^+ and C^+ be the middle and larger A_i^+ values, respectively; and

$$D = \max[B^+C^+, \gamma(C^+ + \gamma)],$$

$$E = \max[\gamma^2 A_*^{-1}(B^+ + C^+ + 2\gamma), \gamma(C^+ + \gamma)],$$

$$\Delta_* = A_1^-A_2^-A_3^- - \gamma^2(A_1^+ + A_2^+ + A_3^+ + 2\gamma).$$

Theorem 1. *Let the admissible region of noise v_i be estimated by the inequality*

$$\left(\sum \beta_i^2\right)^{1/2} < K\alpha,$$

$$K = D^{-1}\left\{\Delta_*\left[\frac{\sqrt{3}}{3}(A^*)^{-1}|\lambda_0^0| - A_*^{-1}\delta^*\right] - E\right\}. \tag{4.1}$$

In this case, problem 1 *is solved by means of controls* (2.6) *and* (3.3) *satisfying given constraint* (1.5).

The **proof** of the theorem is divided into the following three stages:

(i) Applying the scheme used in [1–3], we obtain the estimates

$$\frac{1}{4}\|\mathbf{u}\|^2 \le (\lambda_0^0)^{-2}(A^*)^2\sum \alpha_i^{*2}. \tag{4.2}$$

(ii) Let us estimate v_i^* on the set of possible states of the system specified by Eqs. (2.5) and (3.3). By using the Cauchy–Schwartz inequality and relations $\Delta \ge \Delta_*$ and (1.4), Eqs. (2.4) for v_i^* can be estimated as

$$|v_1^*| \le \frac{1}{2}\Delta_*^{-1}\left[D_1\left(\sum v_i^2\right)^{1/2} + E_1\|\mathbf{u}\|\right] + \frac{1}{2}\delta^*\|\mathbf{u}\|^*$$

$$+ \frac{1}{2}\Delta_*^{-1}D_1\left(\sum g_i^2\right)^{1/2} + \frac{1}{4}|\lambda_1^0|\sum x_i^2 \ (123),$$

$$\|\mathbf{u}^*\| = \left\{\sum [u_i(A_i^-)^{-1}]^2\right\}^{1/2}, \tag{4.3}$$

$$E_i = \max[\sup(P_i^*, Q_i, R_i)],$$

$$D_i = \max[\sup(P_i, Q_i, R_i)],$$

where a supremum is calculated on set (1.2), whereas a maximum is chosen for each i among the three values $\sup(P_i^*, Q_i, R_i)$. In this case, since $|x_1x_2| \le \frac{1}{2}\sum x_i^2$ (123), we have

$$|g_1| \le \frac{1}{2}(|J_2 - J_3| + |J_{13}| + |J_{12}| + |J_{23}|)\sum x_i^2$$

$$\le \frac{1}{2}[(C^+ - A_*) + 3\gamma]\sum x_i^2 \ (123). \tag{4.4}$$

Taking into account inequalities (4.4) and relations $D_i \le D$ and $E_i \le E$, we refine estimates (4.3) as

$$|v_i^*| \le \frac{1}{2}\Delta_*^{-1}\left[D\left(\sum v_i^2\right)^{1/2} + E\|\mathbf{u}\|\right]$$

$$+\frac{1}{2}\delta^* A_*^{-1}\|\mathbf{u}\| + L\sum x_i^2, \tag{4.5}$$

$$L = \frac{1}{4} + \frac{\sqrt{3}}{4}\Delta_*^{-1} D[(C^+ - A_*) + 3\gamma].$$

To estimate $\sum x_i^2$, we solve the system for $\dot{\lambda}_i$ in Eqs. (1.3) with respect to x_i. After corresponding manipulations, we arrive at the equalities

$$x_1 = 2\lambda_0^{-1}[(\lambda_0^2 + \lambda_1^2)\dot{\lambda}_1 + (\lambda_1\lambda_2 + \lambda_0\lambda_3)\dot{\lambda}_2 + (\lambda_1\lambda_3 - \lambda_0\lambda_2)\dot{\lambda}_3] \quad (123), \tag{4.6}$$

which provide the inequality

$$\frac{1}{4}\sum x_i^2 \le \lambda_0^{-2}\sum \dot{\lambda}_i^2.$$

Estimates for $\dot{\lambda}_i^2$ have the form [4]

$$\dot{\lambda}_i^2 \le (\dot{\lambda}_i^+)^2 = |\lambda_i^0|(\alpha_i^*)^{-1}[(\alpha_i^*)^2 - (\beta_i^*)^2].$$

Taking Eqs. (1.5) and (4.5) into account, we obtain

$$|v_i^*| \le \varphi,$$

$$\varphi = \frac{1}{2}\Delta_*^{-1}\left[D\left(\sum \beta_i^2\right)^{1/2} + \alpha E\right] + \frac{1}{2}\alpha\delta^* A_*^{-1} + 4(\lambda_0^0)^{-2} L\sum\{|\lambda_i^0|(\alpha_i^*)^{-1}[(\alpha_i^*)^2 - (\beta_i^*)^2]\}. \tag{4.7}$$

(iii) The resulting estimates (4.2) and (4.7) are applied to prove the theorem. Let us demonstrate that, when conditions (4.1) are satisfied, there are numbers α_i^* and β_i^* such that $\alpha_i^* > \beta_i^*$ and the following inequalities are satisfied on the set of possible states of the system specified by Eqs. (2.5) and (3.3):

$$|v_i^*| \le \beta_i^*, \tag{4.8}$$

which corroborate the specified levels β_i^* of auxiliary noise v_i^* and inequality (1.5).

Taking Eq. (4.1) into account, we set

$$\left(\sum \beta_i^2\right)^{1/2} = K\alpha - \varepsilon,$$

$$\alpha_i^* = \alpha^* = \frac{\sqrt{3}}{6}|\lambda_0^0|(A^*)^{-1}\alpha, \quad \beta_i^* = \alpha^* - \varepsilon_1, \tag{4.9}$$

where $\varepsilon > \varepsilon_1 > 0$ are as small as desired.

In view of Eqs. (4.9), we have $\alpha_i^* > \beta_i^*$ for a given arbitrarily small value $\varepsilon > 0$. Therefore, the auxiliary game problem for linear system (2.5) is solvable.

Then, we demonstrate that Eqs. (4.8) are satisfied on the set of possible states of the system specified by Eqs. (2.5) and (3.3) for a sufficiently small value $\varepsilon > 0$. Indeed, in this case, the value φ in Eqs. (4.7) differs arbitrarily little from the value $\varphi = \alpha^*$. For this reason, taking Eqs. (4.7) into account, we have $|v_i^*| \le \beta_i^*$ on the set of possible states of the system specified by Eqs. (2.5) and (3.3).

Let us also demonstrate that constraints (1.5) are satisfied on the set of possible states of the system specified by Eqs. (2.5) and (3.3) for a sufficiently small value $\varepsilon > 0$. Indeed, taking Eqs. (4.2) and (4.9) into account, we have

$$\|\mathbf{u}\|^2 \le 4(\lambda_0^0)^{-2}(A^*)^2\sum \alpha_i^{*2} = 12(\lambda_0^0)^{-2}(A^*\alpha^*)^2 = \alpha^2.$$

The theorem has been proven.

Remarks. (i) Estimate (4.1) is a sufficient condition and is directly associated with proposed form (2.6) of the control laws. This form is only one of the possible forms of (2.6) (which go over from one to another by rearranging the subscripts) that enable one to consider the problem of reorientation for any initial position of the body. In view of this circumstance and the accepted assumption that $\boldsymbol{\lambda}^1 = (1, 0, 0, 0)$, we can consider that $|\lambda_0^0| \ge \frac{1}{2}$ in Eq. (4.1).

(ii) Condition (4.1) guarantees that the controls specified by Eqs. (2.6) and (3.3) solve problem 1 for a large enough (but finite) τ value. If condition (4.1) is oversatisfied, the guaranteed time τ of reorientation can be found by the algorithm that was mentioned in Section 3 and will be described in Section 5.

(iii) The above approach is associated with the concept of the decomposition of nonlinear controlled systems [10, 11] and is based on results obtained in [12]. The subject under consideration is connected with [13–15].

5. Realization of an algorithm for solving problem 1 and estimation of the guaranteed time of reorientation. Let α, δ_i, and γ be given and estimate (4.1) be oversatisfied, i.e.,

$$\left(\sum \beta_i^2\right)^{1/2} = K\alpha - \sigma, \tag{5.1}$$

where $\sigma > 0$ is a certain number. In this case, the following iteration algorithm can be applied to find τ:

(i) According to Eq. (4.9), $\alpha_i^* = \alpha^*$ is taken, which guarantees the fulfillment of inequality (1.5).

(ii) A probe value $\tau = \tau_i$ is specified, which determines the β_i^* values in view of Eq. (3.4).

(iii) Inequalities $|v_i^*| \le \beta_i^*$ are verified on the basis of estimates (4.7). If these inequalities are not satisfied or are oversatisfied, the value τ increases or decreases, respectively.

One can obtain a direct upper estimate for the guaranteed time of reorientation τ calculated by this algorithm.

Theorem 2. *Let equality* (5.1) *be satisfied. In this case,*

$$\tau \le \tau^* = 2\lambda^*[2(\sigma\Delta_*^{-1}D)^{-1}]^{1/2},$$

$$\lambda^* = \{\max|\lambda_i^0| + 2L[(\lambda_0^0)^{-2} - 1]\}^{1/2}.$$

6. Calculations for a centrally symmetric body. In this case, the A_i^- values are equal to each other ($A_i^- = A^-$) and estimate (4.1) has the form

$$\left(\sum \beta_i^2\right)^{1/2} < K_*\alpha,$$

$$K_* = (DA^-)^{-1}\left\{\Delta_*\left[\frac{\sqrt{3}}{3}|\lambda_0^0| - \delta^*\right] - A^-E\right\}. \quad (6.1)$$

For the same α, λ_0^0, δ_i, and γ values, the region of admissible noise (6.1) is considerably wider than the region of admissible noise (4.1) for an asymmetric body.

7. Example. Let us consider the reorientation of a rigid body from the position $\mathbf{x}^0 = \mathbf{0}$, $\boldsymbol{\lambda}^0 = (0.701, 0.353, 0.434, 0.432)$ to the position $\mathbf{x}^1 = \mathbf{0}$, $\boldsymbol{\lambda}^1 = (1, 0, 0, 0)$.

(i) For $A_1^- = 4 \times 10^4$ kg m^2, $A_2^- = 8 \times 10^4$ kg m^2, and $A_3^- = 5 \times 10^4$ kg m^2, we have $K = 0.1209$ and 0.1819 for $\gamma = 10^3$ kg m^2 and $\delta_i = 0.05$ and 0, respectively, whereas $K = 0.2024$ for $\delta_i = \gamma = 0$.

(ii) For $A_i^- = A^- = 4 \times 10^4$ kg m^2, we have $K_* = 0.3239$ and 0.3783 for $\gamma = 10^3$ kg m_2 and $\delta_i = 0.05$ and 0, respectively, whereas $K_* = 0.4047$ for $\delta_i = \gamma = 0$.

ACKNOWLEDGMENTS

This work was supported by the Russian Foundation for Basic Research (project no. 99-01-00965) and by the Ministry of Education of the Russian Federation.

REFERENCES

1. V. I. Vorotnikov, Prikl. Mat. Mekh. **58** (3), 82 (1994).
2. V. I. Vorotnikov, Dokl. Akad. Nauk **343**, 630 (1995) [Phys. Dokl. **40**, 146 (1995)].
3. V. I. Vorotnikov, *Partial Stability and Control* (Birkhauser, Boston, 1998).
4. V. I. Vorotnikov and V. V. Rumyantsev, *Stability and Control Relative to Part of the Coordinates of Phase Space* (Nauchnyĭ Mir, Moscow, 2001).
5. N. N. Krasovskiĭ, *Game Problems of Movement Meeting* (Nauka, Moscow, 1970).
6. A. I. Lur'e, *Analytical Mechanics* (Fizmatgiz, Moscow, 1961).
7. M. Athans and P. L. Falb, *Optimal Control* (McGraw-Hill, New York, 1966).
8. A. P. Markeev, *Theoretical Mechanics* (CheRo, Moscow, 1999).
9. L. S. Pontryagin, V. G. Boltyanskil, R. V. Gamkrelidze, and E. F. Mishchenko, *The Mathematical Theory of Optimal Processes* (Nauka, Moscow, 1983; Gordon and Breach, New York, 1986).
10. D. D. Siljak, *Decentralized Control of Complex Systems* (Academic, Cambridge, 1990).
11. F. L. Chernous'ko, Izv. Akad. Nauk, Tekh. Kibern., No. 1, 209 (1993).
12. V. I. Vorotnikov, *The Stability of Dynamical Systems Relative to Part of the Variables* (Nauka, Moscow, 1991).
13. A. Miele, T. Wang, and W. W. Melvin, J. Optim. Theory Appl. **49**, 1 (1986).
14. G. Leitmann and S. Pandey, J. Optim. Theory Appl. **70**, 25 (1991).
15. N. D. Botkin, M. A. Zarkh, V. M. Kein, V. S. Patsko, and V. L. Turova, Izv. Akad. Nauk, Tekh. Kibern., No. 1, 68 (1993).

Translated by R. Tyapaev

Doklady Physics, Vol. 47, No. 5, 2002, pp. 410–413. Translated from Doklady Akademii Nauk, Vol. 384, No. 3, 2002, pp. 346–349.

MECHANICS

Constitutive Equations of Two-Phase Filtration in Anisotropic Porous Media with Monoclinic Symmetry of the Filtration Properties

N. M. Dmitriev, V. V. Kadet, and M. N. Dmitriev

Presented by Academician R.I. Nigmatulin January 22, 2002

Received January 29, 2002

In this paper, we present and analyze the law of the filtration of two immiscible fluids in anisotropic media with monoclinic symmetry of the filtration properties. It was shown that the symmetry of the filtration properties can generally change when passing from the absolute-penetrability tensor to the phase-penetrability tensor. In this case, the tensors of phase-penetrability coefficients are not coaxial with each other or with the absolute-penetrability tensor. Furthermore, the position of the principal axes of the tensors of phase-penetrability coefficients can depend on saturation.

Generalization of the classical models that describe the two-phase-filtration of immiscible fluids in terms of the tensors of phase-penetrability coefficients to the case of anisotropic filtration properties is of current interest, because real porous and cracked media that are used as collectors of a hydrocarbon raw material are usually anisotropic. In [1–3], we established the structure of constraints for the tensors of the coefficients of absolute, phase, and relative penetrabilities for media revealing anisotropic filtration properties; wrote and analyzed the tensors of phase and relative penetrabilities; and determined the general form of the functions of relative phase penetrabilities.

However, we considered only the simplest types of anisotropy: the filtration laws for media with transverse-isotropic and orthotropic filtration properties. In media with these types of anisotropy, the position of all the principal axes of the absolute-penetrability tensor is considered to be *a priori* known. In real porous and cracked media, this is seldom the case. For example, in cracked collectors with mutually perpendicular cracks, it is possible to determine the positions of all the principal axes of the penetrability tensor, whereas in porous media with pronounced stratification, it is *a priori* possible to establish the position of only one principal axis perpendicular to the stratification direction. Anisotropic continua for which the position of only one principal axis in the second-rank material tensors is *a priori* known have monoclinic symmetry. There are only three such point symmetry groups, and they are classified as the monoclinic-system symmetry groups in crystallography [4]. For this reason, many real collectors of hydrocarbon raw material have monoclinic symmetry of the filtration properties.

PRINCIPAL RELATIONSHIPS

In the phenomenological theory of the two-phase filtration of immiscible fluids (e.g., oil and water), Darcy's law is assumed to be satisfied for each phase. Thus, along with the tensor k_{ij} of absolute-penetrability coefficients, which satisfies the material properties in Darcy's law for the filtration of a single homogeneous fluid, additional material characteristics are introduced in the form of phase-penetrability tensors k_{ij}^{α}, where the superscript $\alpha = 1, 2$ is the phase number. The tensors k_{ij}^{α} determine and specify the filtration properties for a simultaneous flow of two immiscible homogeneous fluids.

It was experimentally established that the tensors k_{ij}^{α} and k_{ij} for isotropic porous media are related as

$$k^{\alpha}\delta_{ij} = f^{\alpha}(s_1, s_2)k\delta_{ij}, \tag{1}$$

where δ_{ij} is the Kronecker delta; k and k^{α} are the coefficients of absolute and phase penetrabilities, respectively; and $f^{\alpha}(s_1, s_2)$ are the relative phase penetrabilities, which are functions of the phase saturations s_1 and s_2 of the porous medium. Since the sum of the saturations is equal to unity, only one of them can be taken as an argument. Conventionally, the water saturation is taken as the argument and is designated as s.

The generalization of Eq. (1) to the case of anisotropic media has the form [1]

$$k_{ij}^{\alpha} = F_{ijkl}^{\alpha}k_{kl}, \tag{2}$$

where F_{ijkl}^{α} are the components of the fourth-rank ten-

Gubkin State Academy of Oil and Gas, Leninskiĭ pr. 65, Moscow, 117917 Russia

1028-3358/02/4705-0410$22.00

sor symmetric in the first and second pairs of subscripts and their permutation. The components F^{α}_{ijkl} determine and specify the tensors of the coefficients of relative phase penetrabilities. An explicit form of the tensors k_{ij} and k^{α}_{ij} is determined in independent experiments, and, in general, the external symmetries of these tensors (the type of anisotropy) can differ from each other [2]. In this case, the symmetry of the tensor k_{ij} is higher than or coincides with the symmetry of k^{α}_{ij}; therefore, the external symmetry of the tensors F^{α}_{ijkl} generally coincides with the external symmetry of the tensors k^{α}_{ij} [2]. We suppose that the tensors k^{α}_{ij} and F^{α}_{ijkl} have the symmetry groups of the monoclinic system.

The fourth-rank and second-rank tensors for the monoclinic symmetry groups have the respective forms

$$\begin{aligned}
F^{\alpha}_{ijkl} &= c^{\alpha}_{11}a_ia_ja_ka_l + c^{\alpha}_{12}(a_ia_jc_kc_l + c_ic_ja_ka_l)\\
&+ c^{\alpha}_{13}(a_ia_jb_kb_l + b_ib_ja_ka_l) + c^{\alpha}_{22}c_ic_jc_kc_l\\
&+ c^{\alpha}_{33}b_ib_jb_kb_l + c^{\alpha}_{23}(c_ic_jb_kb_l + b_ib_jc_kc_l)\\
&+ c^{\alpha}_{15}(a_ia_jb_ka_l + a_ia_ja_kb_l + b_ia_ja_ka_l + a_ib_ja_ka_l)\\
&+ c^{\alpha}_{25}(c_ic_jb_ka_l + c_ic_ja_kb_l + b_ia_jc_kc_l + a_ib_jc_kc_l)\\
&+ c^{\alpha}_{35}(b_ib_jb_ka_l + b_ib_ja_kb_l + b_ia_jb_kb_l + a_ib_jb_kb_l)\\
&+ c^{\alpha}_{44}(c_ib_jc_kb_l + b_ic_jc_kb_l + b_ic_jc_kb_l + b_ic_jb_kc_l)\\
&+ c^{\alpha}_{46}(c_ib_ja_kc_l + c_ib_jc_ka_l + a_ic_jc_kb_l + c_ia_jc_kb_l\\
&+ b_ic_ja_kc_l + a_ic_jb_kc_l + b_ic_jc_ka_l + c_ia_jb_kc_l)\\
&+ c^{\alpha}_{55}(b_ia_jb_ka_l + b_ia_ja_kb_l + a_ib_jb_ka_l + a_ib_ja_kb_l)\\
&+ c^{\alpha}_{66}(a_ic_ja_kc_l + a_ic_jc_ka_l + c_ia_ja_kc_l + c_ia_jc_ka_l),
\end{aligned} \tag{3}$$

$$k^{\alpha}_{ij} = k^{\alpha}_{11}a_ia_j + k^{\alpha}_{31}(a_ib_j + b_ia_j) + k^{\alpha}_{22}c_ic_j + k^{\alpha}_{33}b_ib_j, \tag{4}$$

where $\mathbf{a} = \mathbf{e}_1$, $\mathbf{c} = \mathbf{e}_2$, and $\mathbf{b} = \mathbf{e}_3$, $\mathbf{e}_i$ are the unit vectors of the crystal system of coordinates and c^{α}_{mn} and k_{kl} are the scalar coefficients. The subscripts in the scalar coefficients c^{α}_{mn} are the same as in crystallography for the matrix representation of fourth-rank tensors [4]. The transition from four to two subscripts is accomplished by the replacement of a pair of subscripts with a single subscript according to the rule

$$\begin{gathered}
(11) \leftrightarrow 1, \quad (22) \leftrightarrow 2, \quad (33) \leftrightarrow 3,\\
(23) = (32) \leftrightarrow 4,\\
(31) = (13) \leftrightarrow 5, \quad (12) = (21) \leftrightarrow 6.
\end{gathered} \tag{5}$$

It should be noted that tensors (3) and (4) differ from those presented for the monoclinic symmetry groups in [5] in the specification of the coordinate axes [4]. Tensors (3) and (4) are written in crystallographic coordinates. In the crystallographic coordinate system *OXYZ*, the *OY* axis coincides with the twofold symmetry axis for the symmetry groups 2 and 2 : *m* (the designation of symmetry groups is given according to A.V. Shubnikov) or is perpendicular to the symmetry plane for the symmetry group *m*. In [5], the coordinate system was oriented so that the *OZ* axis was substituted for the *OY* axis.

Let the tensor k_{ij} also be of the monoclinic symmetry group, i.e., form (4), but without the superscript α in its components. In this case, substituting the tensors F^{α}_{ijkl} and k_{ij} into Eq. (2), we obtain the explicit form of the phase-penetrability tensors in a porous medium with monoclinic symmetry of the filtration properties. The tensors are represented by Eq. (4) where the invariant coefficients are determined by the equalities

$$\begin{aligned}
k^{\alpha}_{11} &= c^{\alpha}_{11}k_{11} + c^{\alpha}_{12}k_{22} + c^{\alpha}_{13}k_{33} + 2c^{\alpha}_{15}k_{31},\\
k^{\alpha}_{22} &= c^{\alpha}_{12}k_{11} + c^{\alpha}_{22}k_{22} + c^{\alpha}_{23}k_{33} + 2c^{\alpha}_{25}k_{31},\\
k^{\alpha}_{33} &= c^{\alpha}_{13}k_{11} + c^{\alpha}_{23}k_{22} + c^{\alpha}_{33}k_{33} + 2c^{\alpha}_{35}k_{31},\\
k^{\alpha}_{31} &= c^{\alpha}_{15}k_{11} + c^{\alpha}_{25}k_{22} + c^{\alpha}_{35}k_{33} + 2c^{\alpha}_{55}k_{31}.
\end{aligned} \tag{6}$$

ANALYSIS OF PRINCIPAL RELATIONSHIPS

As is easily seen from Eqs. (6), the symmetry of the tensors k^{α}_{ij} does not change if the tensor k_{ij} has higher, up to isotropic, symmetry. Indeed, it is necessary to set $k_{13} = 0$ in Eqs. (6) for symmetry groups of the rhombic system (orthotropic filtration properties), $k_{13} = 0$ and $k_{11} = k_{33}$ for transverse isotropy, and $k_{13} = 0$ and $k_{11} = k_{22} = k_{33}$ for isotropy. In all these cases, Eqs. (6) indicate that $k^{\alpha}_{13} \neq 0$ and $k^{\alpha}_{11} \neq k^{\alpha}_{22} \neq k^{\alpha}_{33}$ and therefore the monoclinic symmetry of the tensors k^{α}_{ij} is conserved. Thus, when of passing from the absolute-penetrability tensor to the phase-penetrability tensors, the symmetry of the filtration properties can change. In this case, for the absolute-penetrability tensors with higher symmetry of the filtration properties, the position of only one principal axis remains unknown after passing to a two-phase flow. For monoclinic symmetry of the absolute-penetrability tensor, the direction of the *a priori* known principal axis of the phase-penetrability tensors is also conserved, but the positions of the other two principal axes of the absolute-penetrability tensor can differ from the respective axes of the phase-penetrability tensors. Let us prove the statement. The tensor of the absolute-penetrability coefficients with monoclinic symmetry can be reduced to the principal axes through rotation about

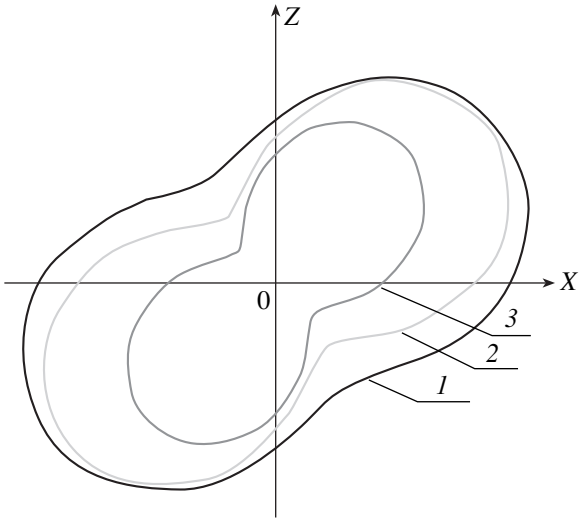

Section of the surface of the tensor k_{ij}^2 of the phase-penetrability coefficients for various values of the functions of relative phase penetrabilities $f_l^2(s, \pi_{ij}) \equiv f_l^2$: (*1*) $f_1^2 = f_3^2 = f_5^2 = 1$; (*2*) $f_1^2 = 0.85$, $f_3^2 = 0.9$, $f_5^2 = 0.375$; and (*3*) $f_1^2 = 0.46$, $f_3^2 = 0.795$, $f_5^2 = 0.295$.

the *OY* axis through an angle φ determined from the equality

$$\tan 2\varphi = \frac{2k_{13}}{k_{11} - k_{33}}. \quad (7)$$

Similarly, to reduce the phase-penetrability tensors k_{ij}^α to the principal axes, it is necessary to rotate the coordinate system about the *OY* axis through the angles φ^α determined as

$$\tan 2\varphi^\alpha = \frac{2k_{13}^\alpha}{k_{11}^\alpha - k_{33}^\alpha}. \quad (8)$$

However, whereas k_{13}, k_{11}, and k_{33} are constant in Eq. (7), and therefore the angle φ is fixed, the components of the phase-penetrability tensors k_{13}^α, k_{11}^α, and k_{33}^α in Eq. (8) depend on the saturation and vary; as a result, the angles φ^α can also vary. Indeed, as follows from relationships (2), the coefficients c_{mn}^α are dimensionless functions of saturation. Therefore, the components of the tensors k_{ij}^α of the phase-penetrability coefficients can be represented in the form $k_l^\alpha = f_l^\alpha(s, \pi_{ij})k_l$, where $\pi_{ij} = \dfrac{k_i}{k_j}$ and the passage from two subscripts to one subscript is performed according to rule (5). In this case, Eq. (8) can be represented in the form

$$\tan 2\varphi^\alpha = \frac{2f_5^\alpha(s, \pi_{ij})k_5}{f_1^\alpha(s, \pi_{ij})k_1 - f_3^\alpha(s, \pi_{ij})k_3}, \quad (9)$$

where $f_l^\alpha(s, \pi_{ij})$ are functions depending on the saturation and the ratio between the components of the absolute-penetrability tensor. The condition that the tensors k_{ij}^α and k_{ij} have common principal axes in the *OXZ* plane imposes the following constraint on the functions $f_l^\alpha(s, \pi_{ij})$:

$$\pi_{13} = \frac{f_3^\alpha(s, \pi_{ij}) - f_5^\alpha(s, \pi_{ij})}{f_1^\alpha(s, \pi_{ij}) - f_5^\alpha(s, \pi_{ij})},$$
$$\pi_{13} = \frac{f_3^1(s, \pi_{ij}) f_5^2(s, \pi_{ij}) - f_3^2(s, \pi_{ij}) f_5^1(s, \pi_{ij})}{f_1^1(s, \pi_{ij}) f_5^2(s, \pi_{ij}) - f_1^2(s, \pi_{ij}) f_5^1(s, \pi_{ij})}. \quad (10)$$

However, it is impossible to verify conditions (10) by comparison with available experimental data, because there are no such investigations for samples with an established type of filtration-property anisotropy [6]. For this reason, we simulate the possible behavior of the phase-penetrability tensor by considering sections of the indicatory surfaces of the k_{ij}^α tensor by the *OXY* plane. The indicatory surface of the filtration properties is determined by the equality

$$k^\alpha(\mathbf{n}) = k_{ij}^\alpha n_i n_j, \quad (11)$$

where n_i are the components of the unit vector specifying the direction along which the phase penetrability $k^\alpha(\mathbf{n})$ is determined. In the *OXZ* plane, Eq. (11) for tensors (4) takes the form

$$k^\alpha(\mathbf{n}) = k_{11}^\alpha \cos^2\beta + 2k_{31}^\alpha \cos\beta \sin\beta + k_{33}^\alpha \sin^2\beta, \quad (12)$$

where β is the angle between the coordinate axis *OX* and the unit vector n_i. Passing from the components of the tensors of phase-penetrability coefficients to the components of the absolute-penetrability tensor, we rewrite Eq. (12) in the form

$$k^\alpha(\mathbf{n}) = f_1^\alpha(s, \pi_{ij})k_1 \cos^2\beta$$
$$+ 2f_5^\alpha(s, \pi_{ij})k_5 \cos\beta \sin\beta + f_3^\alpha(s, \pi_{ij})k_3 \sin^2\beta.$$

Using the results of numerical and laboratory experiments [6, 7], it is possible to analyze the behavior of sections of the phase-penetrability surface preassigned values of functions $f_l^\alpha(s, \pi_{ij})$. The results of this simulation are shown in the figure. Since the component k_{13}^α (or, which is the same, k_5^α) appears in Eq. (12), the orientation of the principal axes of the phase-penetrability tensor varies with varying saturation.

ACKNOWLEDGMENTS

This work was supported by the Ministry of Education of the Russian Federation, project no. T 00-42-764 for fundamental research in engineering sciences.

REFERENCES

1. N. M. Dmitriev and V. M. Maksimov, Dokl. Akad. Nauk **358**, 337 (1998) [Phys. Dokl. **43**, 56 (1998)].
2. N. M. Dmitriev and V. M. Maksimov, Izv. Akad. Nauk, Mekh. Zhidk. Gaza, No. 2, 87 (1998).
3. V. M. Maksimov and N. M. Dmitriev, in *The Problems of Modern Mechanics* (Mosk. Gos. Univ., Moscow, 1998), pp. 76–84.
4. Yu. I. Sirotin and M. P. Shaskol'skaya, *Fundamentals of Crystal Physics* (Nauka, Moscow, 1975).
5. V. V. Lokhin and L. I. Sedov, Prikl. Mat. Mekh. **27**, 293 (1963).
6. A. M. Kuznetsov, Doctoral Dissertation in Engineering Sciences (Moscow, 1998).
7. J. Bear, C. Braester, and P. S. Menier, Transp. Porous Media **2**, 301 (1987).

Translated by V. Bukhanov